Genberg, V. “Structural Analysis of Optics”
Optomechanical Engineering Handbook
Ed. Anees Ahmad
Boca Raton: CRC Press LLC, 1999

Structural Analysis of Optics

Victor Genberg

Notations

1D	= 1 dimensional
2D	= 2 dimensional
3D	= 3 dimensional
BC	= boundary conditions
DOF	= degrees of freedom
FE	= finite element
FEA	= finite element analysis

8.1 Introduction

Typical structural designs in most industries are governed by failure due to stress — either yield, ultimate, or fatigue. An optical structure's performance is usually determined by distortions or displacements rather than stress. Most mirrors or lenses have distortion requirements measured in wavelengths of light (about 25 micro-in.). At this level of distortion, the stresses are usually quite small. Similarly, optical systems typically have tight optical beam-pointing requirements, or tight image motion requirements, which keep stresses in metering structures low. To predict the behavior of optical structures to the level of their performance specifications, analyses must have a high degree of accuracy. Thus, analysis techniques or assumptions commonly used in other industries may not be appropriate for optics.

Closed-form equations for the analysis of plates are useful for determining the general behavior of some optics, especially for determining design rules presented in earlier chapters. When detailed mount configuration and load effects are included, closed-form techniques usually cannot provide the solutions with the desired accuracy. For this reason, the techniques used in this chapter are based on the finite element method.

8.2 Overview of Finite Element Theory

Derivation of Stiffness Matrix

The finite element (FE) method is a numerical technique for converting a system of governing differential equations over a continuous domain to a set of discrete variables defined by a matrix equation. The continuous domain (Figure 8.1) is subdivided into a system of simple elements interconnected at a finite number of points called nodes, which are located at element corners and possibly along the element boundaries. Within each element the form of the behavior is assumed as a function of the nodal variables. In structural mechanics, the displacement (u) anywhere within an element is assumed to be the form:

$$u = \Sigma N_j \delta_j$$

where N_j is called the shape function of node j and δ_j is the displacement of node j. Thus a continuous variable u is approximated as a function of discrete variables δ, which is the fundamental assumption in FE theory. Typically N is a simple polynomial whose order is determined by the number of nodes associated with the element.

Given the choice of shape function, the derivation of the stiffness matrix is usually found from the minimization of potential energy (Π). The strain vector (ε) is found from the appropriate strain-displacement equations involving derivatives of the displacement (u) which lead to derivatives (B) of the shape functions (N).

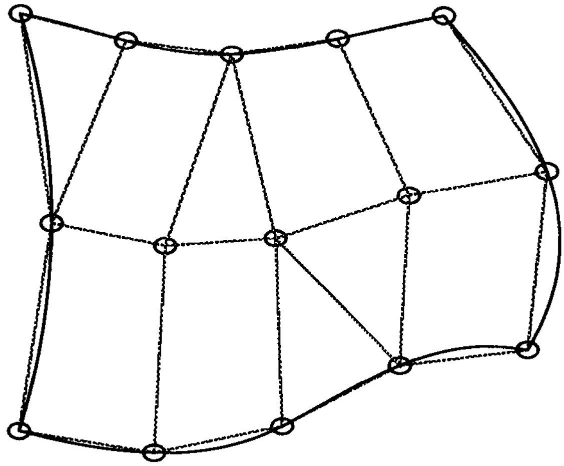

FIGURE 8.1 Finite element representation of a 2D continuum.

$$\{\varepsilon\} = [B]\{\delta\}$$

The stress vector (σ) is found from the appropriate stress-strain relations involving the material matrix (E).

$$\{\sigma\} = [E]\{\varepsilon\} = [E][B]\{\delta\}$$

The potential energy is integrated over the volume of each element:

$$\Pi = \int \{\varepsilon\}^T \{\sigma\} dV - \{\delta\}^T \{F\} = \int \{\delta\}^T [B]^T [E][B]\{\delta\} dV - \{\delta\}^T \{F\}$$

The nodal displacements are discrete variables and put outside of the integration. To minimize the potential energy with respect to the displacements, the partial derivative is set to zero.

$$d\Pi/d\{\delta\} = \int [B]^T [E][B] dV \{\delta\} - \{F\} = \{0\}$$

This has the form of the standard spring equation where the coefficient of displacement is the spring stiffness. Here the element stiffness matrix is

$$[k] = \int [B]^T [E][B] dV$$

integrated over the volume of the element. For any given element type, the above equation is used to find the element stiffness matrix given the material and nodal locations. The element matrices are assembled into a system level equilibrium equation of the form:

$$[K]\{\delta\} = \{F\}$$

Once valid boundary conditions (BC) are applied, the [K] matrix becomes nonsingular and is solvable by Gauss elimination or Cholesky decomposition.

The above is a very brief, simplified overview of finite element theory. For a more detailed description, some very good textbooks are available, such as Logan,[11] Segerland,[16] Knight,[10] or Cook.[3]

Element Types

As a new user, the most difficult parts of using a FE program is in the idealization of the problem, the choice of appropriate element type, and the size of the mesh required. A description of the element types and their application to optical structures follows. The names in parentheses are the names used in the NASTRAN FE program.

Truss Element (Rod)

- Line elements which carry only axial forces, with no bending
- End conditions are perfect ball joints
- Useful for some pinned end strut mounts

Beam Element (Bar, Beam)

- Line elements which carry all forces and moments
- End conditions are perfectly welded
- Symmetric cross sections (I-beam) have shear center at neutral axis
- Asymmetric cross sections (C-channel) have shear center offset
- Short beams require transverse shear factor for accuracy
- Useful for most frame-like optical support structures

Plate/Shell Element (QUAD4, QUAD8, TRIA3, TRIA6, QUADR, TRIAR)

- 2D planar elements with membrane and bending stiffness
- Thin plate elements ignore transverse shear stiffness
- Thick plate elements include transverse shear stiffness
- Plane stress elements are typical plate/shell structures
- Plane strain elements are for 2D cross sections of long structures
- The best elements allow modeling of composite and waffle-type plates
- Accuracy is a function of mesh density, element type, element order
- Useful for thin optics (Figure 8.2) and lightweight mirrors

Solids (Hexa, Penta, Tetra)

- 3D elasticity element, usually having only translational stiffnesses
- Accounts for full 3D effects in structural behavior
- Should allow orthotropic materials
- Accuracy is a function of mesh density, element type, element order
- Useful for thick optics (Figure 8.3), bonded joints, or submodel details

Axisymmetric Solids (TRIAX6)

- 3D elasticity behavior reduced to 2D by axisymmetric conditions
- The structure and BC (and usually the load) must be axisymmetric
- Accuracy is a function of mesh density, element type, element order
- Useful for thick optics, lenses, and lens barrels (Figure 8.4)

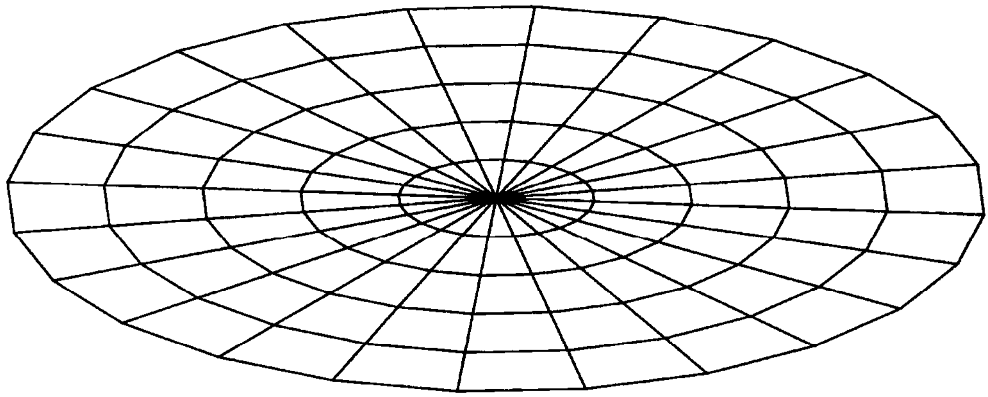

FIGURE 8.2 Shell element model of a mirror, lens, or window.

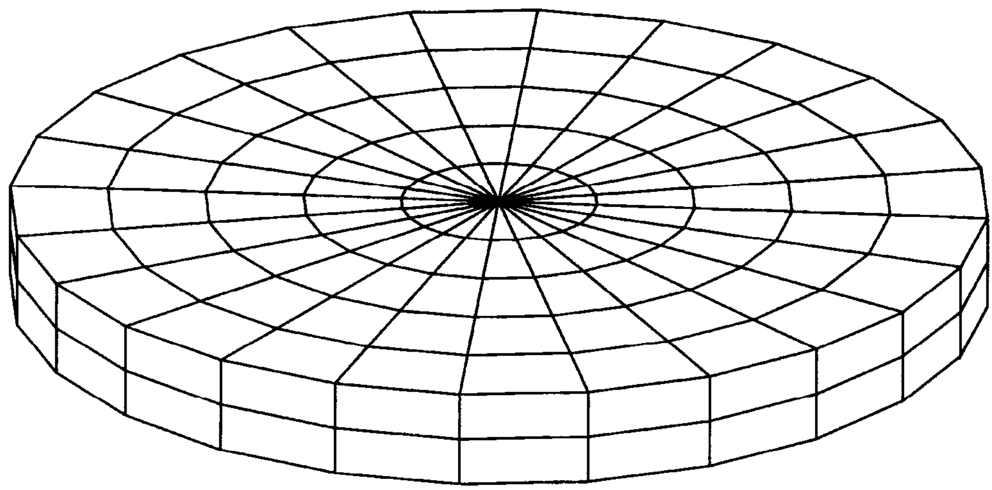

FIGURE 8.3 Solid element model of a mirror, lens, or window.

Springs (ELAS)

- Scalar spring connecting any 2 DOF
- User supplies calculated spring constant
- If connected DOF are not coincident and colinear, then hidden reactions to ground may be created
- Useful for effective joint stiffness in dynamics models

Rigid Element (RBAR, RBE2)

- Absolutely rigid element with no elasticity
- These elements have no thermoelastic growth, so use with care
- Useful for neutral axis offsets in metering structures

Equation Element (MPC, RBE3)

- Add any linear equation to a model with a multipoint constraint (MPC)
- RBE3 can calculate average motion of several nodes
- Useful for calculating image motion in a system level model

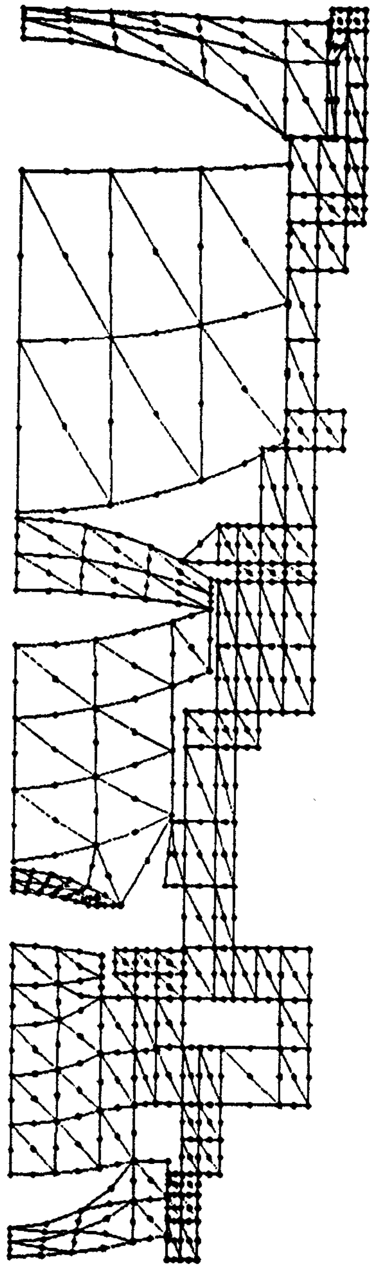

FIGURE 8.4 Axisymmetric element model of a lens barrel.

Element Accuracy

The truss, beam, spring, and rigid elements have the theoretically exact stiffness matrix. Subdividing a beam structure into more beam elements may improve visualization, but does not improve accuracy in a static analysis. In a dynamic analysis, subdivision can improve the distribution of mass with an improvement in analysis accuracy. The plate and solid elements are approximations to continuum behavior, so the element type and number do affect the solution accuracy. The first- and second-order 2D membrane elements are shown in Figure 8.5. For the following discussion, let u and ε be the displacement and strain in the x direction.

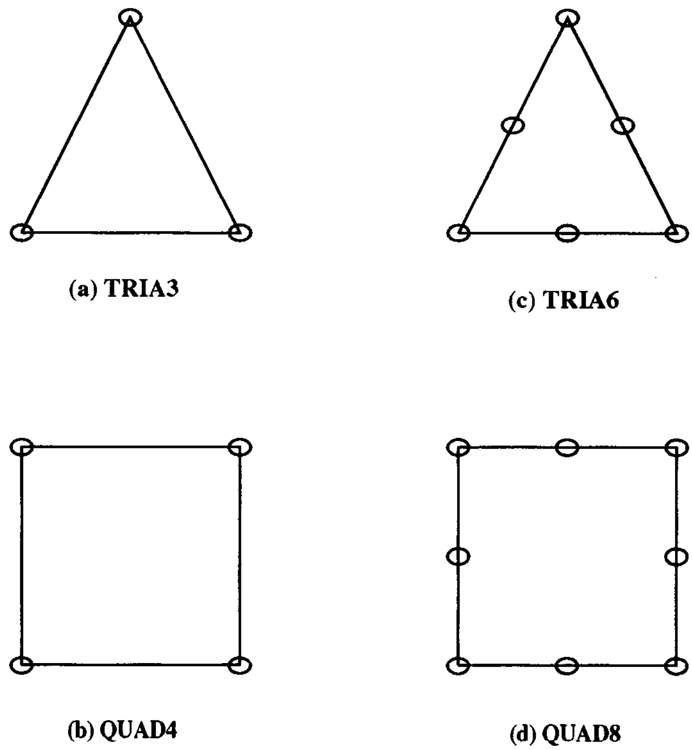

FIGURE 8.5 Shell elements.

1. 3-node triangle: (constant strain)
   $u = a + bx + cy$
   $\varepsilon = du/dx = b$
2. 4-node quadrilateral: (partial linear strain)
   $u = a + bx + cy + dxy$
   $\varepsilon = du/dx = b + dy$
3. 6-node triangle: (full linear strain)
   $u = a + bx + cy + dxy + ex^2 + fy^2$
   $\varepsilon = du/dx = b + dy + 2ex$
4. 8-node quadrilateral: (partial quadratic strain)
   $u = a + bx + cy + dxy + ex^2 + fy^2 + gxy^2 + hx^2y$
   $\varepsilon = du/dx = b + dy + 2ex + gy^2 + 2hxy$

The simple example cantilever beam shown in Figure 8.6 is modeled with the above elements in a regular pattern and with a distorted pattern in Figure 8.7(a). The mesh chosen had nearly equal numbers of nodes, and thus nearly equal size of stiffness matrix. Five load conditions were applied which have the following x direction strain (ε) patterns:

1. Membrane axial force (F_x) causes constant strain ε throughout.
2. Membrane end moment (M_z) causes ε to be linear in y, constant in x.
3. Membrane end shear (F_y) causes ε to be linear in y and linear in x.
4. Bending end moment (M_y) causes ε to be constant in x and y, linear in z.
5. Bending pressure (p_z) causes ε to be constant in y, linear in x and z.

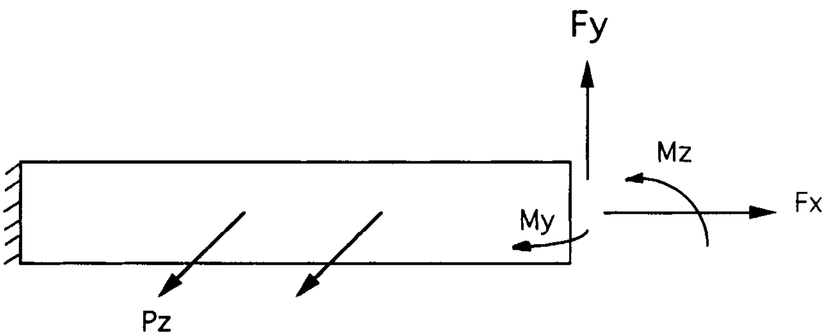

FIGURE 8.6 Thin cantilever beam with in-plane (membrane) and out-of-plane (bending) loads.

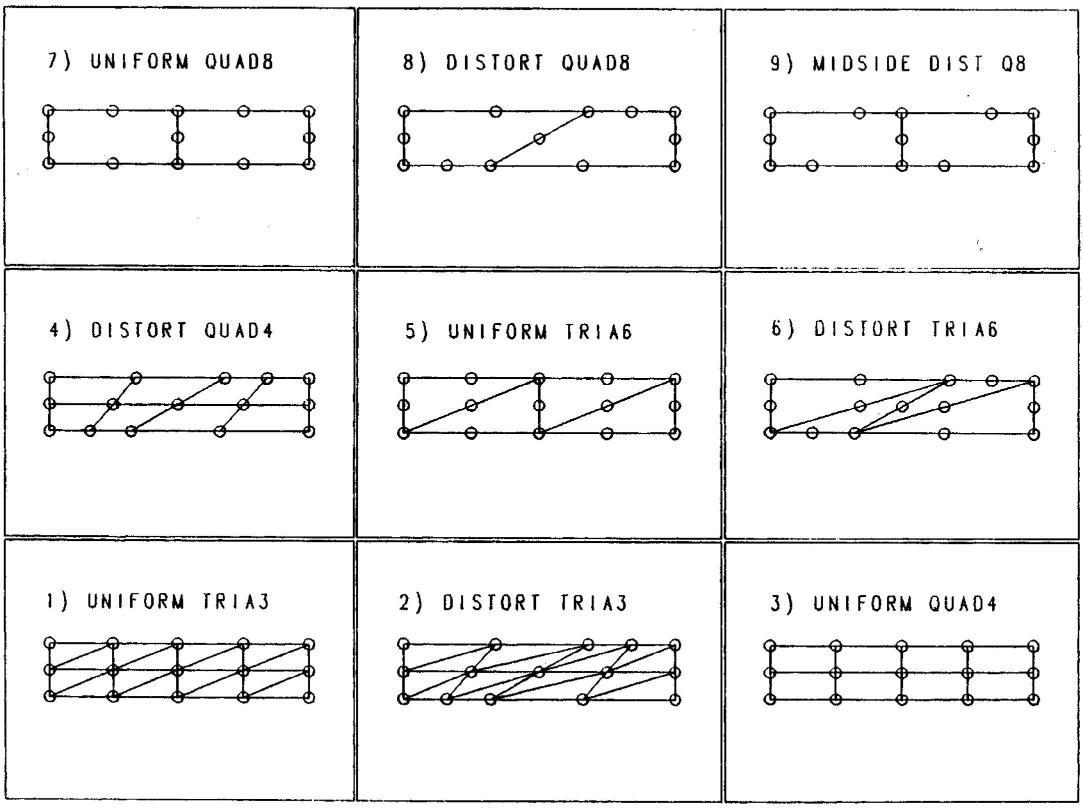

FIGURE 8.7 (a) Finite element models for the cantilever beam.

In each case, the load is picked such that the theoretical end displacement is 1.0. From the resulting displacements in Figure 8.7(b), the following conclusions can be made:

- All elements are good in constant strain.
- All elements are good in plate bending.
- The 3-noded triangle is very poor for any strain variation.
- The 4-noded quadrilateral deteriorates with distortion.
- With second-order elements the added nodes must be at midside.
- The elements with drilling DOF are much better than the originals.

Comparison of 2D & 3D Elements - Cantilever Beam Example

Membrane behavior

1) Fx = Axial load = uniform / constant stress
2) Mz = In-plane moment = axial strain is linear in y
3) Fy = Shear load = axial strain is linear in y & x

Plate behavior

4) My = out-of-plane moment = constant moment
5) Pz = normal pressure = linear moment

Model	F.x	M.z	F.y	M.y	P.z
Conventional Plate Elements					
1)Tria3	1.00	0.30	0.32	0.98	0.98
2)Tria3-Dist	1.00	0.12	0.16	0.98	0.93
3)Quad4	1.00	0.98	0.96	0.98	0.98
4)Quad4-Dist	1.00	0.41	0.47	0.98	0.96
5)Tria6	1.00	1.00	0.96	0.98	0.97
6)Tria6-Dist	1.00	1.00	0.82	0.98	0.81
7)Quad8	1.00	1.00	1.00	0.98	0.96
8)Quad8-Dist	1.00	0.98	0.94	0.88	0.79
9)Quad8-Mid	1.00	0.59	0.59	0.47	0.49
Plate Elements with drilling DOF					
1a)TriaR	1.00	0.87	0.86	0.98	0.98
2a)TriaR-Dist	1.00	0.69	0.67	0.98	0.93
3a)QuadR	1.01	1.00	1.00	0.98	0.98
4a)QuadR-Dist	1.01	0.98	0.97	0.98	0.96

FIGURE 8.7 (b) Results for tip deflections for cantilever beam models.

Note that these results are for the MSC/NASTRAN elements. The elements in other codes may use a different formulation which gives different results. Most notably is the QUAD4 which is not the standard 4-node isoparametric formulation. The standard isoparametric 4-noded quadrilateral would not perform as well as the QUAD4 in the above test. The QUADR and TRIAR have added the drilling DOF (normal rotation or Φ_z) to the formulation, which improves the behavior under distortion. These tests are useful, but not complete. MacNeal[12] has proposed a more complete set of test cases. However, the membrane loadings in this cantilever beam are very similar to the behavior that the core struts in a lightweight mirror experience. Thus, an analyst could use this model as a prototype model in determining the best technique for representing the core structure. An analyst should run a whole series of test cases similar to this to verify the behavior of the FE code to be used in any analysis of optical structures.

Solid elements are a 3D extension of the 2D membrane behavior. Thus conclusions drawn about quadrilaterials and triangles can be extended to hexahedrons and tetrahedrons, respectively. As expected, the 4-noded-tetrahedron performs as poorly as the 3-noded triangle. Since current automeshing capability in 3D structures is generally limited to tetrahedron, the FE code must offer the choice of 10-noded tetrahedron if it is to be used for high accuracy optical structures. This author highly recommends the use of parametric meshing with hexahedron over any automeshing technique for highly accurate optics models.

8.3 Symmetry Techniques

Most optical structures possess some level of symmetry. Techniques which take advantage of symmetry can reduce the computer resources required for a finite element analysis. Typically, only the smallest repeating section is modeled.

Symmetry is defined as a balanced arrangement of structure about a point (spherical symmetry), a line (axisymmetry), or a plane (reflective symmetry). For a structure to be symmetric, both the structure and its boundary conditions must possess the same degree of symmetry. Applied loads may be nonsymmetric, although there are additional efficiencies when the load is also symmetric.

Axisymmetry

Most lenses and lens barrels are axisymmetric (Figure 8.4). The structure may be represented as a finite element model using axisymmetric elements as shown in Figure 8.8. If the load is also axisymmetric, as a circular line load or a uniform change in temperature, then the behavior of one cross-sectional plane represents the solution at any cross-sectional plane. Most finite element programs can solve this problem, because the theory for 2D elements can be extended to axisymmetry by the addition of a hoop stress term. The applied load (F) at a radius (R) is the net force on a full ring of structure subjected to a line load (f) in force/length.

$$F = 2\pi Rf$$

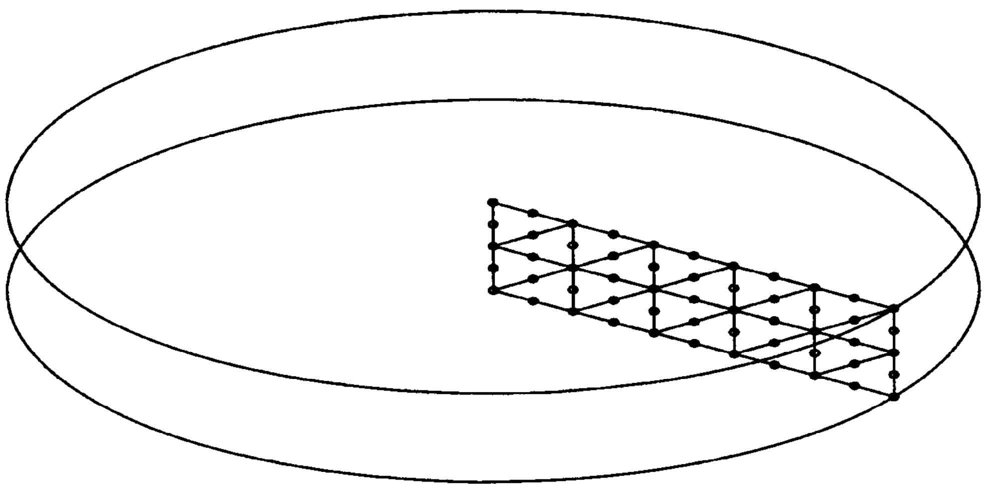

FIGURE 8.8 Axisymmetric element model of an optic.

Displacement results are limited to radial (δ_r) and axial (δ_z), while stress results include radial (σ_r), axial (σ_z), shear (τ_{rz}), and hoop (σ_θ). If the load has a variation in θ which can be represented as a Fourier series, some programs will provide a solution which is also represented as a Fourier series.

An alternative model for axisymmetric behavior is a small slice of pie as shown in Figure 8.9. Since the structure is uniform in θ, then a small slice (<10°) with a single element in that direction is adequate. Symmetric BC must be applied to both symmetry faces to insure the proper behavior.

$$\delta_\theta = 0, \quad \phi_r = 0, \quad \phi_z = 0$$

This model is not as efficient, since twice the number of nodes are required, but it may be possible to use some program features which might not be available in a particular FE program's axisymmetric capability list.

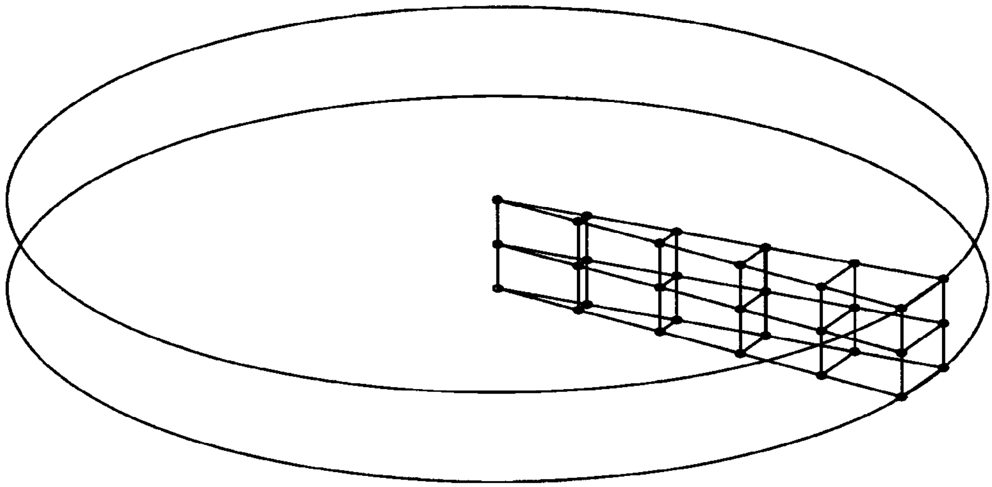

FIGURE 8.9 Solid element wedge model of an optic.

Reflective Symmetry with General Load

Reflective symmetry is very common in most man-made of natural structures. In optical structures there may be several planes of symmetry as shown in a lightweight mirror on a 3-point support in Figure 8.10.

For a single plane of symmetry, where the structure and boundary conditions are symmetric, but the applied load is not (Figure 8.11[a]), the solution is a linear combination of two solutions, a symmetric case (Figure 8.11[b]), and an antisymmetric case (Figure 8.11[c]), each with the loads cut in half. Both (b) and (c) can be solved using symmetric half-models. In Figure 8.12, the half-model (right side) is solved twice, once with symmetric loads (P_s) and symmetric BC to get a displacement vector (δ_S) in Figure 8.12(b), and once with antisymmetric loads (P_A) and antisymmetric BC to get displacement vector (δ_A) in Figure 8.12(c). The load vectors P_S and P_A can be determined from the applied loads on the right side P_R and the left side P_L by the equation:

$$P_S = 0.5(P_R + P_L)$$

$$P_A = 0.5(P_R - P_L)$$

Symmetry can be thought of as a standard reflective mirror. The symmetric BC can be found from intuition using Figure 8.11(b). If at point j on the right side, the x displacement is δ_{xj}, and for the corresponding point k on the left side the displacement is δ_{xk}, then by symmetry,

$$\delta_{xk} = -\delta_{xj}$$

If point j is a point on the symmetry plane, then points j and k are coincident (j = k). The only way the last equation can be satisfied is for

$$\delta_{xk} = -\delta_{xj} = 0$$

For symmetric loads, the displacement normal to the symmetry plane must be zero at the symmetry plane, as are rotations in the symmetry plane. If the x axis is normal to the symmetry plane,

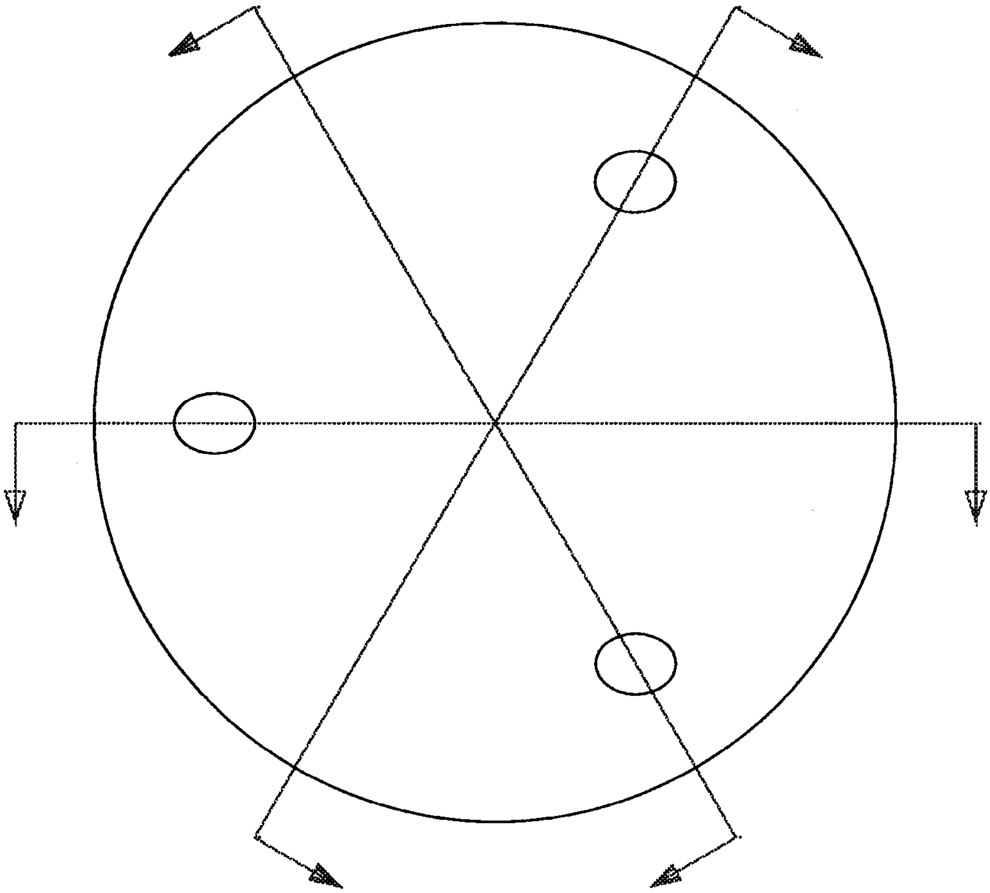

FIGURE 8.10 Planes of symmetry for an optic on a 3-point support.

$$\delta_x = \phi_y = \phi_z = 0$$

Antisymmetry is the negative of a reflective mirror. The antisymmetric BC, which can be determined by a similar argument, are the compliment of the symmetric BC. For Figure 8.11(c), the antisymmetric BC are the two displacements in the symmetric plane and the rotation normal to the plane:

$$\delta_y = \delta_z = \phi_x = 0$$

The resulting displacements δ_S and δ_A are only intermediate results. The desired results on the full structure are found by the linear combination:

$$\delta_R = \delta_S + \delta_A$$

$$\delta_L = \delta_S - \delta_A$$

The displacements on the modeled half (right side) are in a normal right-hand coordinate system. The displacements on the unmolded half (left side) must be interpreted as being in a left-hand coordinate system.

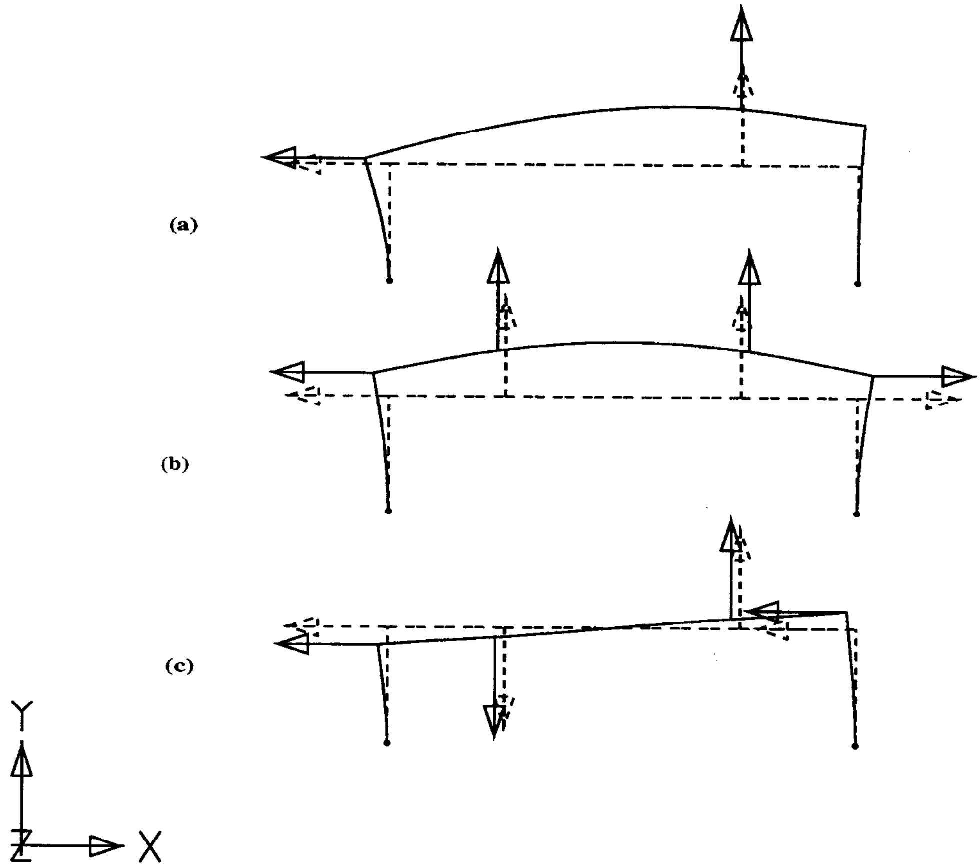

FIGURE 8.11 Symmetric structure with general loads. (a) Solution to general load condition; (b) solution with symmetric load components; and (c) solution with antisymmetric load components.

Some finite element codes allow the solution of multiple BC and linear combinations of results, making the above approach possible in a single execution of the code. The above approach can be applied twice to model two planes of symmetry with a 1/4 model and 4-load cases as shown in Figure 8.13. The double subscripts refer to the type of BC on each side of the model and the integer subscripts refer to the quadrant for which the solution applies.

$$\delta_1 = \delta_{SS} + \delta_{SA} + \delta_{AA} + \delta_{AS}$$

$$\delta_2 = \delta_{SS} - \delta_{SA} - \delta_{AA} + \delta_{AS}$$

$$\delta_3 = \delta_{SS} - \delta_{SA} + \delta_{AA} - \delta_{AS}$$

$$\delta_4 = \delta_{SS} + \delta_{SA} - \delta_{AA} - \delta_{AS}$$

The extension to three planes is also possible, requiring eight combinations of BC.

Reflective Symmetry with Symmetric Load

The application of symmetry is especially efficient for the special case when the applied load has the same symmetry as the structure. In Figure 8.14, there is no antisymmetric load ($P_A = 0$) and,

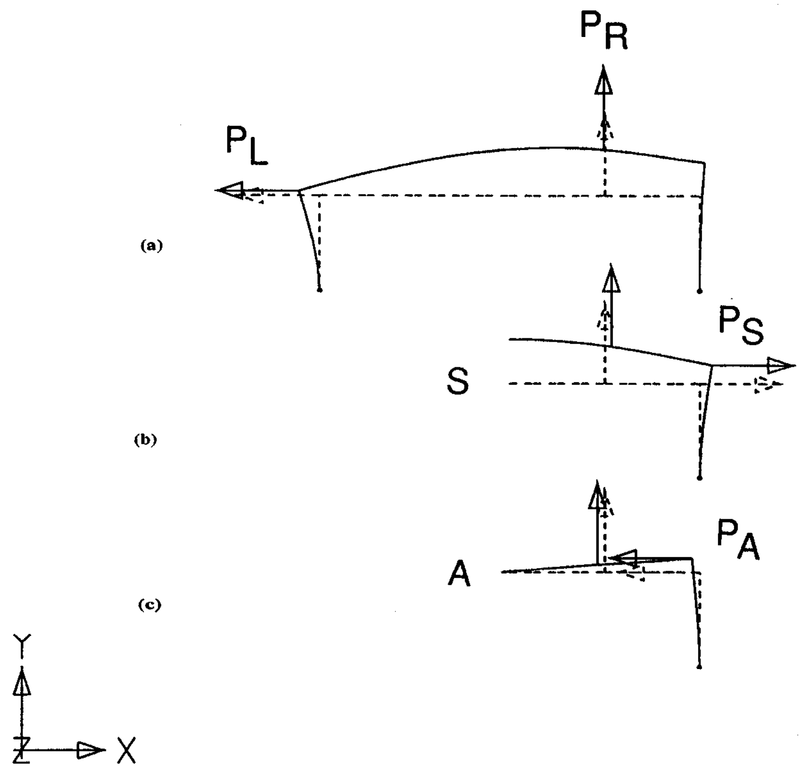

FIGURE 8.12 General solution by using symmetric submodels. (a) Solution to general load conditions; (b) half model with symmetric loads and BC; and (c) half model with antisymmetric loads and BC.

thus, no antisymmetric displacement ($\delta_A = 0$). Only the symmetric case is run, and no combination is required. This is the most obvious and the most common application of symmetry.

Multiple planes of symmetry with symmetric loads are simple to use, if the finite element program allows displacements to be calculated in alternate coordinate systems. Some simple FEA programs require that all displacements be calculated in a single rectangular system, limiting symmetry to the x, y, or z plane. If displacements are calculated in a cylindrical system, then a circular mirror on a 3-point mount with a symmetric load can be analyzed with a 60° model with BC on each cut face,

$$\delta_\theta = \phi_R = \phi_z = 0$$

Note that the displacement normal to the planes is zero and the two rotations in the plane are zero.

Model Size Required

A variety of model sizes are possible in common optical structures. In the following discussion the models are pictured in Figures 8.15 to 8.19. The coordinate axes are oriented so the X axis is on one plane of symmetry and the Z axis is the optical axis normal to the plane of the optic. Symmetric DT includes uniform temperature change, or an axisymmetric temperature variation in the radial or axial direction.

Full Model (360°)

A full model is required for:

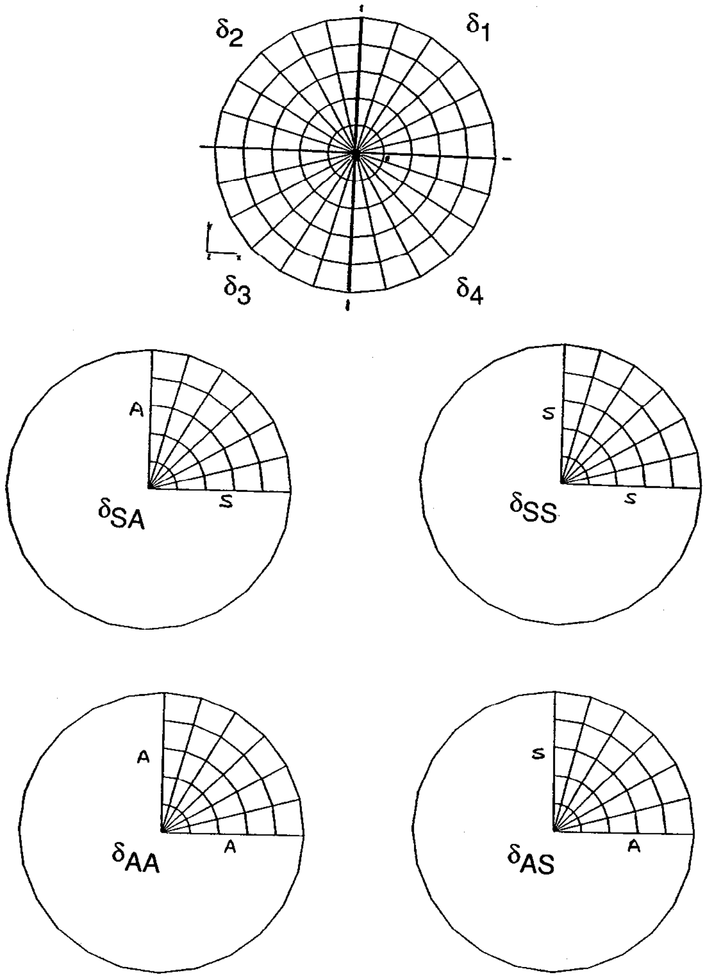

FIGURE 8.13 General solution using two planes of symmetry.

- Nonsymmetric structure (internal core or external shape)
- Nonsymmetric BC (mount location or stiffness)

Even when symmetry exists, a full model can be useful

- To find all dynamic or buckling modes in a single solution
- To get full dynamic response analysis in a single solution
- For nonsymmetric loads solved in a single subcase without combinations
- For plotting and postprocessing of the full structure

Half-Model (180°)

A half-mode applies to:

- Circular, hexagonal, and elliptic optics
- Polar, square, triangular, and hexagonal core structures
- Most mount configurations (uniform, ring, 3, 4, or 6 point)

A half-model is most efficient when:

- Symm BC: loads have 360° symmetry (i.e., Z gravity, symmetric ΔT)

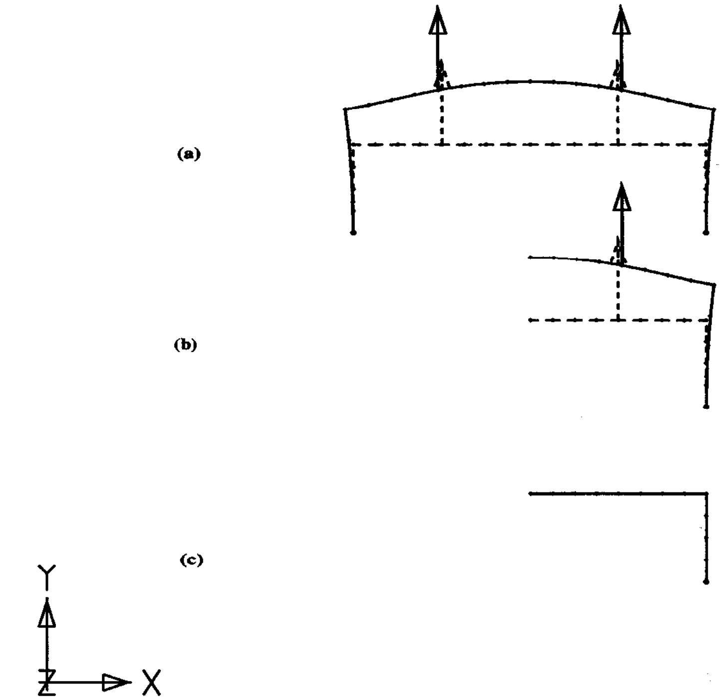

FIGURE 8.14 Symmetric structure with symmetric loads. (a) Full solution; (b) half-model with symmetric loads and BC; and (c) half-model with antisymmetric loads (null).

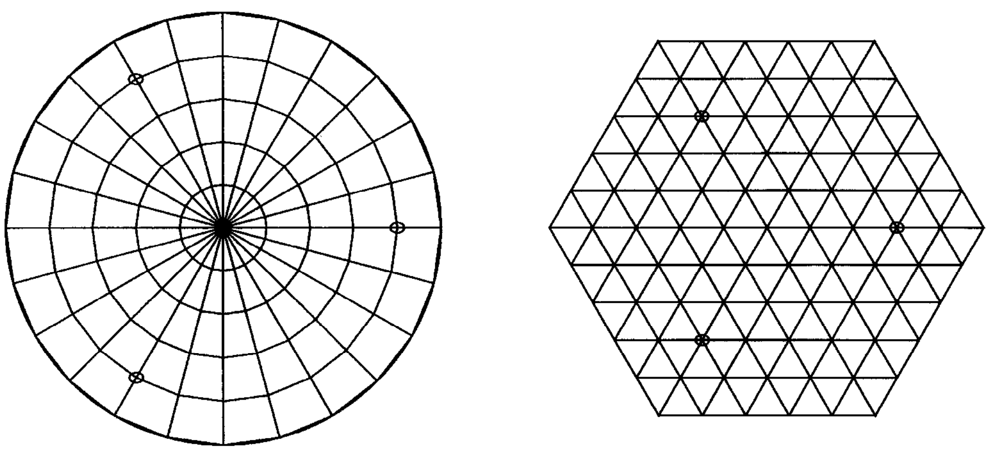

FIGURE 8.15 Full model of an optic (360°)

- Symm BC: loads have 180° symmetry (i.e., X gravity)
- Anti-BC: loads have 180° antisymmetry (i.e., Y gravity)

A half-model requires two solutions (symm BC and anti-BC) to find all dynamic modes.

Quarter Model (90°C)

- Circular, hexagonal, and elliptic optics
- Polar, square, triangular, and hexagonal core structures
- Limited mount configurations (uniform, ring, 4 point, NOT 3 or 6 point)

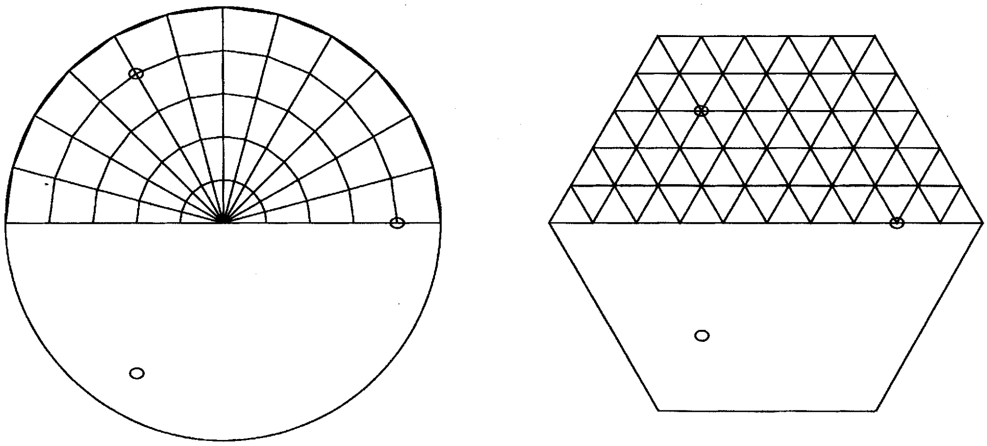

FIGURE 8.16 One-half model of an optic (180°).

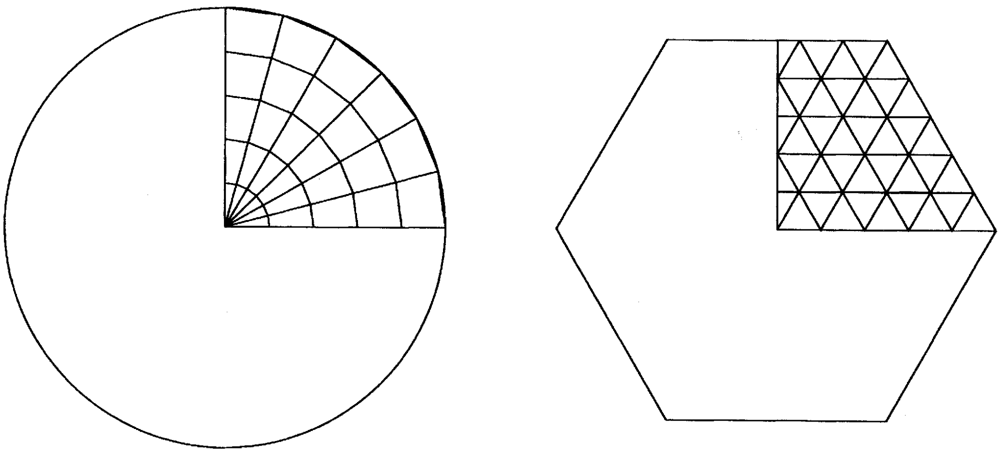

FIGURE 8.17 One-quarter model of an optic (90°).

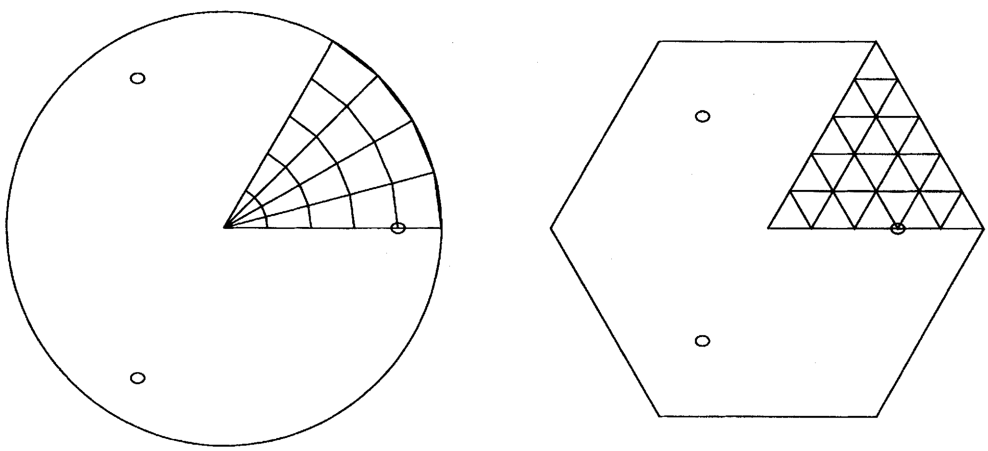

FIGURE 8.18 One-sixth model of an optic (60°).

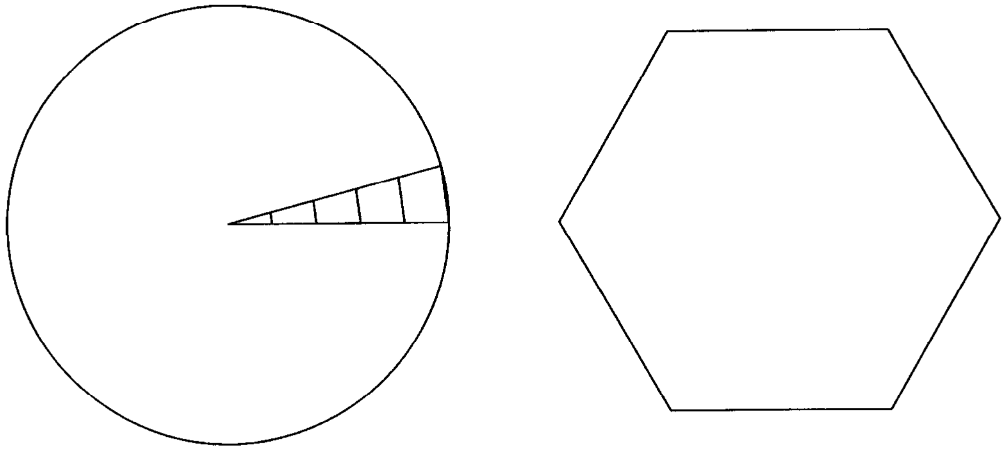

FIGURE 8.19 One-n*th* model of an optic (<10°).

A quarter model is limited to the following loads:

- Symm-symm BC: loads with 360 symmetry (i.e., Z gravity, symmetric ΔT)
- Symm-anti-BC: loads with 180 symmetry (i.e., X or Y gravity)

A quarter model requires four solutions to find all dynamic modes, although some may be mode pairs.

One-Sixth Model (60°)

A 1/6 model applies to:

- Circular, hexagonal, but NOT elliptic optics
- Polar, triangular, and hexagonal, but NOT square core structures
- Most mount configurations (uniform, ring, 3 to 6 point, NOT 4 point)

A 1/6 model is limited to the following loads:

- Symm-symm BC: loads with 360 symmetry (i.e., Z gravity, symmetric ΔT)

A 1/6 model cannot find all dynamic modes, only those with 60°C symmetry.

Thin Wedge Model

A l/n model (<10°) applies to:

- Axisymmetric structure and BC (i.e., circular optic on ring support)
- Axisymmetric loads (i.e., Z gravity, symmetric ΔT)

A l/n model can only find axisymmetric dynamic modes.

Only model sizes are possible in special cases, but the above set describes the most common applications of symmetry.

Advantages and Disadvantages of Symmetry

The obvious advantage of using symmetry in a finite element model is efficiency, but an expanded list would include:

- Faster modeling with fewer grids and elements
- Less model checking required

- Faster run times
- Less memory and disk storage required
- Smaller output files generated

Some disadvantages of symmetry include:

- Cannot get full model plots easily
- Requires multiple solutions and combinations if load is nonsymmetric
- Image side uses left-handed coordinate system for output
- Requires all combinations of BC to get all dynamic modes

In dynamics and buckling, the lowest mode is not necessarily symmetric. All BC combinations must be checked to find the lowest mode. The basic premise of symmetric is linear superposition. If the structure behaves in a nonlinear fashion (material or geometric), then symmetry may not apply. Most optical structures display some symmetry. The analysis can be much more efficient if symmetry is exploited in the modeling scheme.

8.4 Displacement and Dynamic Models for Optics

The primary concern in the structural analysis of optics is the deformation of the optical surface or the pointing of an optical surface, due to static or dynamic loads. Performance of the optical system is controlled by the motion and deformation of the optics, with stress being of secondary concern in most applications. Stress models, which require more detail than displacement models, are addressed in the next section.

Depending on the information required and the resources (manpower and computer) available, the level of detail may vary in a finite element model. The following list is ordered by increasing resolution and model size.

Single-Point Model (Solid or Lightweight Optic)

In a system level model, a "small" stiff optical element may be treated as a single node point in the structural model. For dynamics or gravity loads, the point must have the proper mass properties, including center of gravity and moments of inertia. Since line of action of forces is very important, the mount points must be modeled in their true spatial location (Figure 8.20). The optical mode may be attached to the "softer" elastic mount with rigid elements. However, if thermal loads are to be analyzed, then very stiff elastic beams with the correct CTE should be used to attach to the mount. The stiff elastic beams must be stiff relative to the softer mounts, but not so stiff that they cause numerical difficulty. Suggested stiffness values are 100 to 1000 times the mount stiffness.

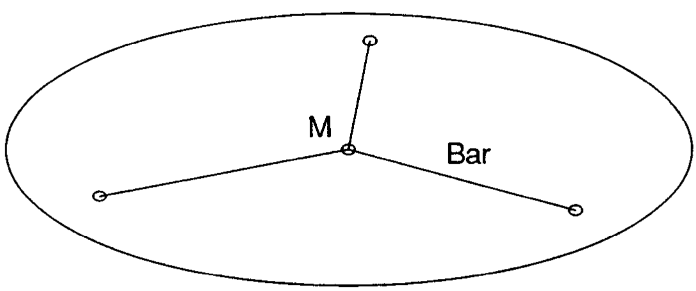

FIGURE 8.20 Rigid, lumped-mass model of an optic.

A slight improvement on this model uses three triangular plate elements with the same 4-node points used in the beam model. Now actual plate thicknesses can be modeled so fewer calculations and assumptions are required. A side benefit is that the graphical display is improved.

A single-point model can be used for optical path pointing analysis, but offers no information about the surface distortion of the individual optic.

2-D Plate Model (Solid Optic)

A plate model (Figure 8.2) incorporates the bending and membrane behavior into the analysis, but does not incorporate through the thickness effects. Bending distortion due to pressure, gravity, or axial gradients, as well as radial growth due to temperature changes, can be found. However, thickness changes caused by temperature cannot be determined from a plate model. The model can account for original thickness variation in the optic by providing different property (thickness) inputs for the various plates.

For high accuracy analysis, traverse shear flexibility must be incorporated in the plate elements. In finite element documentation, this is commonly referred to as thick plate theory or Mindlin plate theory. For a solid flat circular mirror supported at the outer edge by a knife-edge support (simple supported BC), the bending and transverse shear deflection are compared in Figure 8.21. For a diameter/thickness ratio of 10, the shear deflection is 10% of the bending deflection. Although this may seem small, deflections of this magnitude are important to optical performance.

The 2D model is cheap to generate and to run. Dynamic modes are found accurately and cheaply for most conventional optics.

3D Solid Model (Solid Optic)

A finite element model composed of solid elements (Figure 8.3) can accurately predict the distortion of optics including through-the-thickness effects. These include thermal gradients and 3D variations around mounts. Transverse shear is automatically included in the solid elements. Thickness variation of the optic is accounted for by node position on the surface.

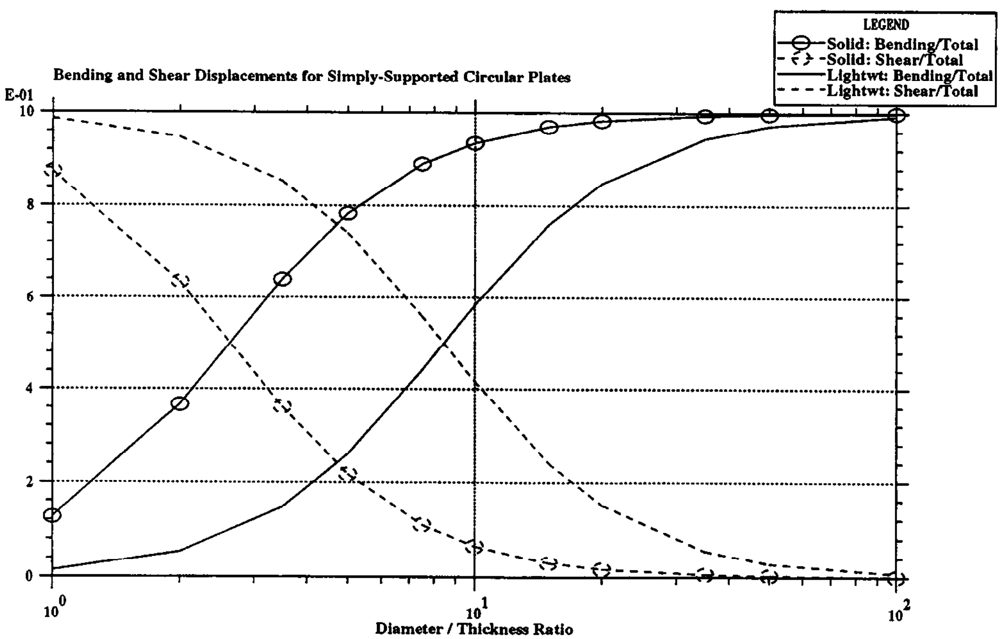

FIGURE 8.21 Bending and transverse shear components of the 1-g-sag displacement of simply supported circular plates.

To get accurate bending behavior from solid models, sufficient model resolution is required in all three dimensions. One layer of 8-noded bricks through the thickness is generally too stiff, causing the deflections to be 10 to 20% too small. At the very minimum, two layers should be used through the thickness. Not all bricks are created equal. Finite element programs may use different formulations and integration rules which can modify the accuracy of a solid model. A suggested approach is to model a flat plate on a ring support using the same elements and resolution to be used on a real optic, to determine the detail required to get the accuracy desired in the analysis program used. The theoretical solution from plate theory (including transverse shear) for a circular plate of radius (R) and thickness (t) subjected to a uniform pressure (p) is

$$\delta_{total} = \delta_{bending} + \delta_{shear}$$

$$\delta_{bending} = [(5 + \nu)pR^4]/[64(1 + \nu)D]$$

$$\delta_{shear} = [3pR^2]/[8Gt]$$

$$D = [Et^3]/[12(1 - \nu^2)]$$

Parametric meshes, as shown in Figure 8.3, provide the most accurate results in general. Most preprocessing programs can create such a mesh under user control. Some programs offer automesh capability for 3D solids. Current technology limits most automeshers to tetrahedron elements. The linear displacement 4-noded tetrahedron is notoriously stiff, causing predicted displacements to be too low. At least eight layers are required through the thickness to predict displacements with less than 10% error. These models often become too expensive to run. The quadratic displacement 10-noded tetrahedron provides much more accurate answers, requiring only two to four layers through the thickness in most cases. Automeshed optics tend to predict nonuniform and nonsymmetric response even for perfectly symmetric problems. The unexpected nonsymmetry can cause the results to be misleading. Since the geometry of most optics is very regular, parametric meshing is highly recommended.

2D Equivalent Stiffness Plate Model (Lightweight Optic)

A typical lightweight optic includes two faceplates bonded to an eggcrate core structure as shown in Figure 8.22. Common eggcrate structures may be triangular, square, or hexagonal patterns. Key dimensions in this structure are the core plate thickness (t_c) and the inscribed circle diameter (B) which define the core density ratio (α).

$$\alpha = t_c/B$$

To first order, the behavior of the core is determined by α regardless of the core pattern.[1] The other key dimensions and properties are (Figure 8.23)

t_p = faceplate thickness
H = overall height
H_c = core height = $H - 2t_p$
E = Young's modulus
ν = Poisson's ratio
ρ = mass density

A lightweight mirror can be represented as a single layer of plate elements with equivalent properties. The membrane (in-plane) behavior is found from the cross-sectional area:

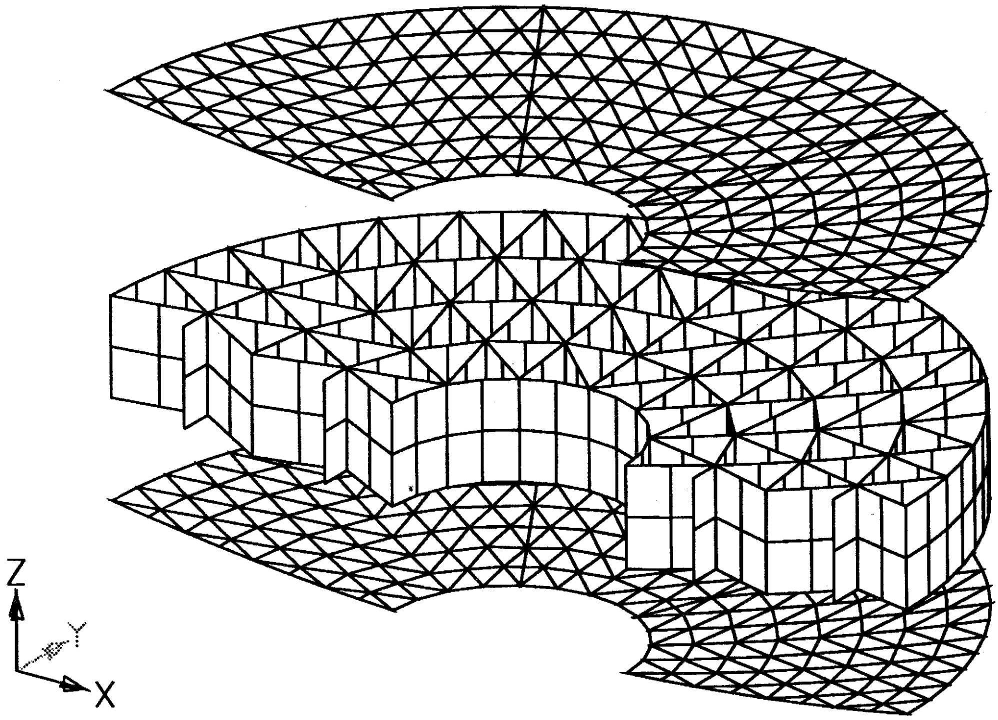

FIGURE 8.22 FE model of a lightweight mirror with triangular core.

$$t_m = 2t_p + \alpha H_c$$

The cross-sectional moment of inertia per unit length is

$$I_b = \left[H^3 - (1-\alpha)H_c^3\right]/12$$

The ratio of I_b to the moment of inertia of a solid plate of thickness t_m is

$$R_b = 12I_b/t_m^3$$

This ratio is always greater than 1, and for most practical designs is on the order of 100 to 1500. Modern designs tend to have higher ratios with more structural efficiency. Transverse shear distortion is even more important in lightweight mirrors than in solids. The transverse shear ratio (R_s) is

$$S = \left[H^2 - (1-\alpha)H_c^2\right]/\alpha$$

$$R_s = (2/3)12I_b/\left[St_m\right]$$

A common approximation is to consider the core to be fully effective in carrying shear, with the faceplates carrying none. Thus the shear ratio is

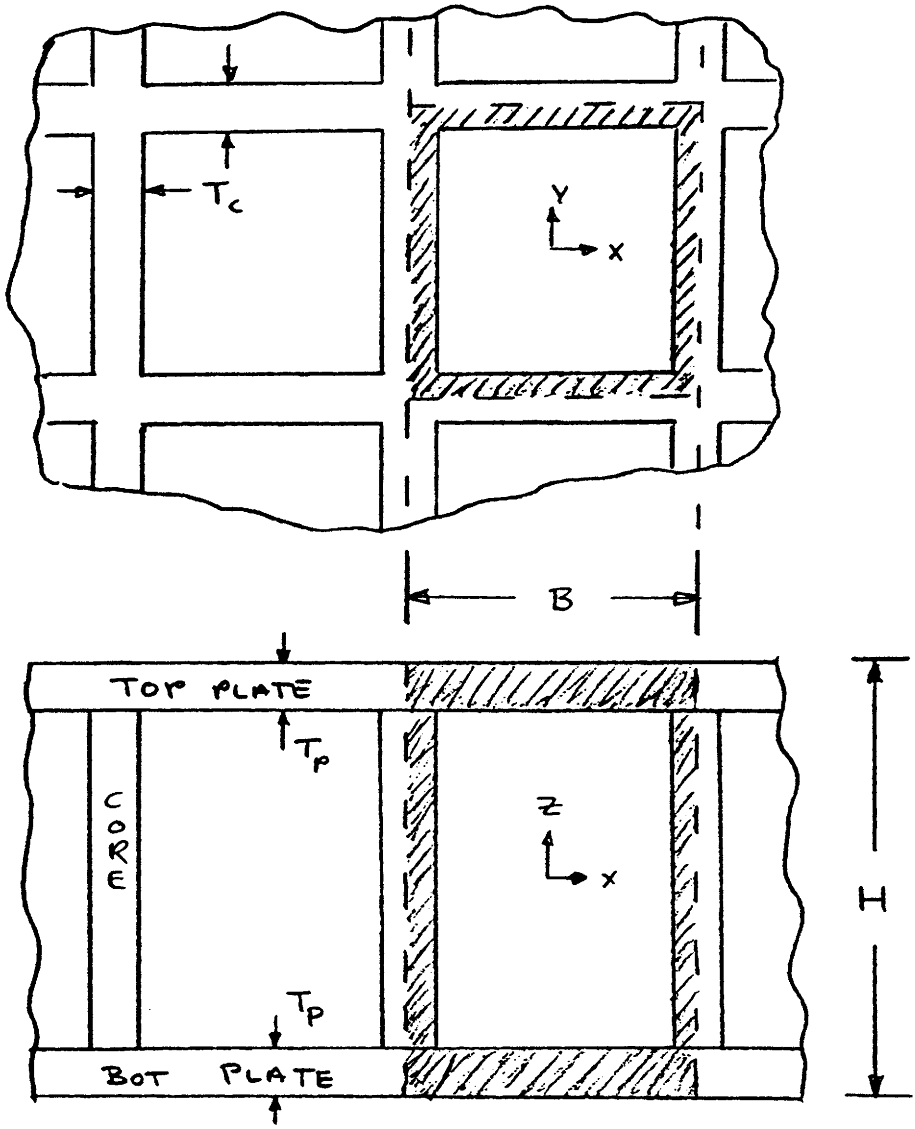

FIGURE 8.23 Lightweight mirror with square cells.

$$Rs = [Ht_c]/[Bt_m]$$

If first-order stresses are to be recovered from these effective plates, the stress recovery points must define the extreme fibers of the mirror:

$$c_1 = H/2 \quad c_2 = -H/2$$

The mass density of the effective plate must be modified, also. The mass is normally calculated from the membrane thickness (t_m) and the mass density (ρ). In this approximation, the membrane thickness is calculated from the cross-section of a cut, which represents core struts in y direction. To account for the core struts in the x direction the effective mass density must be increased.

$$\rho_c = [2t_p + 2\alpha H_c]\rho/t_m$$

To use this approach, the finite element program must allow separate inputs for membrane, bending, and shear properties. A solid, homogeneous plate with a single thickness used for both membrane and bending cannot accurately model a lightweight mirror using this technique.

The advantage of this modeling scheme is the obvious speed and simplicity. The model is easily generated without regard for the internal core geometry. Only the external features such as diameter and mount location need to be considered. The disadvantage of this technique is a slight loss of accuracy, especially in local shear effects around mounts. A plate model cannot predict through the thickness effects. If 3D effects are significant, then a 3D model should be used. As the ratio of diameter/height grows, the optic acts more plate-like and the accuracy of the plate model improves.

3D Equivalent Stiffness Solid Model (Lightweight Optic)

For some optics, a plate model is not accurate enough. Another simplified modeling scheme is available which includes 3D effects. In this scheme, the faceplates are modeled as solid plates of thickness t_p located in their true position. The core is then represented as solid elements of reduced properties (Figure 8.24). Effective isotropic properties are

$$E_e = \alpha E$$

$$G_e = \alpha G$$

$$\nu_e = \nu$$

$$\rho_e = 2\alpha\rho$$

A single layer of solid elements is typically too stiff, so at least two layers through the thickness would improve accuracy.

The isotropic effective properties underestimate the axial stiffness. The use of orthotropic materials could improve that behavior. The orthotropic properties are:

$$E_{xe} = E_{ye} = \alpha E$$

$$E_{ze} = 2\alpha E$$

$$G_{xy} = 0$$

$$G_{xz} = G_{yz} = \alpha G$$

$$\nu_{xy} = 0$$

$$\nu_{zx} = \nu_{zy} = \nu$$

If the program accepts material constants, then the above terms can be used directly. In NASTRAN, the material matrix [C] must be input on MAT9 entries.

$$\{\sigma\} = [C]\{\varepsilon\}$$

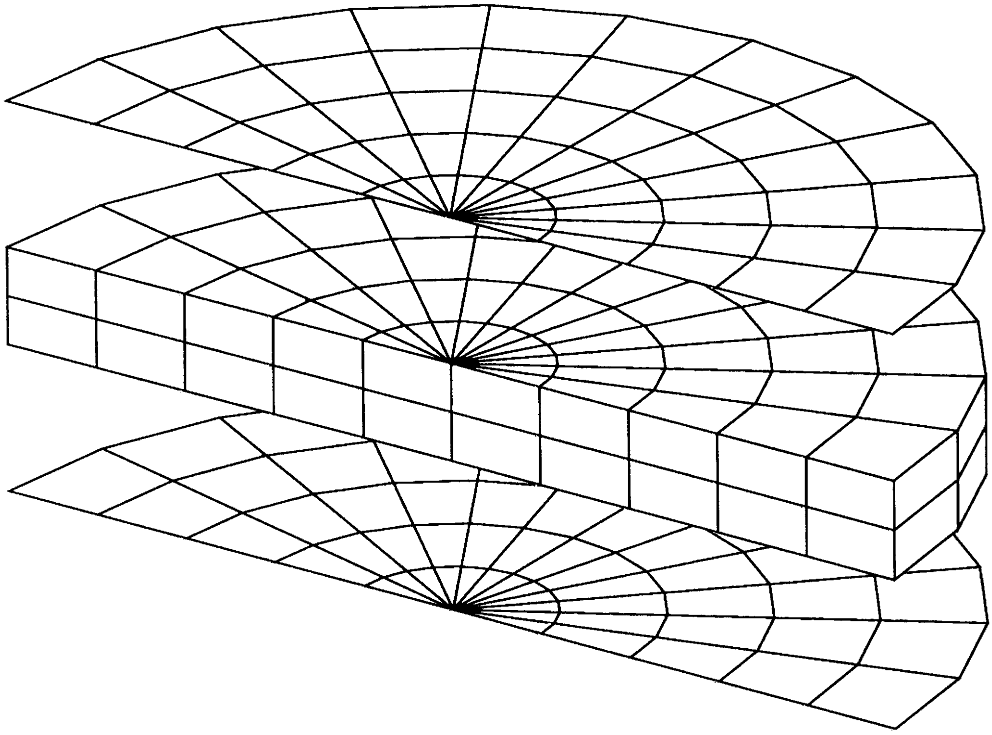

FIGURE 8.24 3D equivalent stiffness model of a lightweight mirror with the core modeled as reduced stiffness solids.

Since C is a symmetric matrix, it is only necessary to define the nonzero terms in the lower triangular portion:

$$K = \alpha E/(1 - \nu^2),\ \ C_{11} = (1 - 0.5\nu^2)K,$$

$$C_{21} = 0.5\nu^2 K,\ \ C_{22} = (1 - 0.5\nu^2)K,$$

$$C_{31} = \nu K,\ \ C_{32} = \nu K,\ \ C_{31} = 2K,$$

$$C_{44} = 0,\ \ C_{55} = \alpha G,\ \ C_{66} = \alpha G$$

This modeling scheme preserves the efficiency advantage of not modeling the detailed core structure. Again the penalty is a slight loss in accuracy, especially in shear effects around point loads and mounts.

In either the 2D or 3D equivalent models, design trades on core geometry, faceplate thickness, and even mirror height are easy to perform. Once a particular design has been chosen from the trade study, then a full 3D model (next section) should be created to verify the predictions.

3D Plate Model (Lightweight Optic)

To obtain high accuracy in the prediction of distortion of lightweight optics, a 3D plate model is required. In this model (Figure 8.25), the faceplates and each individual core strut are modeled as solid, homogeneous plate elements. Since the detailed core geometry is modeled, this approach is quite time consuming. Preprocessing programs can speed up the model generation depending on

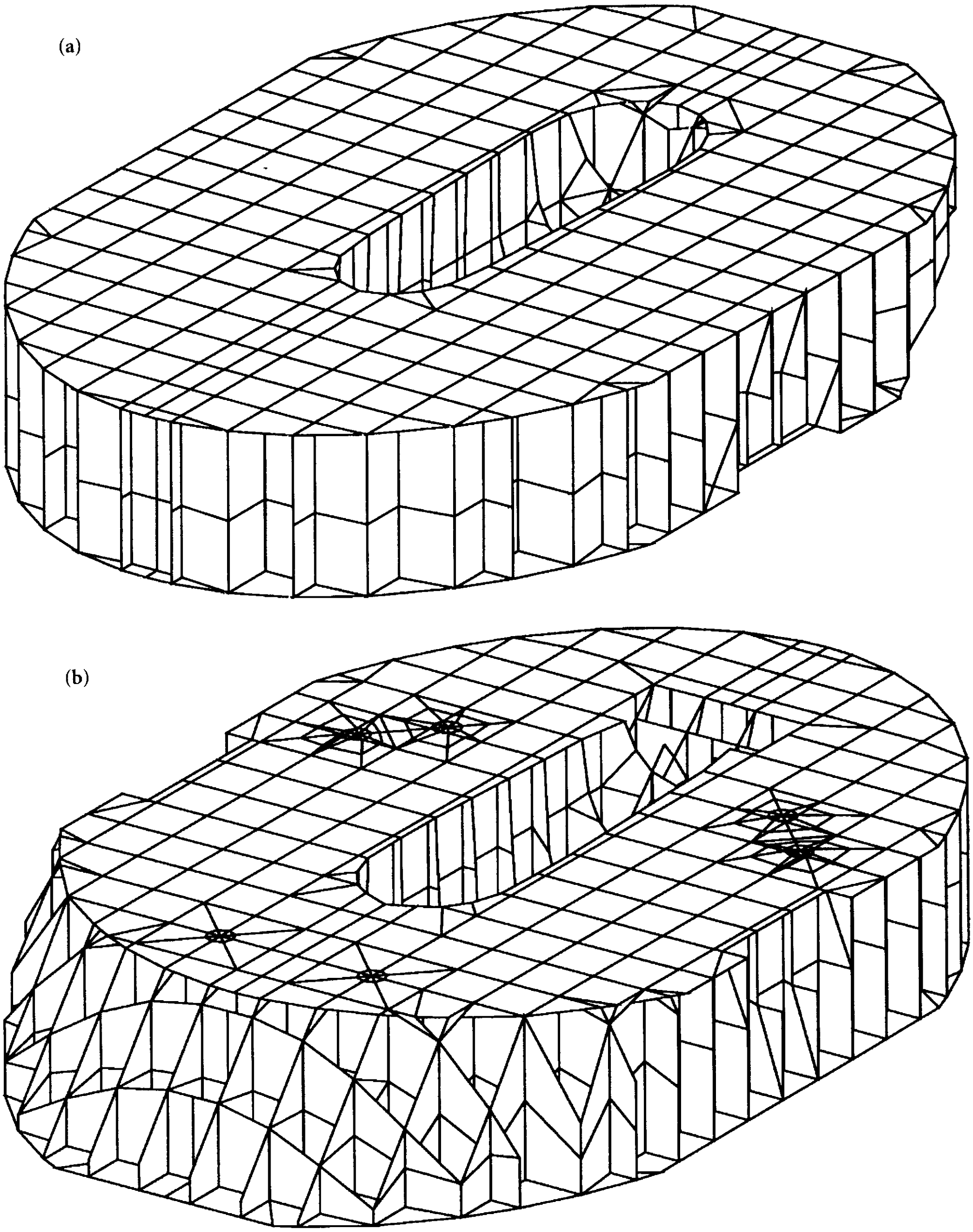

FIGURE 8.25 (a) 3D shell model of a lightweight scan mirror — top view; (b) 3D shell model of a lightweight scan mirror — bottom view.

particular capabilities. Extra detail is required around mounts to accurately model mount geometry, adding to the model generation time.

To accurately predict mirror stiffness, the neutral axis of the plate elements must coincide with the midplane of the faceplates. Thus, either the faceplate nodes lie in the midplane of the faceplate, or offsets are required for the elements. A single layer of plates to represent the core is not accurate enough for most applications. Two or more layers should be used in the core. Meshing on curved surfaces is sometimes difficult and prone to inaccuracies. A lightweight mirror could be modeled in a flat geometry quite efficiently, then curvature could be added to the final model by moving grids in the axial direction, either in a preprocessor or a separate Fortran code. Each node's flat axial position (z_o) must be modified to a curved position (z_n) by using the radius of curvature (R_c) and the angular position (θ) to the node from the center of curvature:

$$z_n = z_o + (1 - \cos\theta)R_c$$

In some analyses, a high degree of accuracy is required on the net mass of the optic. Depending on modeling practices, a 3D plate model may over- or underpredict the true mirror mass. If nodes are located at the faceplate midplane, then the core elements are too tall, overpredicting mass. In many core structures, the joints have extra material (posts or fillets) due to fabrication techniques, so a model will underpredict the weight. The user must adjust the mass density of the core or add nonstructural mass (positive or negative) to the core plates to adjust the mass.

The lightweight mirror depicted in Figure 8.25 had such complex geometry that only a full 3D plate model could predict accurate results. The analytical prediction shows excellent correlation to the experimental results for a 1-g load on edge with a 3-point back mount (Figure 8.26).

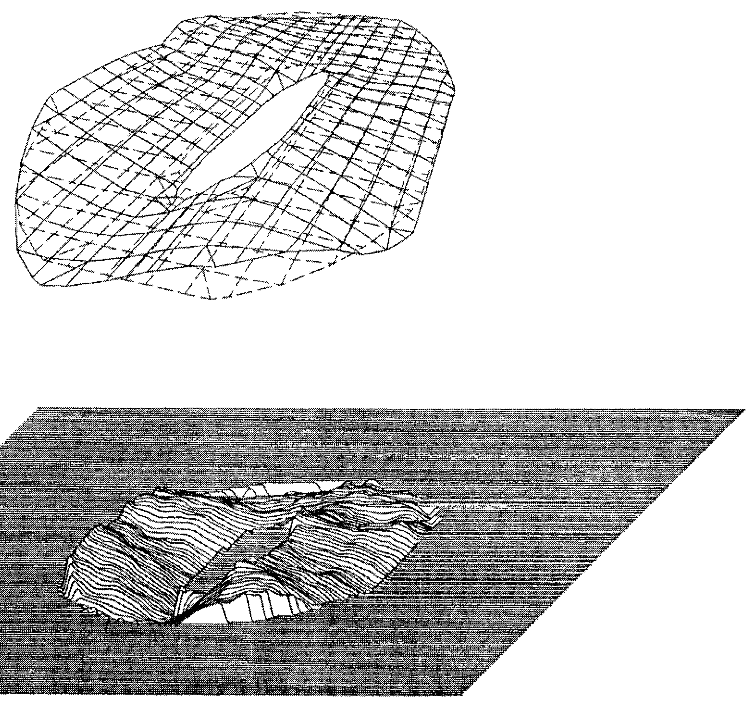

FIGURE 8.26 Comparison of analysis and test surface figures for the mounted scan on edge.

Figure 8.27 shows a more uniform lightweight mirror with extra detail at the core-to-faceplate intersections. In this analysis, the quilting effect due to adhesive joint (dark thick lines) shrinkage was predicted (Figure 8.28). Again, only a full 3D plate model could predict this type of 3D behavior; the equivalent models could not.

Comparison of Models (Lightweight Optic)

A lightweight mirror sitting on a 4-point mount was modeled using 1/4 symmetry to compare the modeling techniques. A full 3D model is shown in Figure 8.29(a) as all plate elements. The 3D equivalent stiffness model is shown in Figure 8.29(b) using a polar mesh for convenience. The

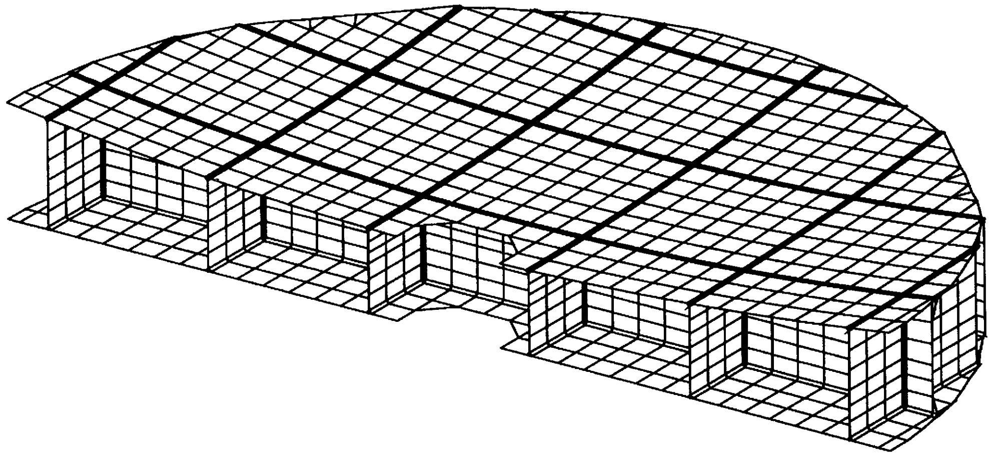

FIGURE 8.27 Lightweight mirror with adhesive bonds between core and faceplates.

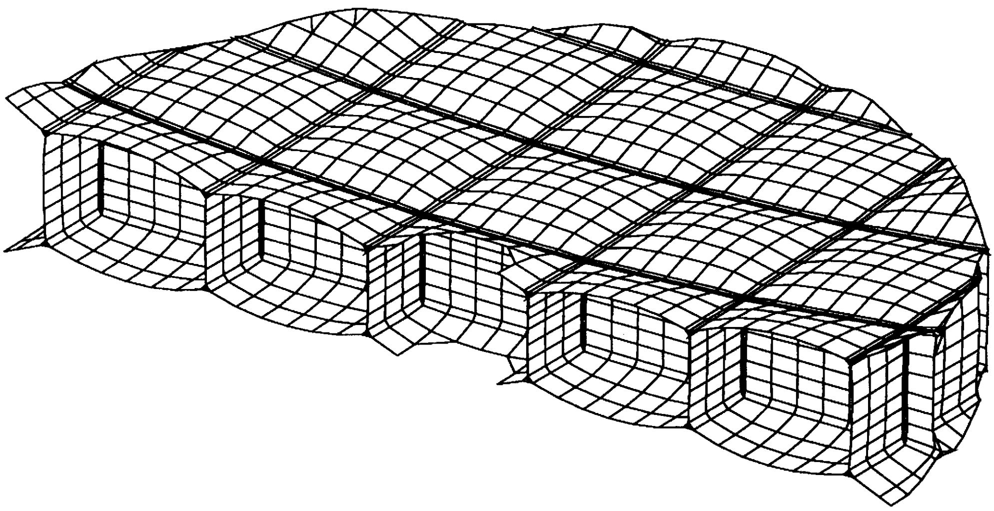

FIGURE 8.28 Deformed shape (scaled) for adhesive joint expansion.

faceplates are modeled as plates with the core modeled as equivalent solids. The 2D equivalent stiffness plate is shown in Figure 8.29(c) as a single layer of plate elements, again with a polar mesh. Deformed shapes are shown in Figure 8.30 where the displacement contours are very similar, except at the mount points where shear has its largest effect. If the rigid body motion is removed (Figure 8.31[a]), the contours are very similar, since the local shear displacement has been subtracted. After the power is removed (Figure 8.31[b]), the contours are nearly identical. A surface fit of the deformed surface shows that they perform optically the same to within 3%. The natural frequencies are very similar, also. For early trade studies, this level of accuracy is usually sufficient for final designs with accurate stresses, a 3D model is usually required.

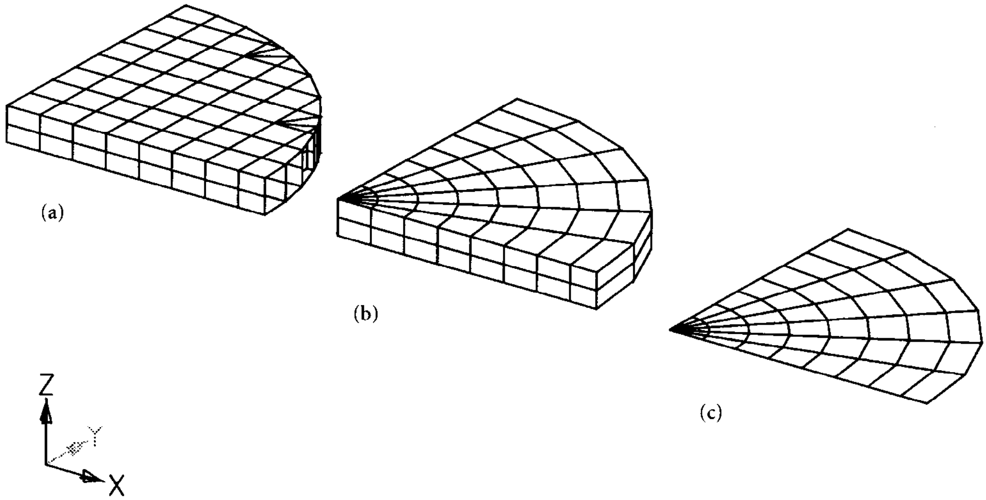

FIGURE 8.29 Three models of a lightweight mirror. (a) 3D shell model with full core detail; (b) 3D equivalent stiffness model with core as reduced solids, and (c) 2D equivalent stiffness model with effective stiffened plates.

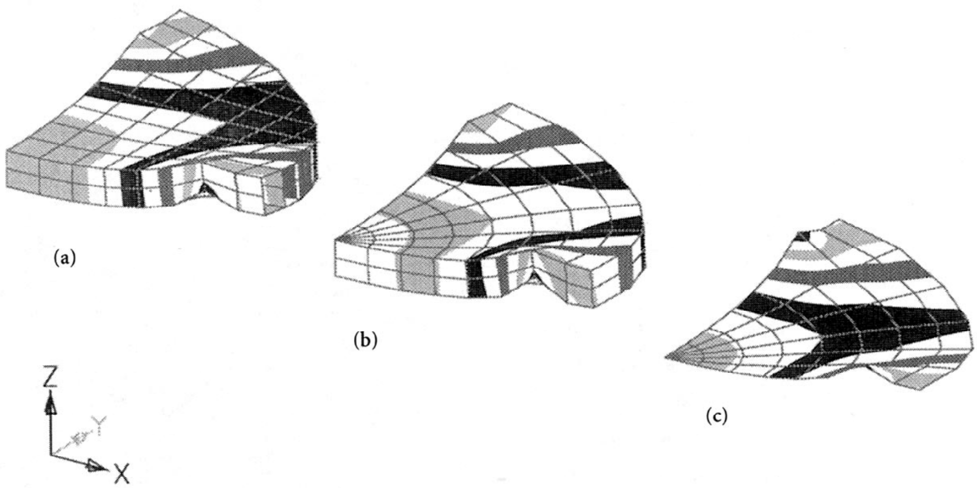

FIGURE 8.30 Comparison of deformed shapes with z displacement contours.

8.5 Stress Models for Optics

Even though displacements govern most optical designs, stresses must be checked. Most optics consist of brittle materials, such as glass or ceramic, which have different failure modes than ductile materials, such as steel or aluminum. To get the accurate stress values from a finite element model, high model resolution is required in the areas of rapid stress gradients. Interpretation of stress output can be sometimes confusing in graphical postprocessing programs to casual users.

Ductile Failure (Most Metals)

A metal mirror will suffer stress failure in a ductile manner in most applications. There are multiple levels of stress failure depending upon the design requirement.

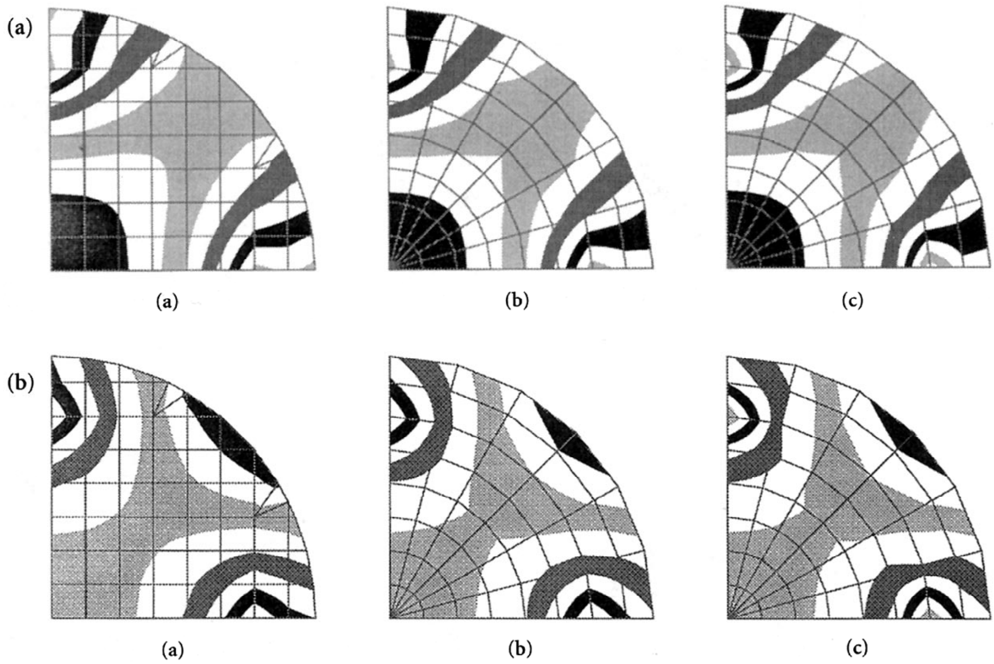

FIGURE 8.31 (a) Displacement contours after best-fit plane removed; and (b) displacement contours after power removed.

(a)
- Fatigue: if the part fails due to repeated cycles of stress
  $\sigma > S_e$ (where S_e is the endurance stress limit)
- Microyield: if the part suffers 0.000001 (1 ppm) permanent strain
  $\sigma > S_m$ (where S_m is the microyield stress limit)
- Yield: if the part suffers 0.002 (0.2%) permanent strain
  $\sigma > S_y$ (where S_y is the yield stress limit)
- Ultimate: if the part features
  $\sigma > S_u$ (where S_u is the ultimate stress limit)

These material properties are obtained from uniaxial tension samples. In a typical structure, the stress state is multiaxial. To compare the multiaxial stress top to a uniaxial property the equivalent stress most commonly used is the Von Mises stress (σ_{vm}):

$$\sigma_{vm}^2 = \left[\left(\sigma_1 - \sigma_2\right)^2 + \left(\sigma_2 - \sigma_3\right)^2 + \left(\sigma_3 - \sigma_1\right)^2\right] \Big/ 2$$

where the principal stresses ($\sigma_1,\sigma_2,\sigma_3$) may be obtained from the directional stresses ($\sigma_x,\sigma_y,\sigma_z,\tau_{xy},\tau_{yz},\tau_{zx}$) by use of a Mohr's circle diagram. A Mohr's circle diagram is shown in Figure 8.32 for a two-dimensional state of stress. For this case the center (C) and radius (R) of Mohr's circle are given by:

$$C = \left(\sigma_x + \sigma_y\right) \Big/ 2$$

$$R^2 = \left[\left(\sigma_x - \sigma_y\right) \Big/ 2\right]^2 \pm \tau_{xy}^2$$

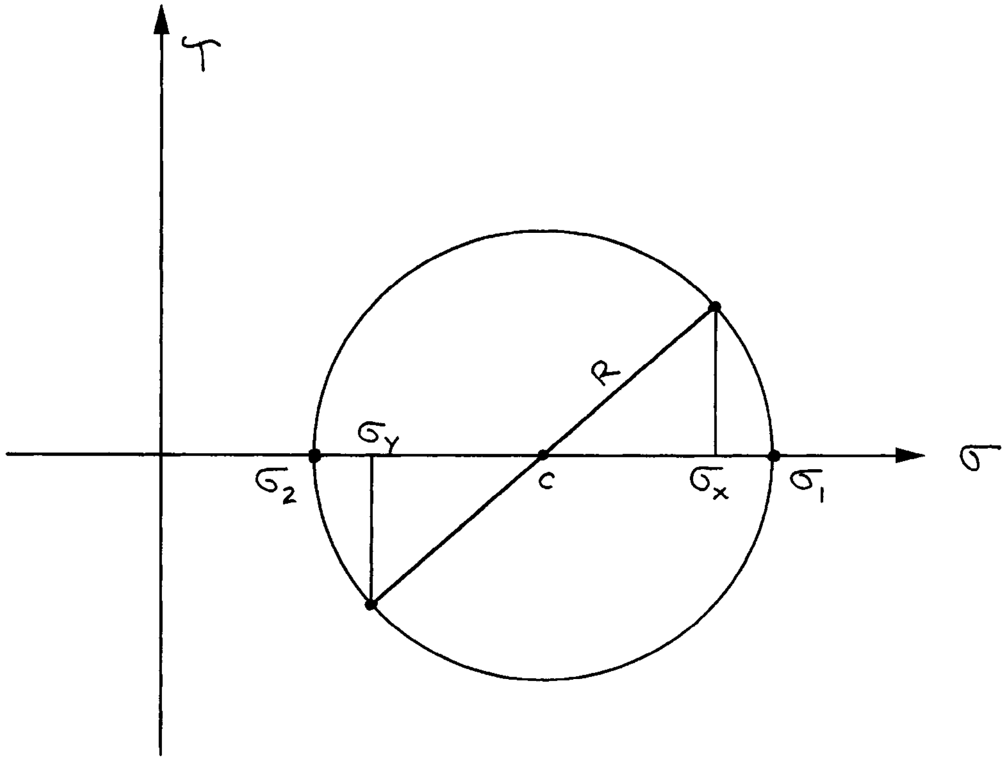

FIGURE 8.32 Mohr's circle for a 2D stress state.

The maximum principal stress (σ_1) is the most positive value, and the minimum principal stress (σ_2) is the most negative value.

$$\sigma_1 = C + R$$

$$\sigma_2 = C - R$$

For example, failure due to yield occurs when:

$$\sigma_{vm} = S_y$$

Thus, when postprocessing a metal part, the user should be plotting Von Mises stress. Note that the Von Mises stress is always positive, even when the directional stresses are negative. Thus, plots of Von Mises cannot distinguish between tension and compression. Although the Von Mises stress is often the largest stress, it is possible for a directional stress or principal stress to have up to a 15% larger magnitude.

In some FE codes, Von Mises stress may not be an option for 3D solid elements. The equivalent stress provided is called octahedral shear stress (τ_{oct}) which can be related to σ_{vm} as:

$$\tau_{oct} = \sigma_{vm}\left[\sqrt{2}/3\right] = 0.577\ \sigma_{vm}$$

When comparing τ_{oct} to failure, use the shear failure stress, which is

$$S_{sy} = 0.577S_y$$

Brittle Failure (Most Glass and Ceramics)

Brittle failure is not as well understood as the ductile failure. Juvenile[9] suggests the use of the modified Mohr theory for the failure of brittle materials. The ultimate stress in compression is usually several times larger than the ultimate stress in tension. A simplifying assumption is that only the tensile failure need be considered. For a multiaxial stress state, the largest tensile stress is the maximum principal stress (σ_1) found from Mohr's circle calculations. Since brittle materials exhibit no yield, failure occurs from fracture when:

$$\sigma_1 = S_u$$

In finite element postprocessing of brittle optics, the analyst should be plotting the contours of maximum principal stress, not Von Mises stress. In many applications the applied load may have a positive or negative value. If the load is reversed in direction, the Mohr's circle is reflected about the origin. Thus, a plot of σ_1 would check failure for a positive force; a plot of σ_2 would check failure for a negative force of the same magnitude.

Fracture Mechanics Approach

If a crack with sharp corners exists in a part, then linear elasticity predicts the stress to be infinite at the crack tip. Any linear finite element code will verify that the stress is infinite. In a series of analyses with successively smaller elements, the program will predict successively higher stresses, while chasing infinity. The results will not converge to a reasonable solution. The fracture mechanics approach can be used to predict when an existing crack will grow, thus causing failure.

According to the theory of fracture mechanics, an initial crack will propagate if the stress intensity factor (K_I) is greater than the material's fracture toughness (K_{IC}). The value of fracture toughness, which is temperature dependent, has units of pressure times square root of length. The stress intensity factor K_I (as opposed to the stress concentration factor K_I) is a function of the initial crack size (a) and the surrounding stress field (σ):

$$K_I = C\sigma\sqrt{a}$$

For a small crack in a large, thin plate, $C = \sqrt{\pi} = 1.8$. If this crack size is not small relative to the plate dimensions, or occurs at the edge of the plate, C increases. For thick plates or solids, the relationship is not as simple.

If cracks are visible in an optic, then the actual geometry of the crack and the part, along with the state of gross stress predicted by the finite element model, should be used to predict K_I. If cracks are not visible, then cracks smaller than the visible threshold should be assumed. For a polished surface with no visible cracks, existing crack size could be as large as 0.001 to 0.005 in. depending on the inspection technique. In this case, a reasonable prediction of K_I is

$$K_I = (1.9)\sigma\sqrt{a}$$

In the above model, the crack detail is not molded. The relatively coarse mesh is used only to predict the "gross" stress (σ).

If a more accurate analysis is required, the stress intensity can be predicted directly by a more detailed model which "zooms" in on the crack. This local model may be part of a larger system model, or it may be a stand-along model which gets its BC from a system level model. There are several ways of predicting K_I from a detailed model, but only two most common will be mentioned here. If the finite element program has a crack tip element, then this element is embedded in a model of standard elements of the same type (i.e., 2D plane stress, 2D plane strain, or 3D solid). The alternative method, available in all FE codes, is to model the crack area with the standard elements. The model is run once with the initial crack area (A_1 = a t) and run again with a slightly larger crack [$A_2 = (a + \Delta a)t$]. The difference in strain energy (U) is used to predict the strain energy release rate (G) and the stress intensity factor.

$$G = \Delta U/\Delta A = (U_2 - U_1)/(A_2 - A_1) = (U_2 - U_1)/(\Delta at)$$

$$K_I = \sqrt{EG}$$

The strain energy release rate is very general and typically more accurate than the crack tip element.

Model Detail Around Stress Conditions

Stress levels change very rapidly around stress concentration effects. When trying to predict stress in a high gradient area like a fillet, the model detail must be fine enough to describe the fillet geometry accurately. More elements are required when using first-order elements (corner nodes only) than when using higher order elements which have one or more nodes along an edge. These higher order isoparametric elements can be used to more accurately describe the geometry as well as to more accurately predict a rapidly varying stress. The analyst must exercise care to verify the accuracy of the stress predictions. Some recommended steps are listed below.

1. Prototype model: Find a theoretical solution to a problem which is similar to the actual problem. Run studies of element type and size to find the required model detail to get within a desired accuracy. Use the prototype results to model the actual problem.
2. Convergence study: When analyzing the actual problem, run an additional analysis with more detail until the change in stress from run to run is within a desired bound.

The conventional approach of adding model resolution by making more elements of smaller size is called “h” convergence. If the size and number of elements are held constant, but their order is increased, then the method is called “p” convergence. Some FE codes offer “p” elements which automatically increase the order and cycle through the solution to reach a desired accuracy of stress. This automated technique offers a higher quality answer for a moderate increase of computer resources.

A more economical approach to the problem is to combine classical stress concentration factors (K_t) with the FE results. In this approach, small details such as fillets are ignored in the model detail. The FE model is used to predict nominal stresses (σ_n) which are then multiplied by a classical K_t to estimate the peak stress (σ_p).

$$\sigma_p = K_t \sigma_n$$

Discrete mount points on lenses and mirrors represent zones of high stress gradients. Extra detail is required in the mount area to accurately describe the stress state. The model shown in Figure 8.22 has sufficient detail for accurate deflection analysis or dynamic analysis. However, to obtain accurate stress results on the same lightweight mirror, the model shown in Figure 8.33 is required. The mirror is flipped over so that the detail around the mount is visible.

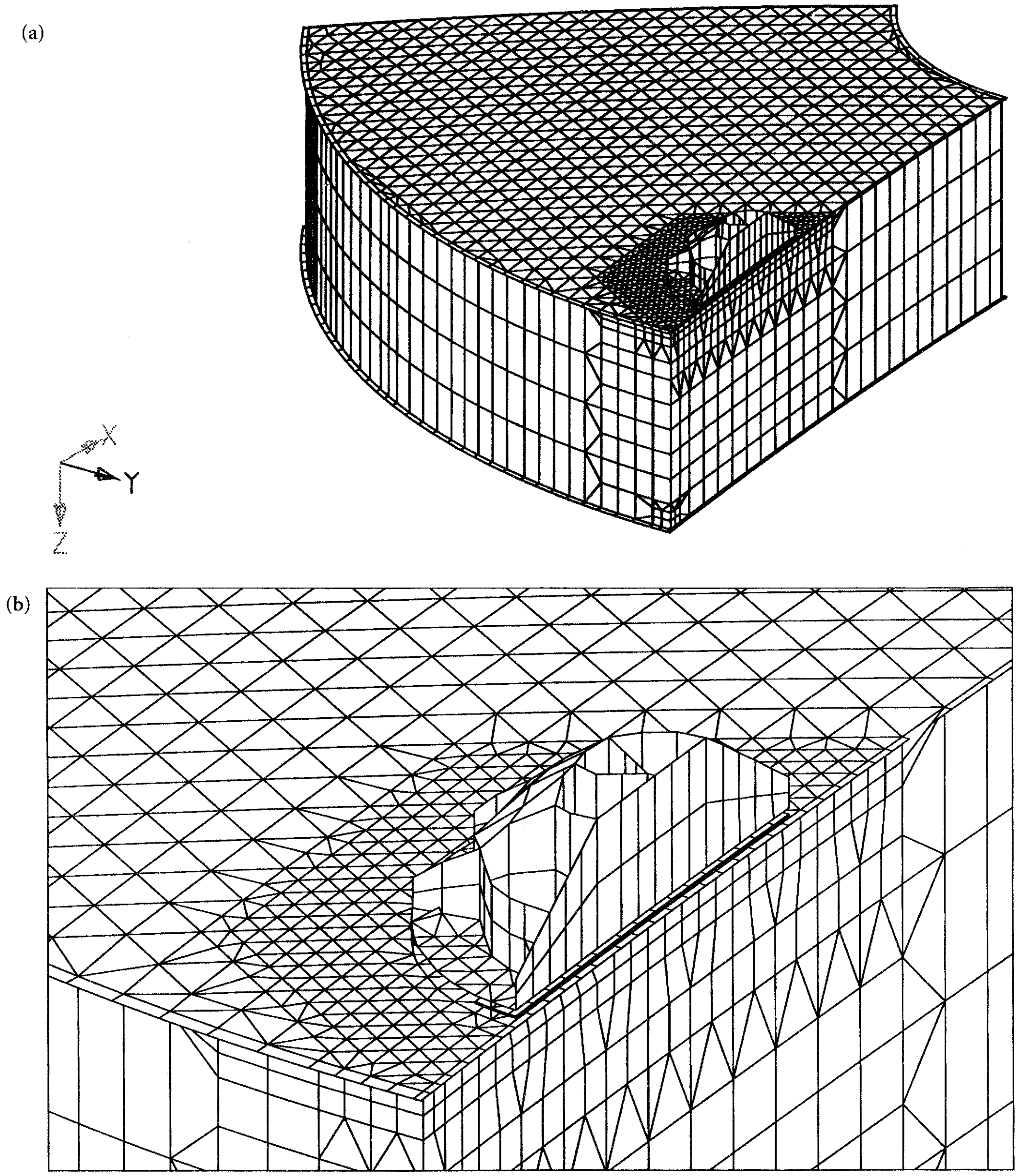

FIGURE 8.33 (a) Stress model of a lightweight mirror on 3-point support — 1/6 segment; and (b) zoom in on detail around mount.

Stress Plots

Most graphical postprocessing programs are not written by the same people who write the FE analysis programs, even if they work for the same company. For that reason, some care must be exercised when interpreting stress plots. For the lightweight mirror segment in Figure 8.34(a), various stress plotting techniques show a wide range of peak stress results all from postprocessing the same FE results file with the same postprocessing program. Thus, the stress plotting technique can add significant error beyond the FE approximation error. The vertical end loads on this model are chosen to give a peak top plate stress of 100 psi at the symmetry plane over the knife edge mount. In Figure 8.34(b), node point values are obtained from averaging centroid stresses of all elements connected to a node. This technique does not consider element orientation or stress coordinate system when averaging the stress. This is the easiest to program, but provides the most inaccurate stress values. In this example, the small core stresses are averaged with the high plate stress to produce a peak stress of 70 psi (30% error) at the wrong location. The results in Figure 8.34(c) are more accurate if the user selects only the top surface elements for averaging. Without the core averaged in, the peak plate stress is 85 psi (15% error). If the FE program provides corner stresses, the graphics program can use them to provide more accurate plots. The common technique of averaging corner stresses at a node improves the stress plot, only if the elements lie on a smooth surface with no breaks or joints and the stresses are measured in the same coordinate system. The best use of corner stresses is to contour each element independently, providing disjoint contours from element to element. The analyst can then see the magnitude and location of stress discontinuities.

The most accurate stress technique averages stress only over continuous surfaces. Whenever a break or joint is encountered the stress is not averaged. Also, element coordinate systems must be accounted for. At a common node, the directional stress from adjacent elements must be converted to a common coordinate system before averaging. The averaged directional stresses are then used in a Mohr's circle calculation to find new values of principal stress or Von Mises stress. An example of the proper technique is the MSC/NASTRAN GPSTRESS module which produced the stress results in Figure 8.34(d) of 100 psi (0% error).

Averaging principal stress or Von Mises stress from element to element is wrong and can result in large errors. For example, suppose two adjacent elements had a state of uniaxial stress where element 1 had $\sigma_x = +100$ and element 2 had $\sigma_x = -100$. In both elements the Von Mises stress is +100, and thus the average Von Mises is +100. If the directional stresses are averaged first, the average $\sigma_x = 0$ and thus the recalculated Von Mises stress is 0, also.

Smooth contour plots are the most appealing, but should only be used for data which is presented as nodal values. When plotting element centroid values the most accurate depiction is a solid, single fill color plot pr element. The averaging of centroid values to get the smooth contours always misses the peak response values that are the goal of the analysis.

An analyst should run experiments with his software to determine the accuracy of the FE results. Additional tests are required to determine how the graphics program alters or interprets those results for plotting. This author's rule of thumb is "The prettier the stress plot, the less accurate the result."

8.6 Adhesive Bond Analysis

Many optics are attached to their mounts with a thin, somewhat compliant, adhesive layer. Even a 3-point mount may not be perfectly kinematic with an adhesive bond. The bond area required to handle the service loads can be large enough to require an analysis of the bond layer effects on the performance of the optic. Bond layers cause distortion of optics due to:

- Bond layer relative growth due to a mismatch of CTE
- Bond layer shrinkage during curing
- Bond layer growth due to moisture absorption

Typical bond layers are

- Very thin (<0.1 in.)
- Very compliant with low modulus ($E < 1000$ psi)
- Rubber-like and nearly incompressible ($\nu > 0.49$)

Each of the above features causes some difficulty in a FE analysis. The sudden change in element size required to describe very thin layers can cause geometrical modeling problems. Due to computer limitations, the optic and mount cannot be modeled with such a fine resolution. Typically,

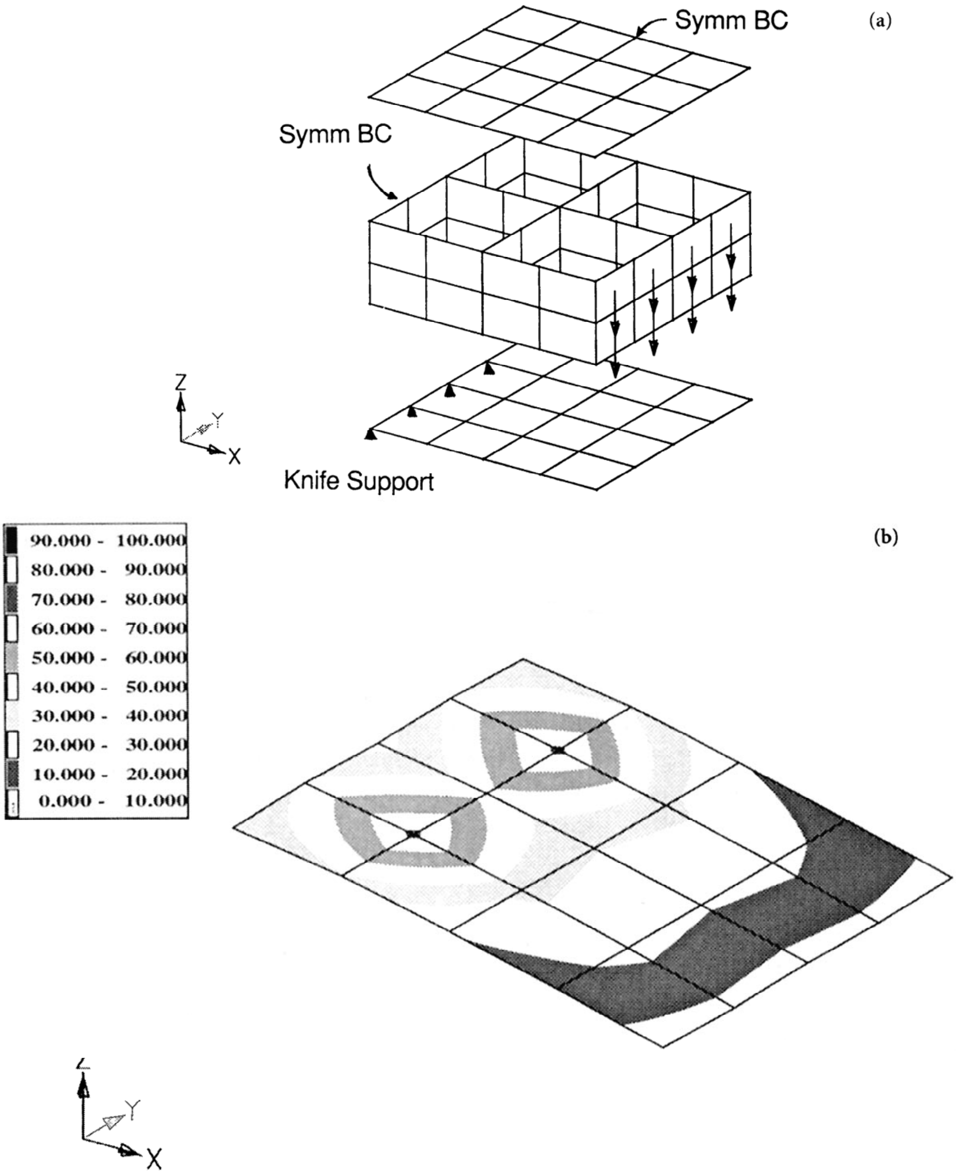

FIGURE 8.34 (a) Lightweight mirror segment with a bending load; (b) stress contours averaging centroid stress of all connected elements;

the thin adhesive elements will have high aspect ratios due to modeling constraints. The low modulus adhesive causes a large stiffness change relative to the much stiffer optic and mount material. Finally, the high Poisson ratio can cause numerical problems because typical element formulations have a term in the denominator of the stiffness matrix of $(1 - 2\nu)$. As ν approaches 0.5, this denominator term goes to zero, causing a divide by zero. Because of these problems, special modeling techniques have been developed for the bonded joints.

If the adhesive is a stiff material with a Young's modulus close to the optic's modulus, then the special techniques used in the following sections do *not* apply. More conventional modeling rules will apply for such cases.

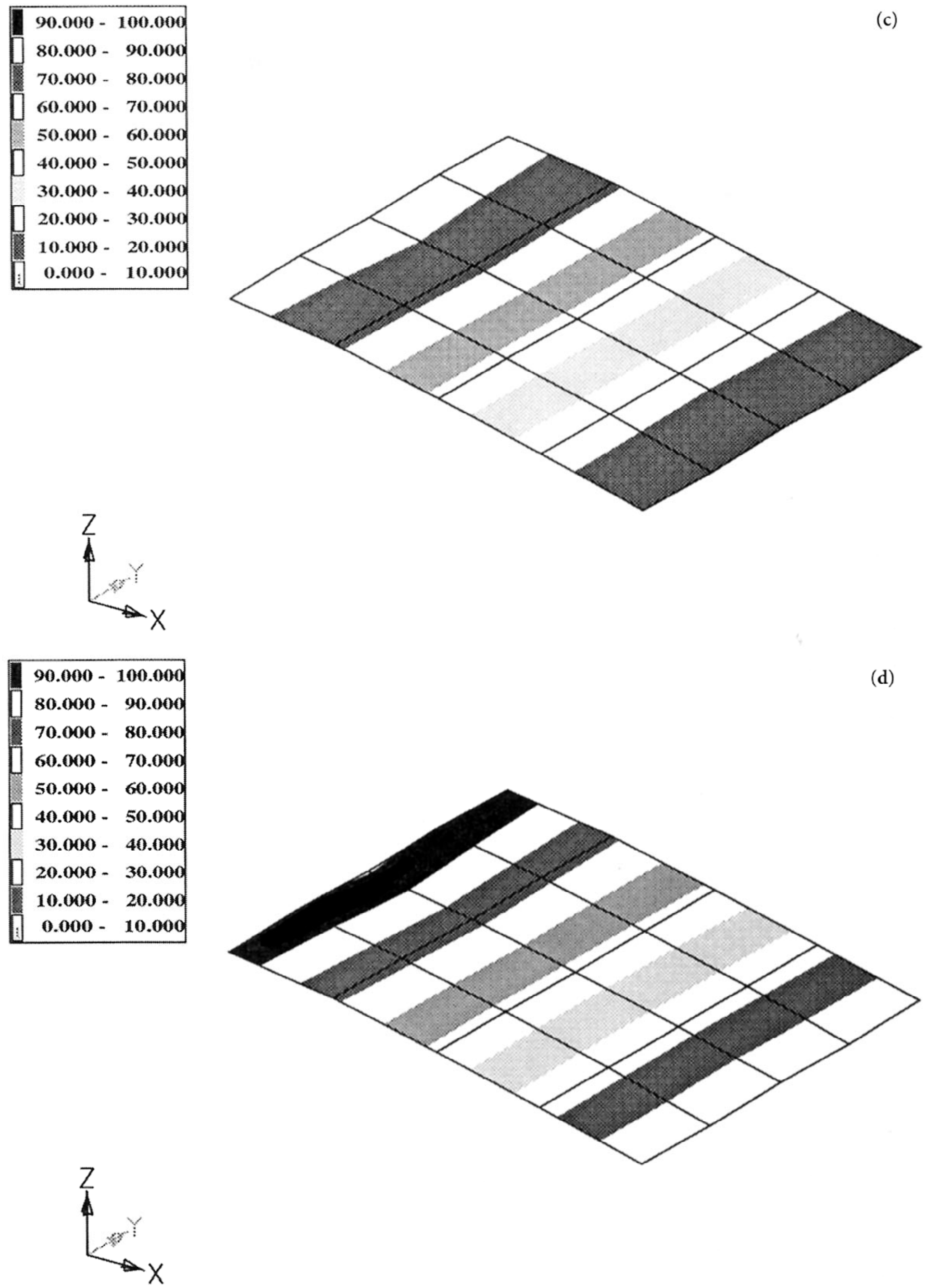

FIGURE 8.34 (c) stress contours averaging centroid stress of top plate elements only; and (d) stress contours averaging corner stress of top plate elements only.

Material Relationships

The following material definitions are used in this section:

E = Young's modulus (measured from a uniaxial tensile test)

ν = Poisson's ratio (the radial contraction during uniaxial tension)

G = shear modulus (measured from a constant volume test)
B = bulk modulus (measured from volume change in constant shape)
M = thin layer modulus (the limiting modulus for very thin layers)
α = coefficient of thermal expansion

For isotropic materials, the shear modulus can be obtained from:

$$G = E/[2(1 + \nu)] = gE$$

where

$$g = 1/[2(1 + \nu)]$$

The bulk modulus can also be obtained from the Young's modulus:

$$B = E/[3(1 - 2\nu)] = bE$$

where

$$b = 1/[3(1 - 2\nu)]$$

Using the full 3D elasticity stress–strain equations, the stress through the thickness is

$$\sigma_z = E/[(1 + \nu)(1 - 2\nu)][(1 - \nu)\varepsilon_z + \nu(\varepsilon_x + \varepsilon_y)] - E\alpha T/(1 - 2\nu)$$

For a very soft, thin layer of adhesive between two much stiffer structures, it can be assumed that the stiff structures prevent any in-plane strain in the adhesive.

$$\varepsilon_x = \varepsilon_y = 0$$

As shown in Figure 8.35, the above is true everywhere except within a thin edge zone width approximately two times the bond thickness. For most bond joints this is negligible compared to the surface area. Using the approximation and neglecting thermal effects, the stress–strain equations reduce to:

$$\sigma_z = (1 - \nu)E/[(1 + \nu)(1 - 2\nu)]\varepsilon_z = M\varepsilon_z = mE\varepsilon_z$$

where

$$m = (1 - \nu)/[(1 + \nu)(1 - 2\nu)]$$

and

$$M = mE$$

For free thermal growth under a uniform temperature change, using the same assumptions of no in-plane strain and $\sigma_z = 0$,

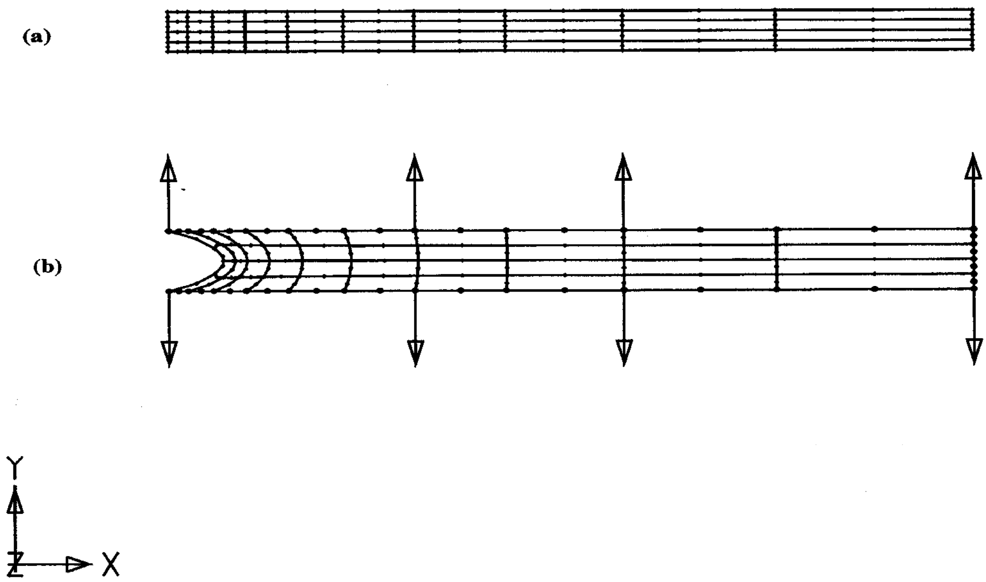

FIGURE 8.35 Adhesive bond distortions for high Poisson's ratio materials. (a) Axisymmetric element model; (b) deformed shape under tension.

$$\varepsilon_z = [(1 + \nu)/(1 - \nu)]\alpha\ \Delta T = a\alpha\ \Delta T$$

where

$$a = (1 + \nu)/(1 - \nu)$$

Curves of all four coefficients (g, b, m, a) vs. ν are given in Figure 8.36. The change in properties over the range of conventional materials ($0.15 < \nu < 0.3$) is relatively small. However, high Poisson materials ($0.45 < \nu < 0.5$) have very high values of m, causing the special thin layer effects. The steep slope of the m curve shows the sensitivity to minor changes in ν, also seen in the following values.

$$\nu = 0.49 \qquad m = 16.7$$

$$\nu = 0.499 \qquad m = 167$$

$$\nu = 0.4999 \qquad m = 1667$$

Each additional 9 adds another power of 10 to the thin layer modulus. The limiting value on coefficient of thermal expansion is 3, which states that all of the volumetric growth is normal to the bond plane as an apparent linear expansion.

The above development assumes that the bond layer is very thin. The obvious question is "How thin is thin?" A series of finite element numerical experiments were run to generate curves (Figures 8.37) of behavior vs. a nondimensional diameter/thickness (D/T) ratio. In these curves, the apparent modulus (E^*) for the particular thickness is compared to the true Young's modulus (E) and

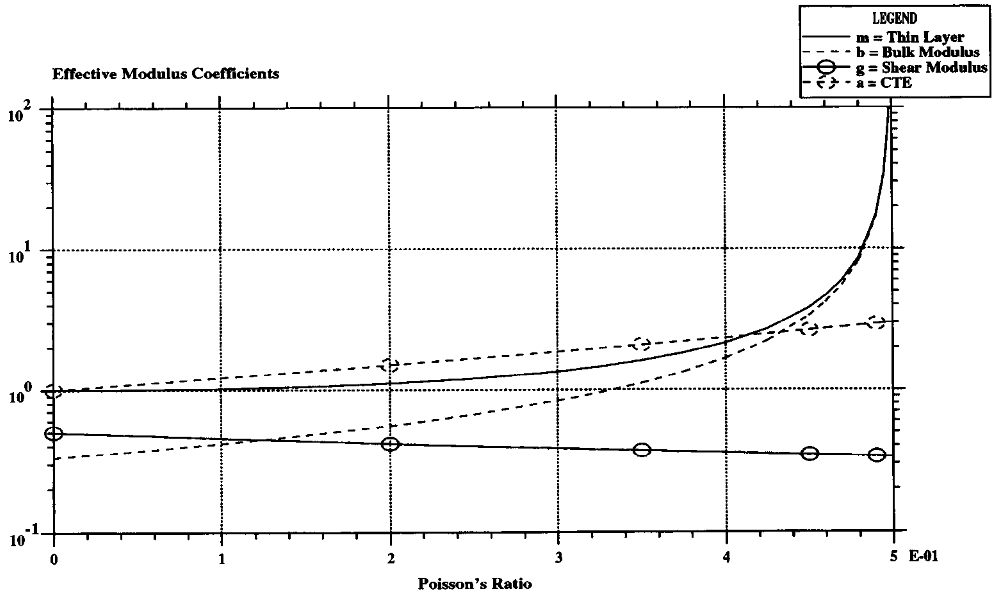

FIGURE 8.36 Effective joint properties as a function of Poisson's ratio.

the thin layer modulus (M), and the apparent coefficient of thermal expansion (α^*) is compared to the actual coefficient (α). For high Poisson materials ($\nu > 0.45$), E^* can be significantly different than E for D/T ratios as small as 10. However, the limiting value of M is not obtained until D/T gets above 100 to 1000. For noncircular sections, the diameter (D) in the curves can be approximated with an effective diameter (D_e)

$$D_e = 4(\text{Bond Area})/(\text{Bond Circumference})$$

For models of adhesive joints, E^* and α^* should be used for the material properties normal to the bond area. The shear behavior and other in-plane behavior are unchanged by the thin layer, so G and the other E values should be the original values. This results in an orthotropic material with a diagonal material matrix:

$$E_x = E_y = E, E_z = E^*$$

$$G_{xy} = G_{yz} = G_{zx} = G$$

$$\alpha_z = \alpha_y = \alpha, \alpha_z = \alpha^*$$

Adhesive Bond Joint Models

Several possibilities exist for models of bond joints depending on the purpose of the analysis.

Option 1: Detailed 3D Solid Model

When investigating the stress state in and around a bond joint, a detailed model with solid elements is required. To get proper edge effects, at least four layers of elements are required through the bond thickness with smaller elements near the free edge. With this level of detail, the elements can accurately predict the Poisson stiffening. Use the original material properties, not the apparent properties. Elements with bubble functions provide better results than standard isoparametrics for high Poisson values. If a Poisson ratio of 0.5 is desired, then special incompressible elements must

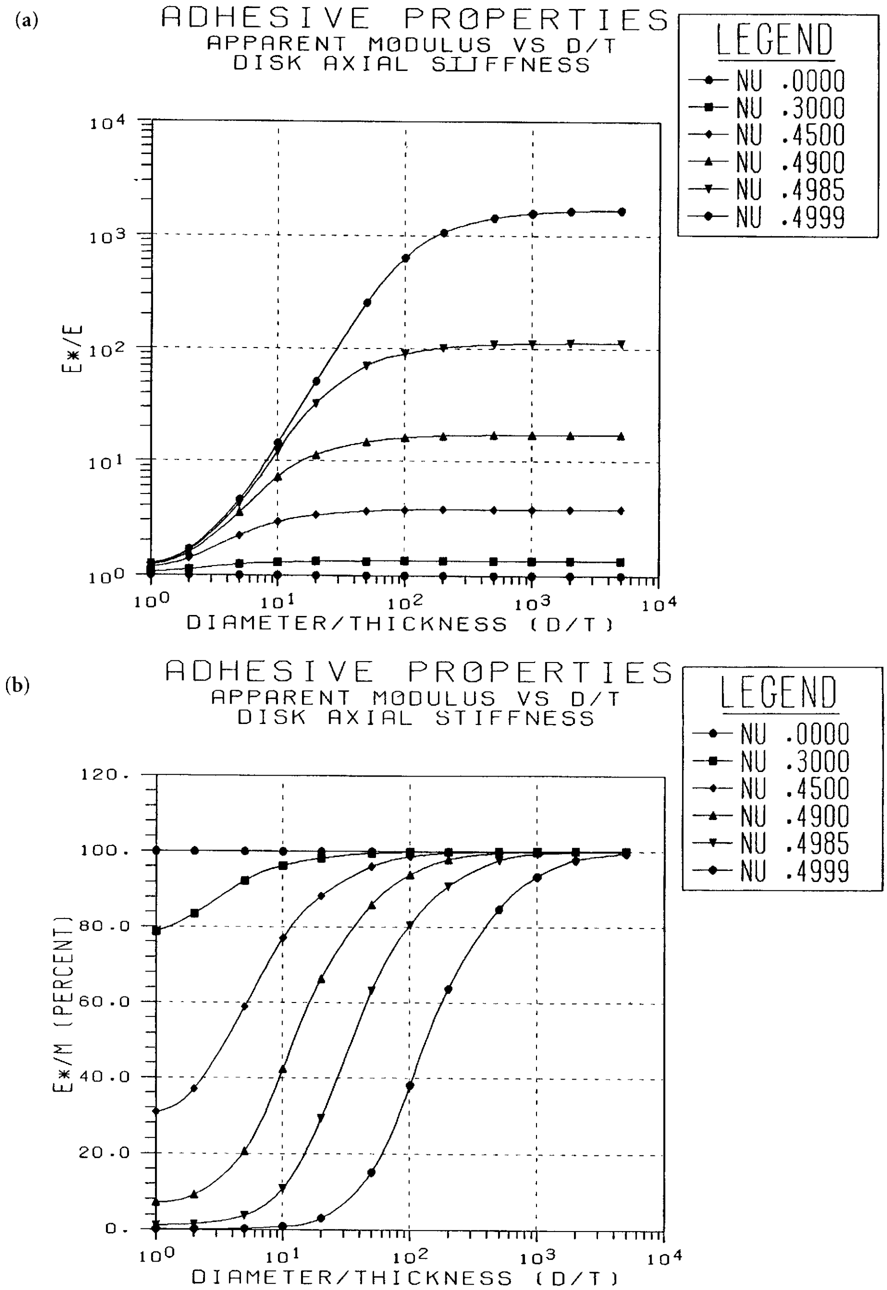

FIGURE 8.37 (a) Apparent modulus ratio (E^*/E) vs. diameter/thickness; (b) apparent modulus ratio (E^*/M) vs. diameter/thickness.

be used, since regular elements will be singular at that value. With this high local detail, this option is usually reserved for a "break-out" submodel or a multilevel superelement model.

Option 2: Coarse 3D Solid Model

In this model, only one layer of elements, usually with a high aspect ratio, are molded through the thickness. This type of model is used to get average or net effects over a bond, rather than a distribution of behavior. This model is too coarse to predict edge effects in the bond. A typical

(c)

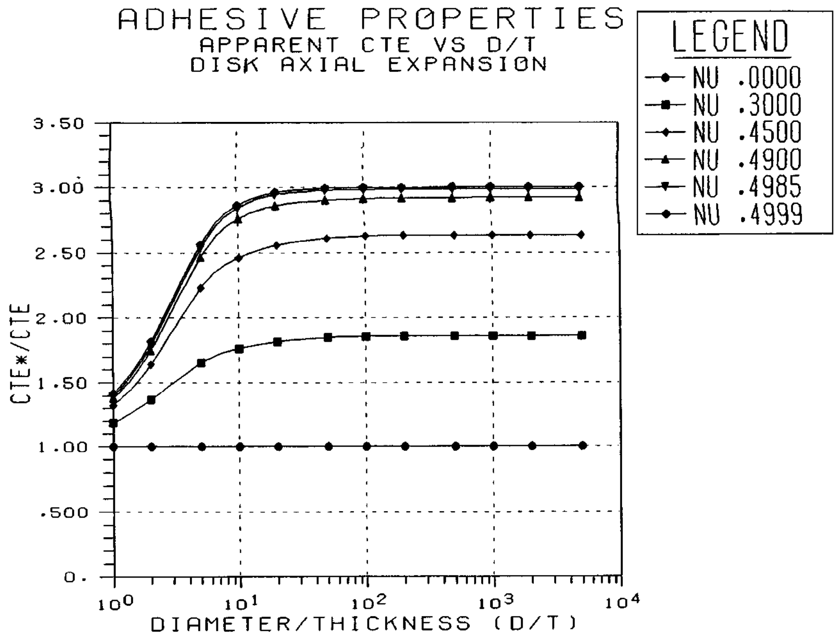

FIGURE 8.37 (c) apparent coefficient of thermal expansion ratio (CTE*/CTE) vs. diameter/thickness.

application is the prediction of bond shrinkage effects on optical surface distortions. Effective orthotropic bond properties are required to get accurate behavior.

In-plane modulus = E
Out-of-plane modulus = E^*
Shear modulus = G
In-plane coefficient = α
Out-of-plane coefficient = α^*

Option 3: Single Beam Normal to the Bond Plane

This approach would be used in a very coarse model trying to predict the first-order deflections or dynamic response. The bond surface geometry is used to predict the cross-sectional beam properties. Since bond layers are typically very thin compared to their surface area, the resulting beams are very short. For short beams, transverse shear effects can dominate the bending behavior. Figure 8.38 shows how the displacement due to bending and the displacement due to shear vary with beam length for a cantilever beam. The two contributions are equal when the length of the beam is 0.7 of the height of the beam. For bond layers, the beam length/height ratio is much less than 0.1, so the shear represents the full effect. The material properties of the beam should use E^* for axial effects, G for shear effects, and α^* for coefficient of thermal elasticity. Note that the isotropic relationship does not hold for the effective properties, so G is not equal to $E^*/2(1 + \nu)$. If the default shear factor is zero, a nonzero value must be input to the program. This model will predict the thermoelastic displacement of the optic normal to the bond, but will not predict the distortion of the optic due to in-plane bond effects.

Option 4: Equivalent Spring Model

The bond layer is represented as a set of springs which produce the equivalent stiffness of the bond layer. This scheme is used in a system level dynamics model which is trying to keep the number of nodes to a minimum, yet includes all of the soft elements in the system which contribute to the lower modes, especially whose which involve the image motion. This model is very similar to the

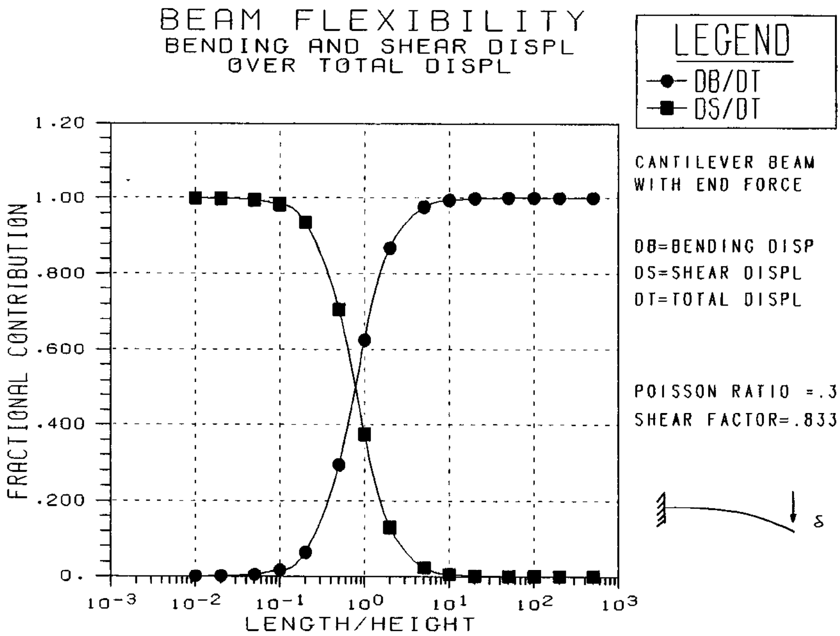

FIGURE 8.38 Relative bending and shear deflections for a cantilever beam with a square cross section.

beam model in Option 3 except that the springs offer no thermoelastic effects. The effective spring constants are

$$K_x = K_y = GA/t$$

$$K_z = E^* A/t$$

$$K_{\theta x} = K_{\theta y} = E \times I/t$$

$$K_{\theta z} = GJ/t$$

where A, I, and J are the cross-sectional properties of the bond, and t is the thickness of the bond. Note that whenever using the spring elements, the node points should be coincident in space and their displacement coordinate system must be aligned. Otherwise, hidden springs to the ground may be created which will cause errors in the results. Exceptions to this rule are possible, but should only be used by a trained analyst.

Bond Joint Failure Analysis

According to linear elasticity, the state of stress in the adhesive at the end of the joint bondline is infinite. Detailed stress models of the joint will chase infinity as the model is refined. To predict failure, fracture mechanics theory is required. As in Section 8.5, an initial crack is assumed. The stress intensity factor is calculated and compared to the fracture toughness of the adhesive. Buettner[2] compares the use of crack-tip elements to predict the stress intensity with conventional elements and strain energy release rate to predict K_I in a bond joint. Also in Buettner,[2] the multimesh extrapolation is shown to be a useful technique in predicting the error and improving the calculation of stress intensity. In Devries,[4] it is shown experimentally that high Poisson materials will fracture first at the edge for a small diameter-to-thickness ratio (D/t < 10), but will fracture at the center for high diameter-to-thickness ratio (D/t > 40). The reason fracture initiates at the center is that the stress intensity is higher at the center than the at the edge for the high Poisson material.

8.7 Mounts and Metering Structures

The analysis of optical systems requires careful modeling of the mounts and metering structures to get an accurate description of optical surface distortion and image motion. This section deals with modeling techniques important to precision optical structures, rather than more common stress-limited structures.

Determinate Structures

A structure is "statically determinate" if the force distribution can be determined solely by the equations of static equilibrium. An optical mount which is statically determinate is also called "kinematic", "exact" or "strain-free", because of the properties associated with these systems.

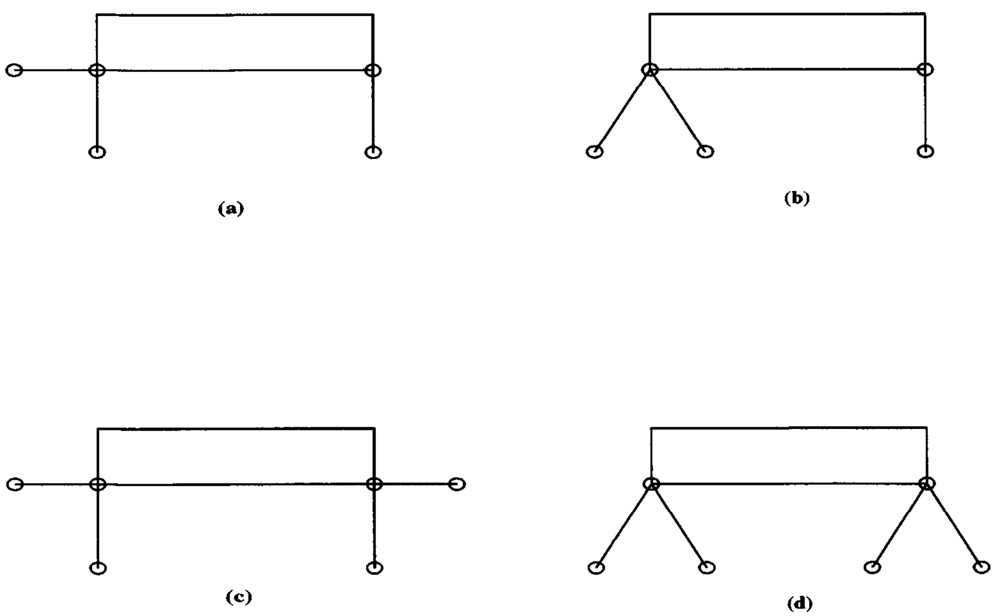

FIGURE 8.39 Mount configurations in a 2D plane using pinned jointed members: (a) and (b) are statistically determinate; (c) and (d) are statically indeterminate.

Figure 8.39(a) and (b) shows examples of two statically determinate, stable mounts in a 2D space. The elements have pinned ends and carry only axial force, with no moments or shear. In each case, the three unknown element forces can be determined from the three equations of equilibrium:

$$\Sigma F_x = 0$$

$$\Sigma F_y = 0$$

$$\Sigma M_z = 0$$

When additional, or "redundant", members are added to a determinate system (c and d), more unknowns are added; but no new equations are added, making the system "indeterminate". The system can be solved only by adding the equations of elasticity to the system. Not all 3-force systems are valid statically determinate, stable mounts. Figure 8.40 gives four examples of systems which are unstable mechanisms.

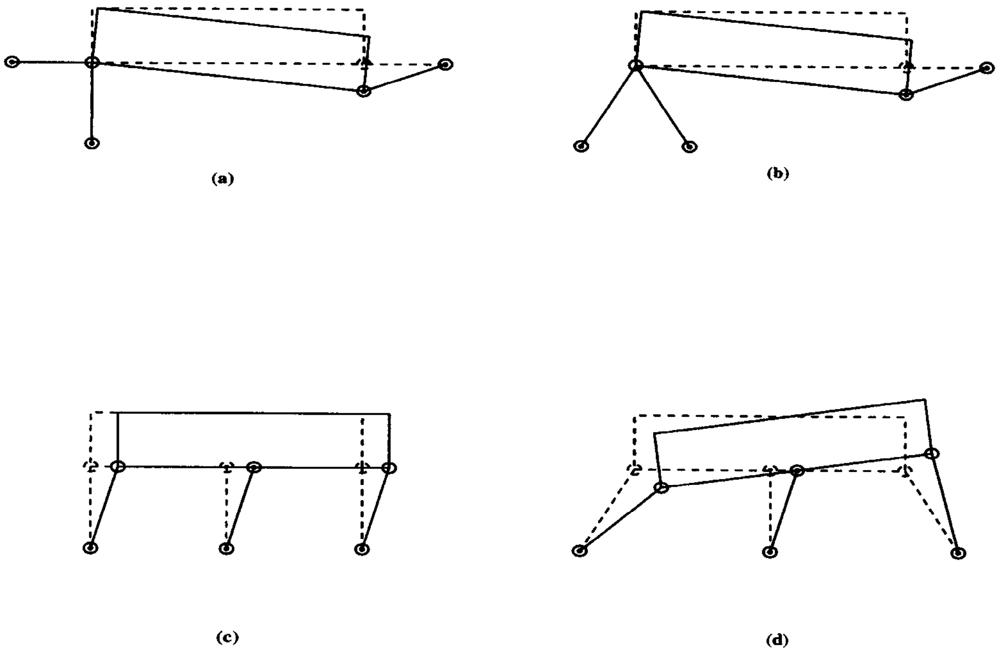

FIGURE 8.40 Unstable mount configurations in a 2D plane.

In 3D space, six rigid body motions are possible, requiring six constraints. There are also six equations of equilibrium available to determine those six element forces. Figure 8.41 shows three sets of constraints which are stable and statically determinate. Figure 8.41(a) is the common ball, slot, and flat mount. Figures 8.41(b) and (c) could be a 3-slot mount, or a 3-bipod mount. Figure 8.41(a) has no symmetry, 8.41(b) has a single plane of symmetry, and 8.41(c) has three planes of polar symmetry. As noted in Section 8.3, a significant improvements in solution efficiency is possible if symmetry is used.

The real significance of a determinate mount is not in the ease of solution of the mount forces, but in the uncoupling of the optic's internal behavior from its mount behavior. As noted below, this uncoupling effect is important to precision structures. No matter how, or for what reason the mount support moves, the optic moves only in a rigid body sense, with no distribution of the optic itself. Thus the error created is only a pointing error and not an image quality error.

As shown in Figure 8.42(a), the support motion for a determinate mount causes only a rigid body "strain free" motion of the optic, as opposed to the redundant mount in 8.42(b). This mount displacement could be due to mechanical or thermal loads, either static or dynamic. Initial imperfections, fabrication errors, and tolerance buildup also cause only the rigid body motion without a surface distortion. These pointing errors are more easily corrected in the system than the image quality errors. In a statically indeterminate design (Figure 8.42[d]), uniform temperature changes can cause strain and distortion due to a difference in the coefficients of thermal expansion. The determinate designs, on the other hand, allow for a strain-free thermal growth as shown in Figure 8.42(c). This is especially important in optical systems fabricated at room temperature, but used

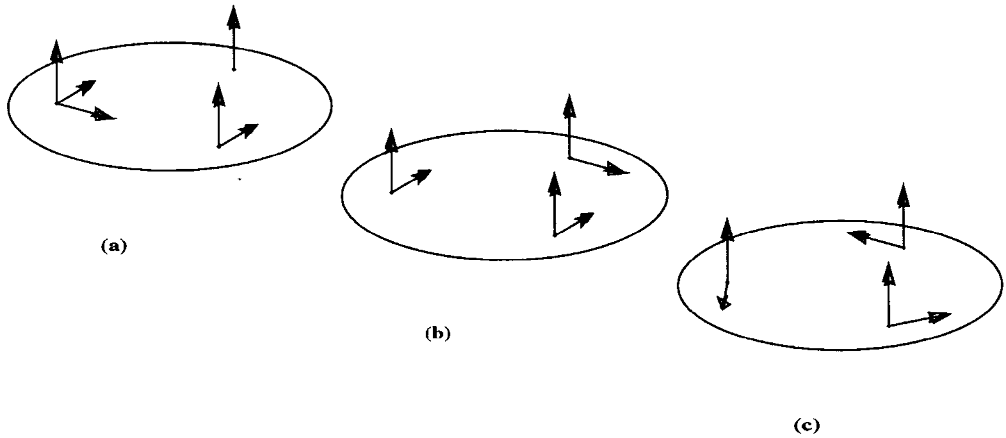

FIGURE 8.41 Statically determinate mount schemes in 3D space. (a) 3-2-1 which is common for a ball, groove, slider mount; (b) three grooves or bipods in a rectangular configuration; and (c) three grooves or bipods in a polar configuration.

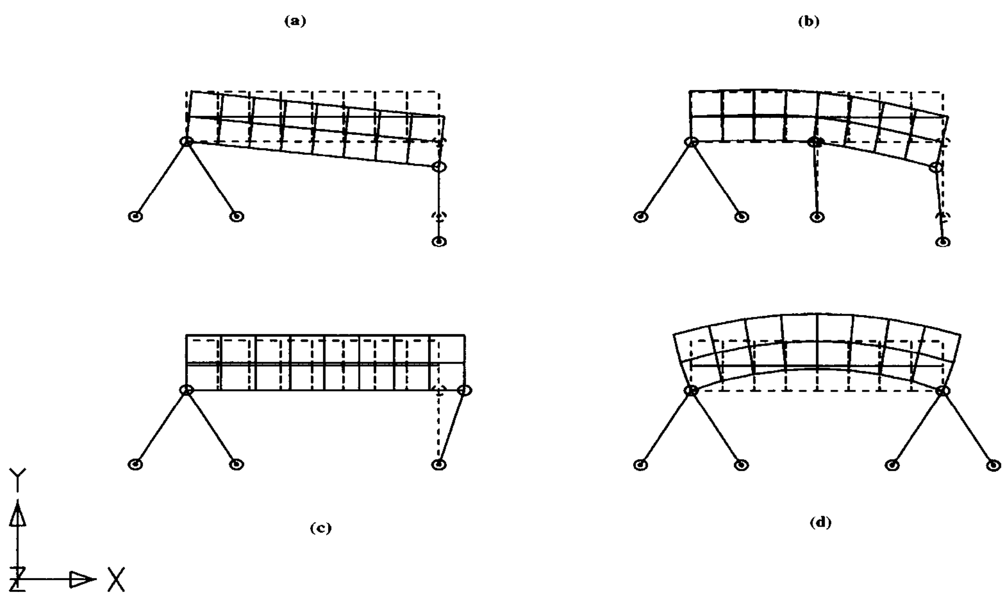

FIGURE 8.42 Determinate vs. indeterminate mount schemes. (a) Determinate mount with strain-free mount motion; (b) determinate mount with strain-free thermal growth; (c) indeterminate mount with distortion due to mount motion; and (d) indeterminate mount with distortion due to thermal growth.

at high or low temperatures. Note that the thermal gradients within the optic will still cause distortion, but it will be uncoupled from any distortion in the mount.

Real mount systems usually try to be as determinate as possible, but are not perfectly kinematic. In the analysis model, the mount can be made "exactly" determinate. The feature is useful in debugging and checking of the finite element models. In a kinematic system, the analyst should always check the mount forces or reactions for any load condition. If the load condition is a uniform temperature change, any nonzero reaction is a modeling error and causes unreal distortions in the optic for this and other load conditions. If the load condition is mechanical, the sum of the applied forces and moments on the optic should exactly equal the sum of reaction forces and moments at the optic mounts. These can be easily checked by using the six equilibrium equations.

From a reliability point of view, the determinate mount may have some drawbacks. Since there is no redundancy in the system, the failure of one element causes failure of the full system. In an optical system, a precision operation is usually more important than stress, so the statically determinate scheme is often used.

Models of Determinate Mounts

A common mount scheme for large mirrors is the use of six struts in a bipod pair arrangement (Figure 8.43). To make each strut an axial force-only member, the ends are ball-in-socket joints. This scheme is exactly represented as the truss members (ROD). For most applications, this is a good first-order model which can be used in design trade studies. In a real mount, the ball joint often has friction which causes some extra forces and moments to be introduced in the optic as a second-order effect. Up until slip, the friction could be molded as rotational springs. If slip or slop is to be included. then a nonlinear analysis with gap elements is required. Also, once the moments are added, the strut must be modeled as a bending element (BEAM).

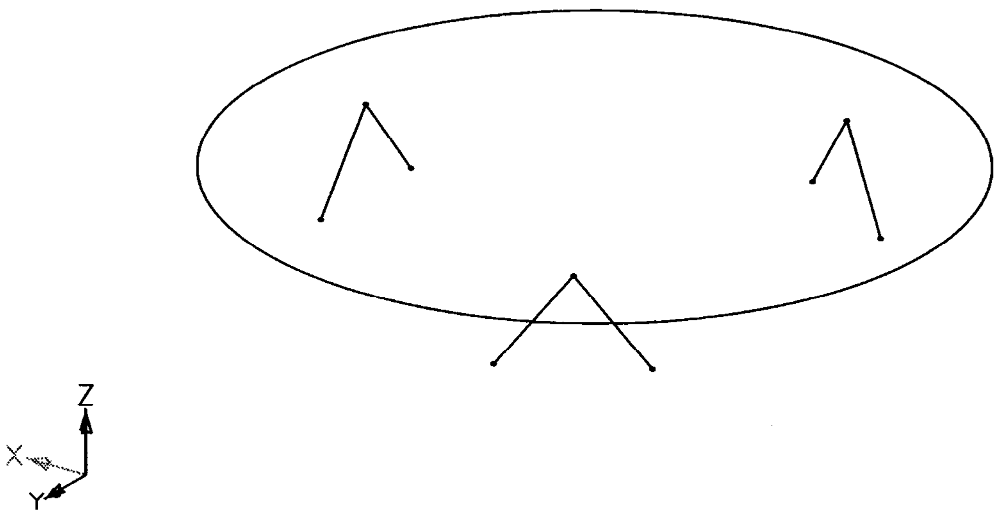

FIGURE 8.43 Three-bipod mount determinate scheme.

A variation on strut arrangement which eliminates the nonlinearities associated with slip and slop in the ball joint is a flexure mount. In this design, each ball is replaced by a necked-down section in the strut which transmits only a small, but highly predictable moment to the mirror. Again, to a first order, a truss element model is possible, but a beam model is required to include the small transmitted moments. This remains a linear analysis, static or dynamic, to very high load levels. Since the loads may be in compression, a buckling analysis is required to verify that the system will not buckle due to the necked down regions.

Many other kinematic mount schemes exist, including the blade flexures, finger flexures, pin-in-hole, ball-in-groove, and flat-in-flat point mounts. To a first order, each can be represented as a determinate mount, but may require the incorporation of second-order effects when a very high precision is required.

Zero G Test Supports

Since many optical systems are used in space, it is necessary to simulate a zero-gravity situation when testing an optic here on earth. These test systems try to support a mirror by applying a distributed load over the back surface. Since these are only approximations, it is necessary to analyze the effect these supports have on mirror distortion. The following are first-order models which predict the primary behavior of the optic. If higher accuracy is required, then more detail is required in the mount model.

An inflatable, fluid-filled rubber bag is used to support the mirror on its back surface. This can be represented as a uniform pressure over the loaded surface. A first FE analysis run is required to calculate the FE model weight and to calculate the net support force caused by the support. By comparing the net vertical force to the model weight, a scale factor on pressure is determined which will exactly balance the mirror weight. Since an FE model requires a nonsingular stiffness matrix, a set of kinematic BC are required to create a valid model. A check of the reaction forces in the second run will determine how accurately the scale factor was chosen. In some read applications, a small, nonzero 3-point support force is desired so that the exact mirror position is determined, rather than floating in an unknown vertical position or tilt. Again, this residual force can be obtained by a proper choice of the scale factor.

An alternative approach is to use a multipoint constraint (MPC) equation. From 8.44, an equation can be written that states that the volume change ΔV in the bag is zero.

$$\Delta V = 0 = \Sigma A_j \delta_j$$

where δ_j is the normal displacement of node j and A_j is the nodal area associated with node j. In an FE model, this area is easily determined by applying a unit pressure to the loaded surface and obtaining the area from the calculated load vector. Since the net volume change is zero, this equation constrains the mirror from having a net vertical displacement. Note that this is a single constraint on the vertical motion which does not prevent a rotation about the horizontal axes. In most models, the rotation would be eliminated by symmetry of BC. This technique removes the requirement to balance the loads as in the reverse pressure method above.

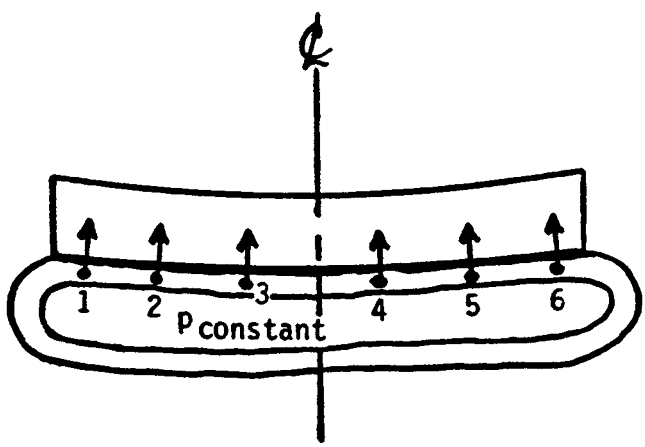

FIGURE 8.44 Optic supported on a zero-g simulation airbag.

Note that neither technique accounts for the in-plane elastic stretch of the bag or its frictional drag on the mirror surface. In actual tests, precautions are taken to minimize this effect. If the mirror surface is highly curved and a liquid-filled bag is used, then the change of hydraulic head from center to edge should be incorporated in the model.

A whiffle tree (Figure 8.45) may be used to simulate a zero-gravity state. In this scheme a system of pin-jointed levers is used to support the mirror in a uniform manner. This scheme is tuneable by varying the lever arm lengths. Note that this exactly determined by a set of lever equations (MPC) or the MSC/NASTRAN RBE3 element (called a whiffle tree element). In a 2D representa-

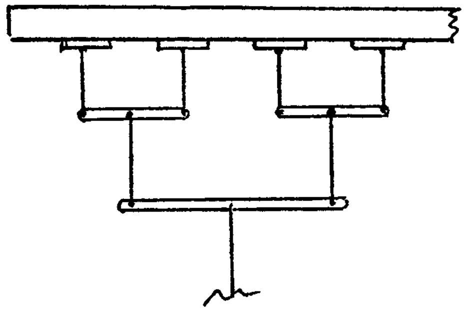

FIGURE 8.45 Optic supported on a zero-g simulation whiffle tree.

tion, each node point has two equations (sum vertical forces = 0 and sum moments = 0) to determine the two forces at the level ends. In 3D, an additional moment equation is used to find the third vertical force on the corners of the triangular lever arm. Note that this model ignores the frictional effects in the points.

Metering Structures

The structure which holds all of the optical elements together to form a system is called a metering structure, because the relative position and motion of the optics are critical to the system level performance. With the wide variety of metering structures possible, only some simple modeling guidelines will be offered in this section.

The most important rule is that the model must contain all effects which cause the distortion of optics or alters their position. This means that any nonkinematic effects at the mounts which pass forces or moments to an optic should be included if the magnitude is significant. This may require the submodel of a mount to determine the magnitude of the unwanted forces and a subsequent optics analysis to determine the magnitude of the effect on surface quality. The effects of friction in ball joints or the moments passed through the flexures are examples.

In a metering structure, the line of action of a member force is important. If the neutral axes of members do not intersect, the resulting moments may cause significant rotations of members. These moments and rotations can cause pointing errors which may not be predicted by a model in which the neutral axes incorrectly intersect. An example is a force from one member which does not pass through the shear center of an attached c-channel. Another example is an offset lap joint which creates bending under axial tension, which might be modeled as an in-line butt joint which has no bending (Figure 8.46). Ring-stiffened cylindrical shells behave differently whether the ring is inside or outside of the shell. The model must include the offset between the ring and shell to get the proper behavior. To get all effects molded correctly, the analyst must understand and use the concepts of neutral axis and shear center for the cross sections involved. The finite element program must allow for the proper independent offset of neutral axis and shear center. Rigid bodies are often required when the lines of action do not intersect at a point.

If the analysis is to include thermal loads, then the rigid bodies must be used with care since they have no thermoelastic growth. Figure 8.47 shows a ring and stringer-stiffened shell offset with rigid elements. If all the material has the same coefficient of thermal expansion, then a uniform temperature change causes stress-free uniform growth. In the example, the rigid offsets have no growth, so the radial growth is not uniform, causing the distortion shown in the contour plot (Figure 8.48). If the structure was a flat stiffened plate, rather than a shell, the thermal growth would be uniform. Thus, some modeling conditions are affected more than others. A good check of the rigid body effect is to convert all material to the same coefficient of thermal expansion. Apply a uniform temperature change, then plot the stress in the structure. Any nonzero stress indicates a modeling problem. One fix is to replace the rigid elements with very stiff elastic elements

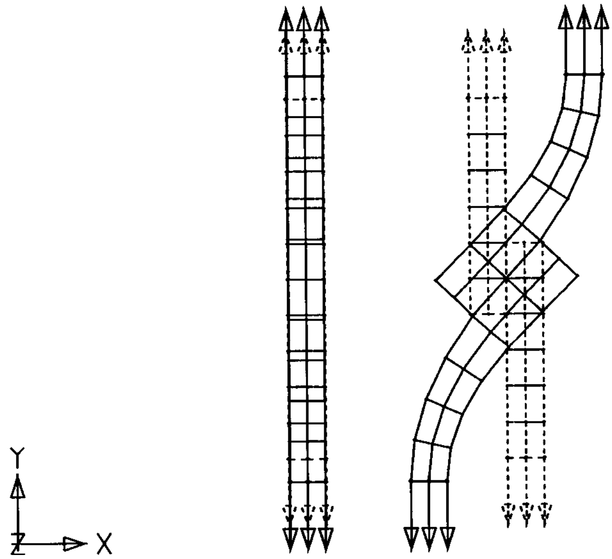

FIGURE 8.46 Comparison of bending caused line-of-action forces for in-line butt joints vs. offset lap joints.

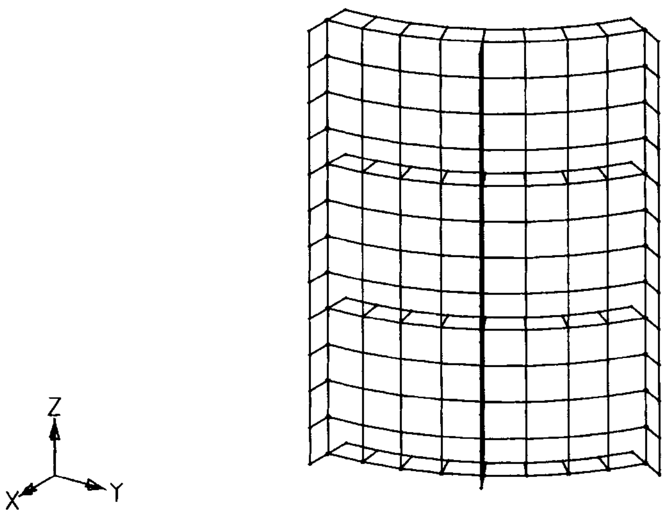

FIGURE 8.47 Curved shell with internal rings and external stringers modeled as beams with rigid offsets from the shell midsurface.

which have thermoelastic growth. Very stiff in this case means a stiffness of three to five orders of magnitude larger than the surrounding stiffness, but not so large as to create numerical problems. Whenever using stiff elements or rigid elements, the analyst should carefully check all the warning messages and error checks (EPSILON) put out by the analysis program.

When using gravity loads or dynamic loads, the center of gravity (cg) is important. A small error in the cg of a large optic can cause a significant moment error in a metering structure resulting in pointing errors. The correct mass moments of inertia are required for all large lumped masses to get a proper dynamic response.

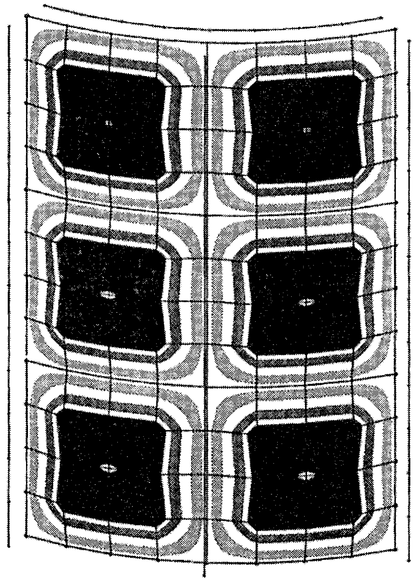

FIGURE 8.48 Radial displacement contours caused by a uniform temperature increases when using rigid offsets in a shell.

8.8 Optical Surface Evaluation

Typical finite element results include the deformed shapes of optical surfaces, usually in contour plot form. Although these data are useful, the distortion of the surface is often masked by a large rigid body motion which may be aligned out of the system. A useful postprocessing feature is to fit selected polynomials to the deformed surface to decompose it into meaningful components.

Polynomials

Let a function be defined as a summation of a polynomial series:

$$D(z,\theta) = \Sigma\Sigma[A_{nm}P_{nm}(z)\cos(m\theta) + B_{nm}P_{nm}\sin(m\theta)]$$

where

D = displacement normal to surface = axial (radial)
z = radial (axial) position
θ = circumferential position
n = radial (axial) wave number
m = circumferential wave number
P = polynomial function of (n,m,z)
A = cosine coefficient
B = sine coefficient

Zernike polynomials represent the common aberrations over conventional optics, such as power, astigmatism, coma, trefoil, etc. (Figure 8.49). For Zernike polynomials (z = radial position):

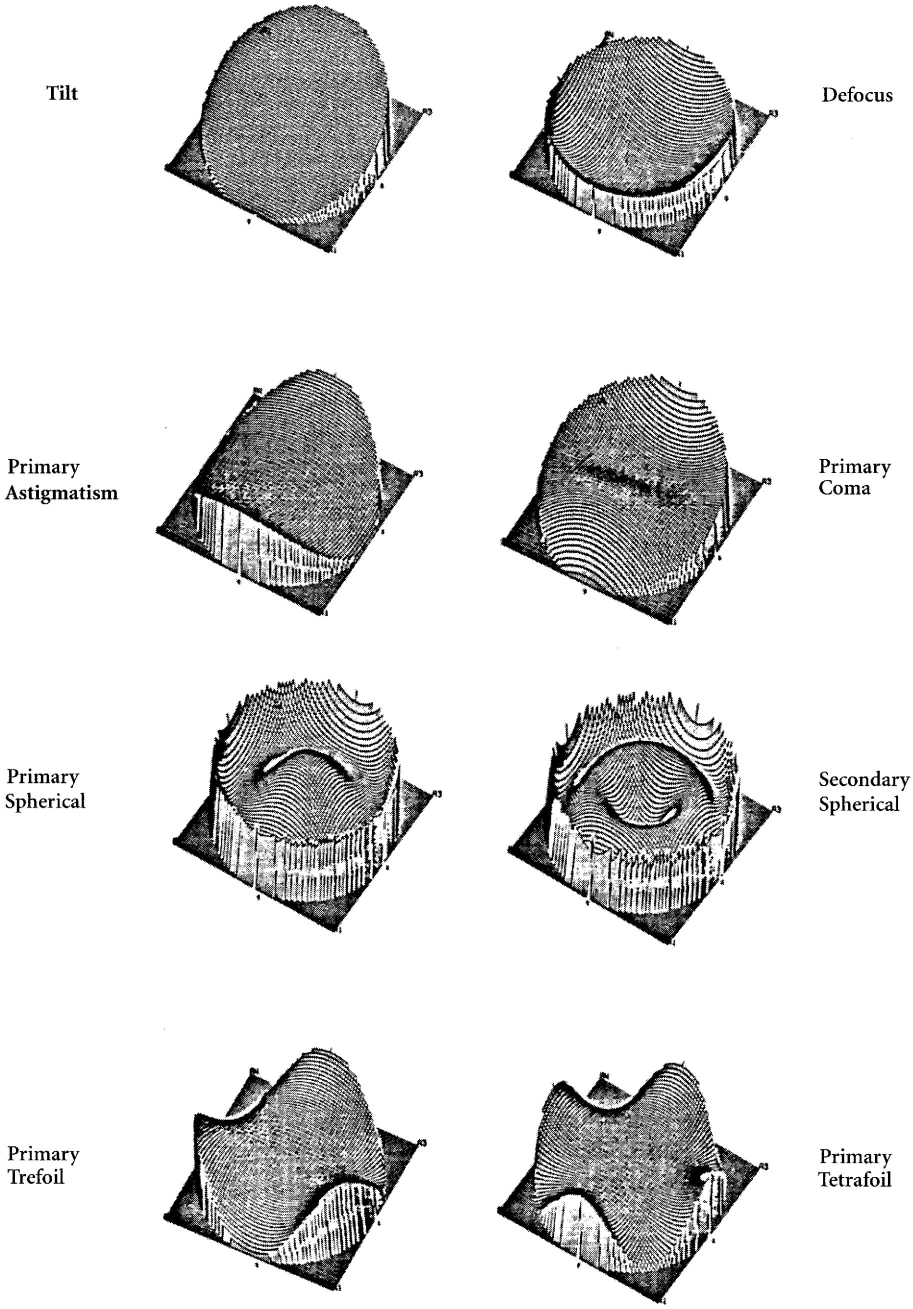

FIGURE 8.49 Typical Zernike polynomial terms for conventional optics.

$$P_{nm}(z) = \Sigma C_p(n,j) z^{n-2j}$$

$$C_p(n,j) = [(-1)^j (n - j)!]/\{j![(n + m)/2 - j]![(n - m)/2 - j]!\}$$

where the series is summed for m < n and for alternate values of n.

Legendre-Fourier polynomials are similar to Zernike polynomials, but fit cylindrical optics (Figure 8.50). For Legendre-Fourier polynomials (z = axial position):

$$P_{nm}(z) = \Sigma C_p(n,j)z^{n-2j}$$

$$C_p(n,j) = [(-1)^j(2n - 2j)!]/[2^n j!(n - j)!(n - 2j)!]$$

where the series is summed for all values of n and m.

Since both series are orthogonal and complete, their representation is exact. If the series is truncated, then it becomes an approximation in general. The series terms may be represented as the coefficients of cosine and sine (A,B) as above, or as magnitude and phase (M,Φ) where:

$$M_{nm} = \mathrm{SQRT}\left[A_{nm}^2 + B_{nm}^2\right]$$

$$\Phi_{nm} = (1/m)\mathrm{ATAN2}\left[A_{nm}/B_{nm}\right]$$

ATAN2 is the standard FORTRAN arc tangent function with two arguments.

Surface Fitting

Given a deformed shape of an optical surface from a FE solution, the error between the FE solution and a polynomial approximation is defined by Genberg[5] as:

$$E = \Sigma W_i(\delta_i - D_i)^2$$

where

i = node number
δ_i = FE displacement of i*th* node
D_i = polynomial displacement of the i*th* node
W_i = area weighting of the i*th* node

In a typical FE model the mesh varies throughout the model so each node point does not represent the same amount of surface area. W_i is the area weighting factor which can be determined from the load vector calculated from a unit pressure over the surface. If the series for D is written symbolically as:

$$D_i = \Sigma c_j f_{ji}$$

then

$$E = \Sigma W_i(\delta_i - \Sigma c_j f_{ji})^2$$

To find the best-fit polynomials, minimize the error E with respect to the coefficients c_j.

$$dE/dc_j = 2\Sigma W_i(\delta_i - \Sigma c_j f_{ji})f_{ji} = 0$$

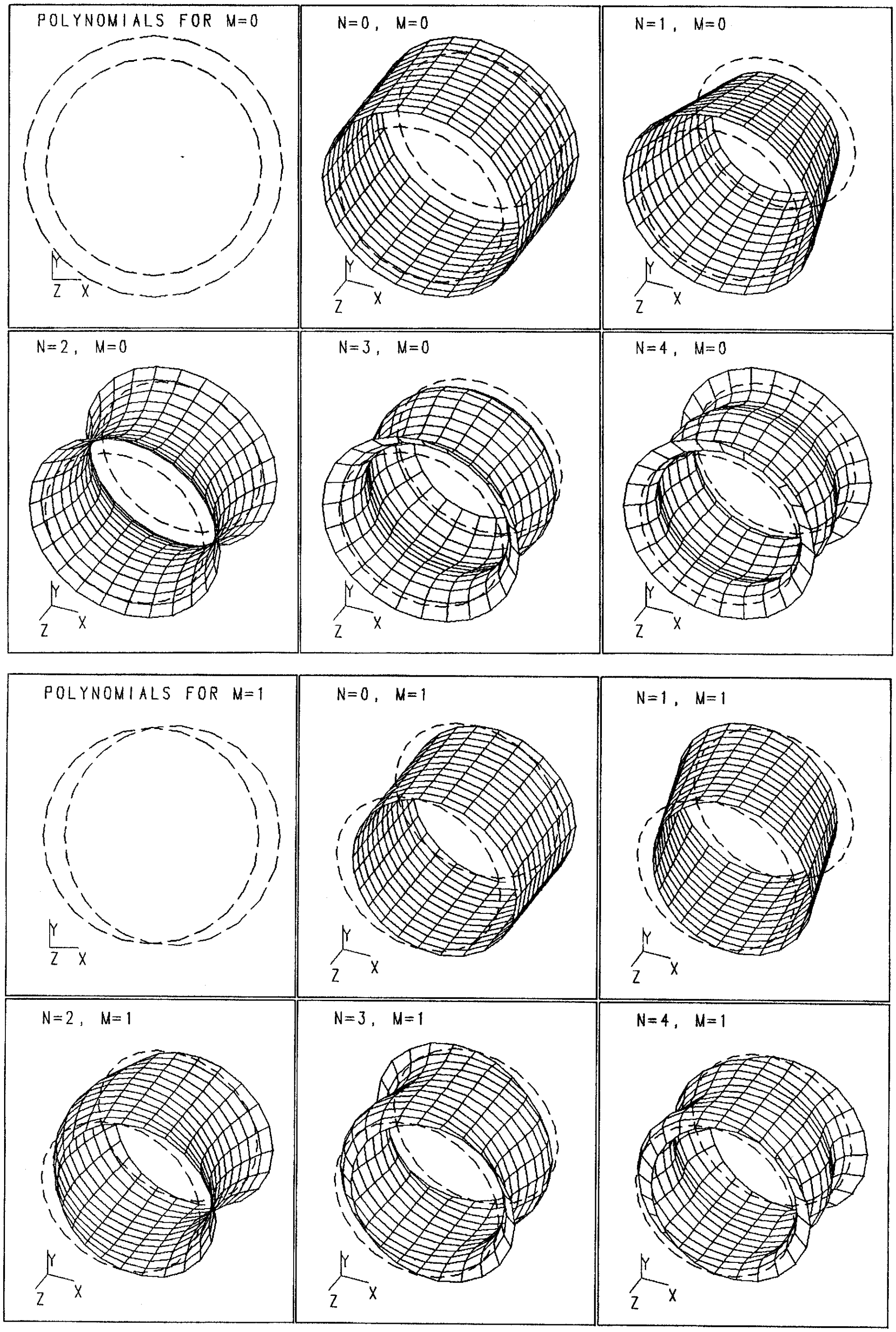

FIGURE 8.50 Typical Legendre-Fourier polynomial terms for cylindrical optics.

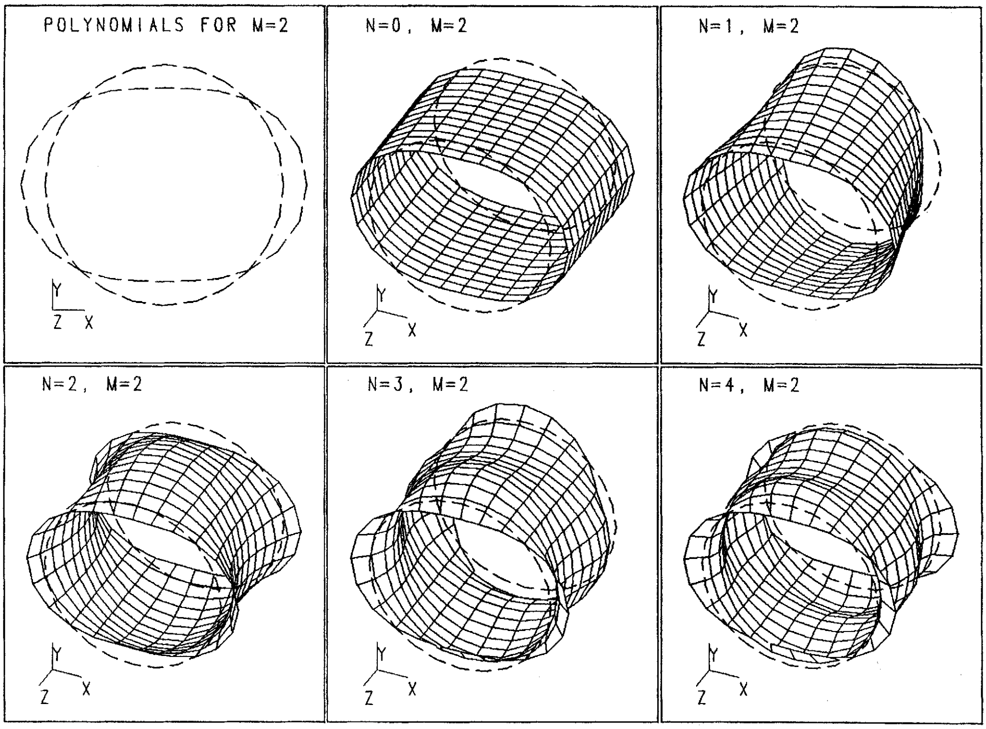

FIGURE 8.50 (continued).

Collecting the terms and writing in a matrix notation:

$$[H]\{c\} = \{p\}$$

where

$$H_{jk} = 2\Sigma W_i f_{ji} f_{ki}$$

$$p_j = 2\Sigma W_i \delta_i f_{ji}$$

This is a liner system with a square, symmetric coefficient matrix solvable by Gauss elimination. The best-fit coefficients (c) can be represented as the original series coefficients (A,B) or as the magnitude and phase (M,Φ) for each polynomial term. These polynomials are orthogonal over a full circular geometry, so their coefficients are constant regardless of the number of terms used in the series. If the geometry is irregular or obstructions exist, the coefficients may vary with the number of terms used in the series. It is useful to calculate the error term, both root-mean-square (RMS) error and peak-to-valley (P-V) error, after each term in the series is subtracted from the original deformed surface. This error indicates the amount of surface distortion not accounted for by the previous polynomials.

Interpretation

Both polynomial series considered above include the rigid body motion. In the Zernike series, for example, the first two terms are rigid body and the third is power:

Bias: n = 0, m = 0
Tilt: n = 1, m = 1
Power: n = 2, m = 0

Any optical system which has pointing and focusing capability can adjust out the bias, tilt, and power terms. Thus these terms do not affect image quality in such a system. All of the higher order terms represent aberrations in the surface which do affect the image quality. The measure of surface quality is the error calculated after the first three terms have been removed, not the error in the original FE deformed shape. Figure 8.51 shows a mirror on a 3-point, delta frame mount system oriented at 45° with gravity. Contours on the original deformed shape are dominated by bias, tilt, and power. The contours after these three terms are removed show the actual surface quality which affects imaging. Figure 8.51(f) gives the magnitude and phase angle of each of the terms, as well as the RMS and P-V error after the term is removed from the surface. In this example, the original P-V error is 90 waves, but after the bias, tilt, and power are removed, the P-V error is 8 waves. Obviously, the original FE surface displacements are not an accurate measure of surface quality, until postprocessed by a surface-fitting program.

The decomposition of a surface into a series is useful for understanding the important factors in the optics behavior. In the above example, all of the trefoil effect can be attributed to the 3-point mount and all of the coma is due to the in-plane gravity. If the mirror had a lightweight square core, then its effect would show up as tetrafoil. In many cases, this can be useful in improving the performance of a system.

To be a useful surface-fitting program the following features should be incorporated:

- Submodels using symmetric BC
- Multiple, nested coordinate systems defining the node location and output
- User coordinate system to define the polynomial centers and orientation
- Apertures and obstructions to limit the amount of surface fitted
- Units conversion to arbitrary output (i.e., wavelengths)
- Linear scaling and combining of loadcases (displacement vectors)
- Residual surface output format suitable for plotting

8.9 Modeling Tricks for Optical Structures

In this section, three modeling tools useful in optical structures are discussed.

Image Motion Calculation

For the small displacements and rotations common in optical structures, the image motion calculation is a linear equation. This is true for rather complex assemblies of flat mirrors, curved mirrors, and lenses. For the simple system shown in Figure 8.52, the image motion shown (δ_i) affected by the rotations (Φ) of the two mirrors (a,b) and their respective path lengths (L):

$$\delta_i = (L_2 + L_3)\Phi_a - 2(L_3)\Phi_b$$

For more complex systems, all of the mirrors' motions (translations and rotations) enter into the image motion equation. For powered elements, the effective lengths are modified. An optical analysis program may be needed to determine the appropriate coefficients of each optic's unit motions.

Absolute motion of the image is not important to the system performance, but the relative motion of the image to its receptor is. In a copier, the relative motion is measured as smear. Given the receptor's motion (δ_r), the smear (δ_s) is

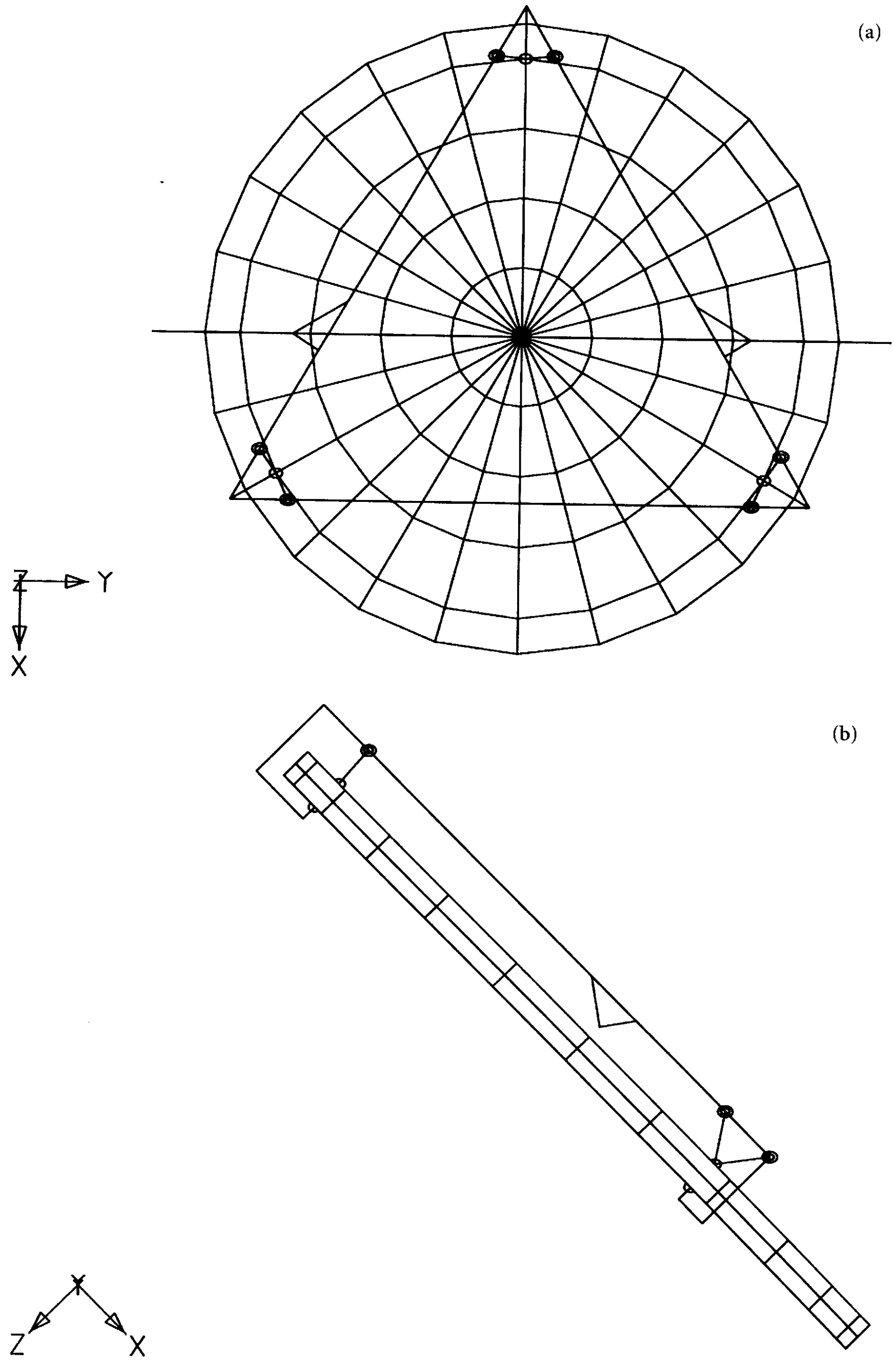

FIGURE 8.51 (a) Flat turning mirror on a delta frame mount — front view; (b) flat turning mirror on a delta frame mount — side view.

$$\delta_s = \delta_i - \delta_r$$

If the optical system is modeled, then the FE program will determine the mirror and receptor motions. If the program has the capability to include the user written equations (MPC), then δ_i or δ_s can be directly calculated and output by the FE program. For the simple system shown, this

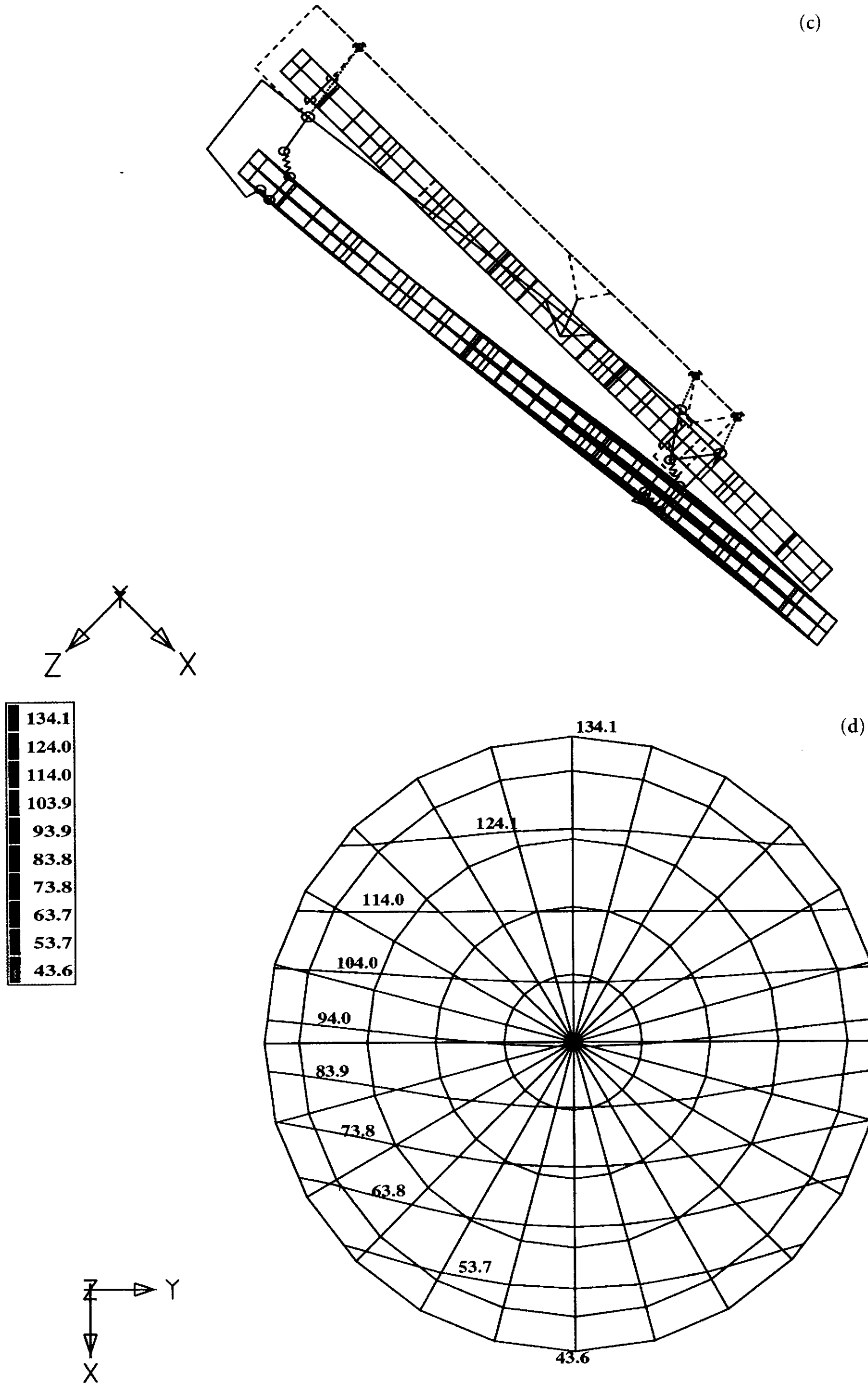

FIGURE 8.51 (c) flat turning mirror on a delta frame mount — deformed side view; (d) flat turning mount — contours of normal displacements.

may not represent a big savings in data postprocessing outside of the FE code. However, for systems with many elements, and considering all six degrees of freedom of each optic, this can represent

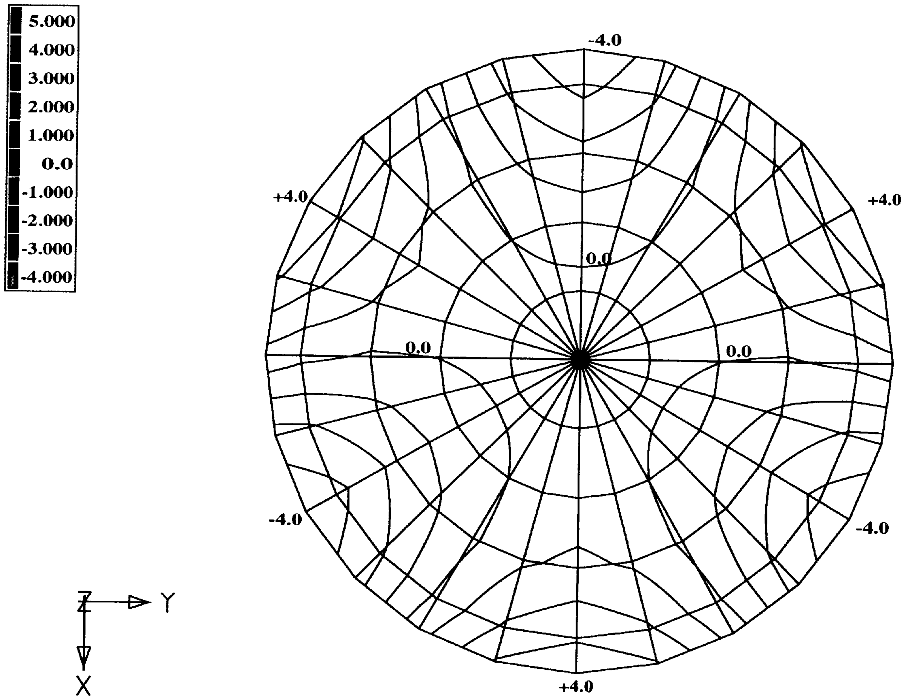

Zernike Polynomials for Surface= 1 Subcase= 1 Multiplier= 1.000E+00

Order k	n	m	Surface Aberration	Functional (Units)	Phase (Deg)	Residual RMS	Residual P-V
			Input Surf			24.8842	90.4800
1	0	0	Bias	91.58552	0.0	24.8842	90.4800
2	1	1	Tilt	98.43091	179.9	2.2940	9.7651
3	2	0	Power	-5.43184	0.0	1.5996	8.0006
4	2	2	Pri Astigmatism	0.07498	89.8	1.5995	8.0074
5	3	1	Pri Coma	0.02916	-180.0	1.5995	8.0147
6	3	3	Pri Trefoil	8.68164	0.0	0.2345	1.0534
7	4	0	Pri Spherical	0.53040	0.0	0.1599	0.9565
8	4	2	Sec Astigmatism	0.01820	0.0	0.1599	0.9564
9	4	4	Pri Tetrafoil	0.02178	0.0	0.1599	0.9445
10	5	1	Sec Coma	0.00148	-0.1	0.1599	0.9451
11	5	3	Sec Trefoil	0.70869	60.0	0.1102	0.5993
12	5	5	Pri Pentafoil	0.00523	-0.1	0.1102	0.6029
13	6	0	Sec Spherical	-0.05257	0.0	0.1096	0.6029
14	6	2	Ter Astigmatism	0.00095	-89.8	0.1096	0.6033
15	6	4	Sec Tetrafoil	0.00390	0.0	0.1096	0.6033
16	6	6	Pri Hexafoil	0.74367	30.0	0.0331	0.1716
17	7	1	Ter Coma	0.00113	0.0	0.0331	0.1717
18	7	3	Ter Trefoil	0.06975	60.0	0.0311	0.1999
19	7	5	Sec Pentafoil	0.00493	36.0	0.0311	0.1968
20	8	0	Ter Spherical	0.00171	0.0	0.0311	0.1968
21	8	2	Qua Astigmatism	0.00117	-89.9	0.0311	0.1971
22	8	4	Ter Tetrafoil	0.00232	44.9	0.0311	0.1960
23	8	6	Sec Hexafoil	0.14599	0.0	0.0228	0.0908

FIGURE 8.51 (e) contours after best-fit plane and power removed; and (f) surface fit results with the magnitude and orientation of the Zernike polynomials and the resulting surface RMS and peak-valley after the term is removed.

a very useful capability. The amount of data processed increases significantly in the dynamic analysis where the smear is calculated at each time step. Nowak[14] shows a laser printer system with 13 independent optical elements analyzed for the frequency response as well as transient response.

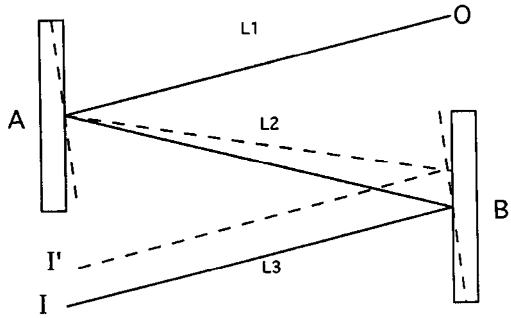

FIGURE 8.52 Image motion due to mirror rotations.

Poor Man's Spot Diagrams

Wolverton[23] describes a procedure to provide a simulated spot diagram directly from the FE output, without any additional postprocessing. The procedure involves the following steps:

- Define a spot center at twice the focal length
- Create a node at the spot center for each node on the optical surface
- Add rigid beams from the optical surface to the spot center
- Add a circle of grounded beams to represent the blur circle
- Plot the deformed nodes at the spot center to get a spot diagram

Note that this spot diagram is a standard FE output without further postprocessing. The individual rigid elements (or ray bars) are not connected to each other. They represent massless cantilevers off the optical surface with no effect on the surface response. The spot diagram is located at twice the focal length (2L) since an incoming ray sees twice the node rotation (Φ) (angle of incidence + angle of reflection):

$$d_i = L(2\Phi) = (2L)\Phi$$

Optical Pathlength Calculation

When a planar optical wave passes through a planar window of a constant index (n), it stays planar as it exits. If the window has a variation in optical index, then the pathlength may be different for different rays, causing the exiting wave to be nonplanar. The index may vary with temperature and stress level.

The variation from planarity is called the optical pathlength difference (OPD). To find the OPD, two finite element runs are necessary. First, a heat transfer analysis is conducted using the techniques discussed in the next chapter. The result is a new temperature (T) at every node. In the second analysis, the OPD is output directly using the following analogy to thermoelastic expansion:

$$OPD = L[n + (dn/dT)\Delta T] - L(n)\Delta T = L(dn/dT)\Delta T$$

which has the same form as the thermal expansion:

$$\delta = L\alpha\Delta T$$

In the second model:

- Set the material properties to $E = 1$, $G = 0$, $\nu = 0$.
- Set the coefficient of thermal expansion (CTE) to dn/dT.
- Constrain all in-plane displacements to zero.
- Constrain the first (incident) surface normal displacements to zero.
- Apply the new temperature vector as a thermal load.
- The normal displacement of the second (exit) surface is the OPD.

This second surface displacement vector may be postprocessed for Zernike coefficient if desired. An example of a window in a vacuum chamber with an incident laser beam is shown in Figure 8.53. The resulting OPD map correlated closely to the experimental results.[6]

The above calculated OPD is one contributor to the total OPD. Other affects such as the true thermoelastic expansion may be added, but are typically much smaller than the index change effect. This calculation is exact within FE theory for the planar windows, but may be a useful approximation for lenses, also. The suggestion is that the element boundaries should be parallel to the path of the rays to improve the quality of the approximation.

Plastic optics may absorb moisture and change in index. The moisture absorption can be analyzed by analogy to heat transfer with the appropriate property changes. The OPD due to index change can be calculated using the method above where the temperature is replaced with moisture concentration. A similar procedure can be used to predict the OPD due to stress effects (birefringence).

8.10 Ray Tracing

A finite element program presents its analysis results at the node points. A ray tracing program which bounces random rays off of the deformed optical surfaces requires an accurate displacement and slope information at ray–surface intersection points which are, in general, not at the node points as shown in Figure 8.54. High accuracy is required on the slope data because it usually has a large effect on the final ray position at the image plane. Other postprocessing programs for optical evaluation may require the deformed surface data on a regularly spaced square pattern which typically do not line up with the finite element node points (Figure 8.55). This section presents a highly accurate technique for obtaining deformed surface data at points on a finite element model which are not at node locations. The technique, which is more accurate than spline fitting, extracts the maximum information from a finite element model because it uses the same theory to postprocess the data as was used in the finite element program to solve the problem. The technique applies to a variety of mirror surface geometries including flat, spherical, or cylindrical. Additional details are available in Genberg.[7]

In a ray trace program evaluating a deformed surface, the plate or shell bending behavior is required for accurate slope information at intermediate ray–surface intersection points. The technique described applies to the low order plate and shell elements (QUAD4 and TRIA3). This restriction is not usually a major limit on the model. If the optic is modeled of solid elements, then a "thin" coating of plate elements is applied to the reflective surface. Since most solid elements do not have rotational stiffness, this coating of thin plates provides the necessary node point rotation data required for the cubic interpolation.

Nonrectangular quadrilaterals are converted to two triangles. The rectangles and triangles are used because their Jacobian transformation matrix (J) is a constant throughout the element and not a function of spatial location as in a general quadrilateral. The transformations can be calculated once and then stored for the search routine. The element transformation matrices from spatial coordinates $\{x\}$ to parametric coordinates $\{\xi\}$ are calculated for the resulting rectangles and triangles. For element m,

$$[J_m] = [dx/d\xi\ldots]$$

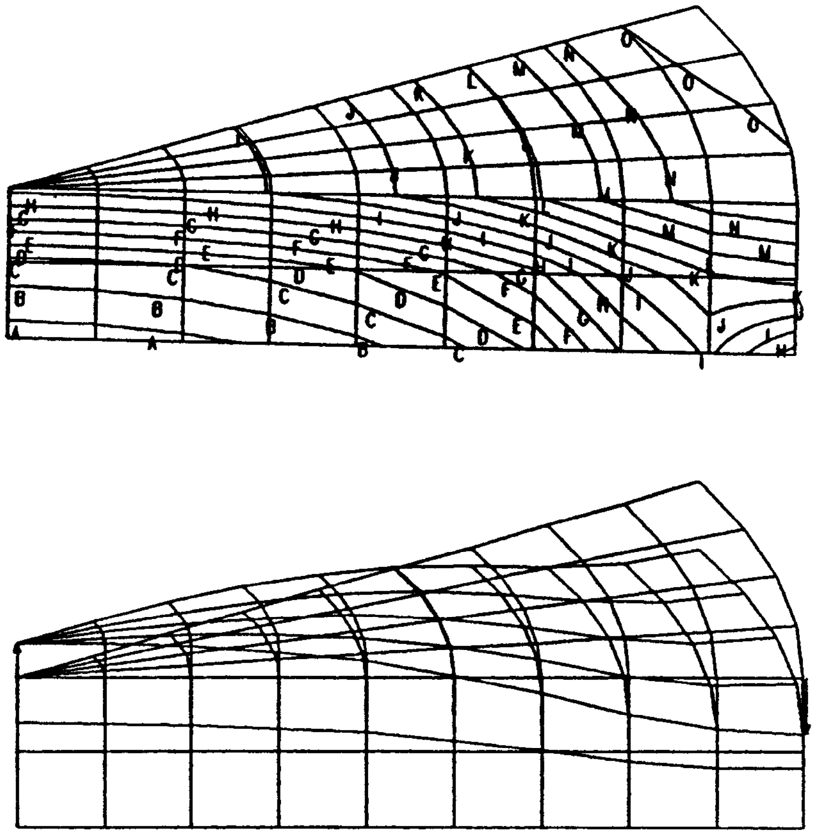

FIGURE 8.53 Optical pathlength analysis due to temperature-dependent index of refraction due to laser beam heating in a test chamber window. (a) Temperature due to laser beam heating; (b) wavefront change due to index change.

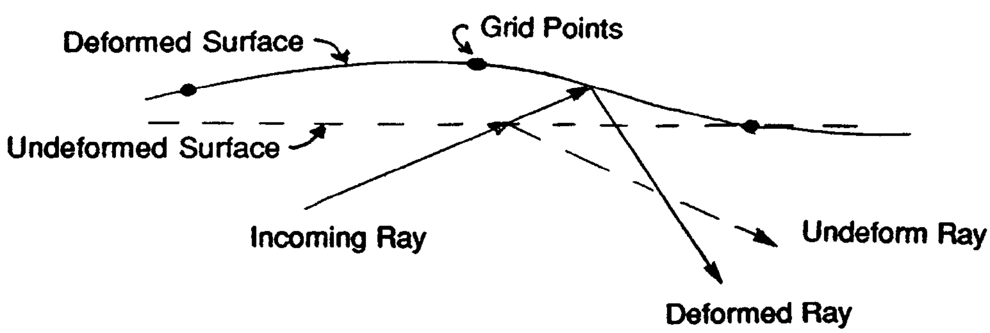

FIGURE 8.54 Ray tracing from deformed analysis results.

The origin of element m in parametric coordinates $\{\xi_0\}$ can be found from the geometric center $\{x_0\}$

$$\{\xi_0\} = [J_m]^{-1}\{x_0\}$$

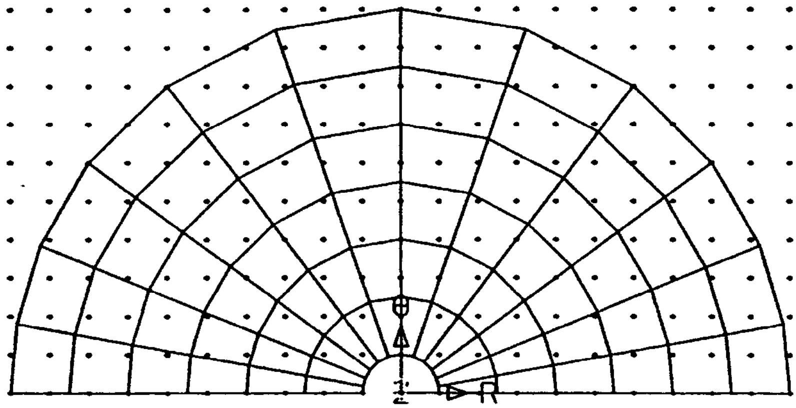

FIGURE 8.55 Uniform grid (x-y) pattern of results interpolated from a polar FE model of an optic for optical postprocessing.

For every ray point $\{x_p\}$, a search over all elements is conducted. The point is converted to element m's parametric coordinates $\{\xi_p\}$

$$\{\xi_p\} = [J_m]^{-1}\{x_p\} + \{\xi_0\}$$

then tested to see if contained within element m.

$$-1 < \xi_p < +1$$

When the proper element is found containing the point, the interpolation takes place using the element's shape functions (N) and the element's nodal results, such as displacements (δ). In-plane motion is found from membrane behavior

$$u(x_p) = \Sigma N_j\{\xi_p\} \times \delta_j$$

The out-of-plane displacement $w(x_p)$ and slopes w_z and w_y are found from plate bending behavior as given in Yang.[24] The equations have the general form of

$$w(x_p) = \Sigma[f_j W_j + g_j W_{xj} + h_j W_{yj}]$$

where W_j, W_{xj}, and W_{yj} are the nodal displacements and rotations. The cubic shape functions (f, g, and h) depend on the plate formulation chosen. It is suggested that fully compatible elements be used in the interpolation so that the surface slope is continuous in both directions at all element boundaries. This continuity condition provides for smoother behavior for rays that bounce from nearby points across the element boundaries.

The two-mirror system shown in Figure 8.56 was used to test the ray-trace algorithm which used interpolation over the shell surface. The incoming rays are collected at the focal plane by very low angle-of-incidence rays grazing off mirrors which are nearly cylindrical. The interpolation was verified by forcing a known functional displacement over both mirror surfaces. The interpolated rays were then compared to the rays from the perfect functional surface, again with an excellent agreement. Additional details are presented in Genberg.[7]

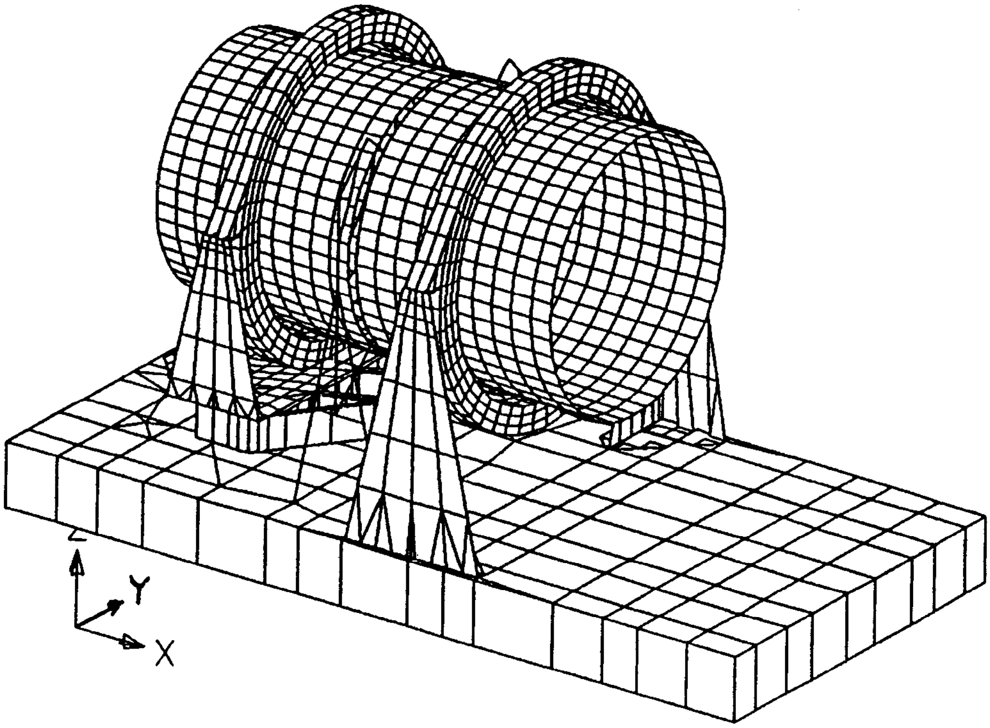

FIGURE 8.56 Cylindrical optics which were ray-traced from deformed FE results.

8.11 Model Checkout

Included below is a checklist for the model creation and checkout. It is suggested that a novice user refer to this list before and during the analysis process.

1. Is FE necessary for this problem?
   - Can a closed form solution be found?
   - Use both if possible, since each verifies the other.
2. Why is the analysis required?
   - What are the analysis goals?
   - Conceptual design vs. detail design verification?
   - Statics vs. dynamics, deflection vs. stress?
   - Accuracy required vs. time and resources available.
3. Check FE program documentation.
   - Does the FE program have the required capabilities?
   - Read about the solution method and element types.
   - Check the current error list for program bugs.
4. Idealize the problem.
   - What is the important behavior — beam vs. shell vs. solid?
   - Consider constraints/loads/element types/ material.
   - Consider symmetry — structure, BC, loads.
5. *Always* run a *prototype* model!!
   - Small model with important features of the true problem.

- Prototype problem should have a theoretical solution.
- Compare with theory to determine the accuracy vs. mesh density.
- Test program input/output/restarts/plots/alters — all features that may be new to the analyst.

6. Model true problem.
   - Keep the model simple; don't overkill with too much detail.
   - Add detail later as required.
   - A small model is easy to debug and understand.
   - A big model has more errors which are hard to find.
7. Know your model generator (preprocessor).
   - Are circles really circles or are they parametric cubics?
   - How symmetric are the generated models?
   - What is the accuracy of generated node points?
   - Know about equivalencing/element normals/coordinate systems.
8. Run graphical checks on model.
   - Plot the model using hidden lines and shrunken elements.
   - Check free boundaries for unwanted cuts in the model.
   - Check element normals for reversal for pressure loads/stress.
   - Check element geometry for warp/skew/aspect ratio.
   - Display of loads/BC/constraints.
9. Use checkout runs to validate the model.
   - 1-g static loads in all directions.
     - — Check max displacements/reactions.
     - — Check mass properties of the model, compare to known values.
     - — Look for symmetry of the response where appropriate.
     - — Perform sanity checks, compare to hand solutions.
     - — Is the response realistic and sensible?
     - — Check epsilons t see if small.
     - — Compare the sum of loads to the sum of reactions.
     - — Plot deformed shape/stress plots for discontinuities and peaks.
   - Uniform thermal soak with all materials having a uniform CTE.
     - — Check stress caused by the offsets, rigid bodies.
     - — Deformation should be a stress-free growth.
   - Rigid body error checks.
     - — Remove constraints to the ground.
     - — Give one node a unit translation/rotation, to see if stress free.
   - Natural frequency analysis.
     - — Check for near mechanisms (Freq = 0)
     - — Check for reasonableness.
   - Compare to any test data of similar structures.
10. Run production analyses.
    - Run statics before dynamics.
    - Run linear before nonlinear.
    - Make all sanity checks/comparisons as above.

11. Understand your postprocessor.
    - Stress averaging vs. extrapolation and fitting?
    - Over what set is averaging done?
    - Does it use nodal values/centroid values?
    - Does it know which stress component is which?
    - Does it know the element coordinate systems?
    - Does it label the output correctly?
    - Can it interpret the displacements in the local systems?
    - How does it treat the midside nodes?
12. Interpret the answers.
    - Look at the analysis results file *before* creating the plots.
      — Look for the warning/error messages.
      — Check epsilon/maximum displacement/sum loads/sum reactions.
    - Look at the stress gradients and strain energy density.
      — Are model refinement and reanalysis required?
    - Are results linear or is a nonlinear analysis required?
      —Are displacements large?
      — Is stress above the yield?
      — Is buckling possible due to high compression?
    - Is redesign required based on the analysis results?
      — Use design sensitivity and optimization.
13. Document the model assumptions and analysis results.
    - Keep a notebook — sketches, calculations, section properties.
    - Keep listing of the input data file with lots of comments.
    - Make many plots of the model and results with labels.
    - Keep the input file or data base for important analyses.
    - Document the labor, cpu time, and calendar time for future estimates.
    - Report the assumptions, model description, results, and conclusions.

The most common sources of errors in FE models are listed below with some recommended checks to locate these errors:

- Bad geometry — find by plots and the mass properties.
- Bad elements — use shrink plots, free boundary plots, normal checks.
- Bad beam orientation — check v vector, section properties, stress points.
- Bad MPC/rigid bodies/offsets — compare sum of the loads to reactions, run rigid body error check, and thermal soak with a uniform CTE.
- Bad BC — same as above, also check for nonsymmetry in the results.
- Bad properties — check for the wrong units, wrong exponents, mixed units.

8.12 Optimum Design

High performance mirrors such as those used in the orbiting telescopes or large, ground-based observatories require a light-to-moderate weight, low stress, and small deflections under static and dynamic loads. The design approach in the past has been through parametric studies to achieve the "best" design within the trade space studied. In this section, the automated optimum design techniques based on nonlinear programming will be discussed as applied to optical structures, in general, and the lightweight mirrors, in particular.

Nonlinear programming techniques were first applied to structural design by Schmit.[15] Early work was limited to the problems where the designer could write the analysis equations as a subroutine and embed them in a general purpose optimization program such as DOT.[20] This limitation prevented the technique from becoming a popular design tool for complex structures. When the theory became available for design sensitivity[19] of general purpose structures through finite elements, the optimization gained favor quickly.

Design Problem Statement

Any design problem can be stated as a general nonlinear programming problem.

Minimize	$F(X)$
Subject to:	$g_j(X) \leq 0$
and	$XL_i < X_i < XU_i$
where	F = objective function
	g = inequality constraints on behavior
	X = vector of design variables
	XL, XU = power and upper bounds on variables

If equality constraints are present, they may be treated as two inequality constraints.

$$h_j \Rightarrow 0 \geq g_j \leq 0 \text{ and } g_{j+i} \geq 0$$

Note that the functions F and g are nonlinear functions of X. In a finite element code, the constraints on displacement and stress are found numerically (not analytically). A constraint on displacement written as:

$$\delta \leq \delta_U$$

where δ_U is an upper limit on displacement, can be converted to the general form as:

$$g = (\delta - \delta_U)/\delta_U \leq 0$$

Design Sensitivity

Nonlinear programming methods are iterative in nature, moving from one design to a better design. An efficient optimization code requires the first derivatives of the responses to determine a proper move direction in the design space. Finite difference operations are too time consuming for most applications. The efficient alternative is the use of implicit derivatives for the design sensitivity of constraints with respect to the variables.[19] In a static analysis, the system equation

$$[K]\{\delta\} = \{F\}$$

is varied by the implicit derivatives

$$[K]\{d\delta/dX\} + [dK/dX]\{\delta\} = \{dF/dX\}$$

To find the response derivative, an additional "load case" is applied to the system equation, where the right-hand load terms are easily calculated.

$$[K]\{d\delta/dX\} = [dF/dX] - [dK/dX]\{\delta\}$$

Note that the additional load vectors are just another column of multiplication, vs. the alternative of new decompositions of the stiffness matrix as required by a finite difference approach to the response derivatives. Finite element programs which provide these sensitivities internal to the code are efficient in a general design optimization program.

Design Variables

Almost all FEA programs which offer the design optimization offer the *sizing* variables which include beam cross-sectional properties and plate thicknesses. These variables effect the "property" cards (pbar or pshell), but not the node locations. A more general capability would include the *shape* variables which change the node point locations. In a continuum structure such as a mirror, the individual node points should not normally be independent variables, but rather overall shape parameters are the variables. Shape optimization can be approached with a variety of techniques, but two methods are prevalent:

1. Basis vector technique
2. Automesh technique

In the basis vector method, a valid mesh of the nominal structure is created. This mesh is perturbed in various directions which represent the candidate designs. The node and element numbering are unchanged in each candidate vector. The optimizer then finds the scale factors for the linear combination of all candidates which yields the "best" design. This is highly efficient, but is limited in the amount of variation possible before a remesh is required.

The automesh technique allows a greater amount of variation in the design because an automatic remesh is redone at every design step. However, an automatic mesh requires a good error evaluation technique which tests the accuracy of the automesh and modifies the mesh for sufficient accuracy. This extra iteration loop, combined with the automeshing algorithm, can be quite time consuming when buried inside a shape optimization loop. Another bothersome feature of automeshing is that symmetric response is not maintained for the symmetric structures such as optics. Any level of asymmetric response for the symmetric checkout loads usually signals a modeling error.

Design Constraints

Optical systems must survive and operate in a variety of environments. For example, during transportation and handling, the stresses must be less than the allowable stress, during launch the natural frequency must be greater than a minimum value, and during operation the surface deformations must be less than an allowable value. A design approach which optimizes for the static stress by providing a soft mount will often violate the dynamic response with low natural frequencies. To obtain a truly optimum mirror, both the static and dynamic constraints must be considered simultaneously. If the finite element code is to be useful, it must have the combined analysis capability. In fact, a very desirable feature is to include the frequency response, transient responses, and buckling as simultaneous analysis and constraint options along with the static and natural frequency constraints.

Since the optical surface performance is often difficult to relate to the raw finite element displacements, some user function capability is required. For a mirror which has a large tilt, but whose surface remains perfectly smooth, the results will show large finite element displacements. However, if the optical system has a pointing capability, the smooth surface will perform satisfactorily (see Section 8.8). What is needed is the ability to find relative motions by writing the responses as equations, or by letting the user include the subroutines, such as surface fitting subroutines, to calculate the response functions. This would allow the constraints to be placed on the RMS error after the rigid body motion and power have been removed.[17]

Algorithms

Many iterative algorithms have been created for the solution of general nonlinear programming problems. In the DOT optimizer,[20] the method of modified feasible directions and the method of sequential linear programming are chosen for their efficiency and robustness. The key issue when combined with a finite element program is the efficiency, especially as related to the number of full FE analyses required per design optimization. In order to reduce the number of full FE analyses, the best procedure is to create an approximate problem which is a first-order Taylor series expansion of the design responses:

$$R(X) = R(X_0) + dR/dX(X - X_0)$$

where R is any response quantity, X_0 is the current design, and dR/dX is found from the design sensitivity. This approximate problem is optimized to get a new design. A full FE analysis is then run on the new design, along with design sensitivity, to create a second approximate problem. At each cycle, the constraints are checked, sorted, and the inactive ones temporarily dropped. Using this approximation technique, the typical designs require five to ten full FE analyses to reach an optimum design.[13]

Lighweight Mirror Design Issues

The previous fabrication and assembly techniques limited the lightweight mirrors to regular, uniform spacing, with a uniform wall thickness. Therefore, the mirror cores were restricted to square, triangular, or hexagonal cells of constant size (B) and a constant wall thickness (t_c). Recent advances in waterjet cutting have allowed a very general core structure to be a possibility.[22] Now the core can be created with an irregular geometry (spacing, shape, and thickness) over the whole mirror which provides an extensive new design freedom.

In the past, the mirrors were polished to a high figure by polishing laps rubbing on the surface. The pressure forced the center of the cell to deflect relative to the cell edge, causing a nonuniform pressure with associated nonuniform material removal. The core print-through effect on the finished surface was labeled quilting. The cell spacing (B) was determined by the polishing quilting displacement (q) which is a function of the cell geometry and faceplate thickness.

$$q = \text{function}\left(B^4 / t_p^3\right)$$

New procedures using ion figuring[22] can place a finished surface of very high quality on a mirror without the use of surface pressure. This allows a greater freedom in the core geometry with larger cell sizes.

In a solid mirror, the only structural design variable is the thickness. Conventional lightweight mirrors can be described structurally by a few parameters as defined in Section 8.4:

H = overall height
t_p = faceplate thickness
t_c = cell wall thickness
B = effective cell spacing

In most applications, the mirror diameter and curvature are specified by the optical requirements. Since the usual goal is the lightest weight mirror which satisfies all the performance criteria, the design problem could be stated:

$$\text{Find the design} = X\ (t_p, t_c, B, H) \text{ which will minimize } W = \text{weight}$$

subject to:

q < quilting limit (polishing)
σ < stress limit (handling, transportation, launch)
δ_{pv} < peak-to-valley displacement limit (test, use)
δ_{rms} < rms displacement limit (test, use)
f_n > natural frequency limit (transportation, launch)

Two general approaches to the design optimization of lightweight mirrors are possible with today's capabilities in finite element analysis. Depending on the mirror complexity and the program's capability, either the sizing or shape design may be used.

Sizing Optimization

Sizing optimization is limited to changes in the effective plate thickness (PSHELL entries). Thus any 3D model can use as many independent design variables as desired to change the core thickness or faceplate thickness. The mirror height (H) and cell size (B) cannot be changed since that involves changes in the node position.

If a mirror is regular enough such that a 2D equivalent stiffness plate model can be used accurately, the equations in Section 8.4 show that the mirror height (H) and cell spacing (B) can be treated as sizing variables.

For highly irregular geometry of the core, a 2D equivalent stiffness "plate" model is very difficult to create and has questionable accuracy. For these irregular mirrors a 3D shell model is required for the design/analysis.

Shape Optimization

A more general and more accurate capability for design optimization is the combination of sizing and shape optimization. With this capability, a full 3D shell model of the mirror is used. The design variables could include the faceplate and individual core wall thicknesses as sizing variables, with cell strut intersections, mount locations, and overall height as the shape variables.

Genberg and Cormany[8] presents a comparison of a conventional mirror design with a shape-optimized lightweight mirror. The elliptic mirror (27 in. × 14 in.) shown was to be mounted at 3 points on the back surface with the gravity acting normal to the face. Due to the space requirements, the mirror thickness was limited to 2 in. The design problem can be summarized as

Objective function:
Min wt = minimize total weight on mirror

Design constraints:
δ_{pv} < 4 m-in. = max P-V under 1 g

As a reference, four design solutions are presented.

1. A regular square core mirror with a hexagonal outline
2. A solid elliptic mirror
3. An unconventional lightweight mirror resulting from parametric studies
4. An unconventional mirror using the optimization techniques

The square core mirror was presented as a design option by an unknown source, so the amount of design effort is unknown. The solid mirror represented the cheapest solution from both a fabrication and a design effort measure. The "parametric" mirror was the "best" design available after a large amount of the design effort from experienced engineers supported by several finite element analyses. The optimized mirror was the result of two trial runs with the new GENESIS program[21] combining the sizing and shape optimization. A plot each of the finite element models appear in Figure 8.57. Symmetric half-models were used for the efficiency. Comparing the unconventional designs, the optimizer moved the mount locations (shape variables) and changed many of the core strut thicknesses (size variables). It was the combination of these changes that was successful and could not be found from the parametric studies. A summary of the resulting designs was

Design	Displacement (m-in.)	Weight (lb)
Square core	8.8	31.6
Solid	8.0	53.6
Parametric	6.0	38.1
Optimized	3.8	30.1

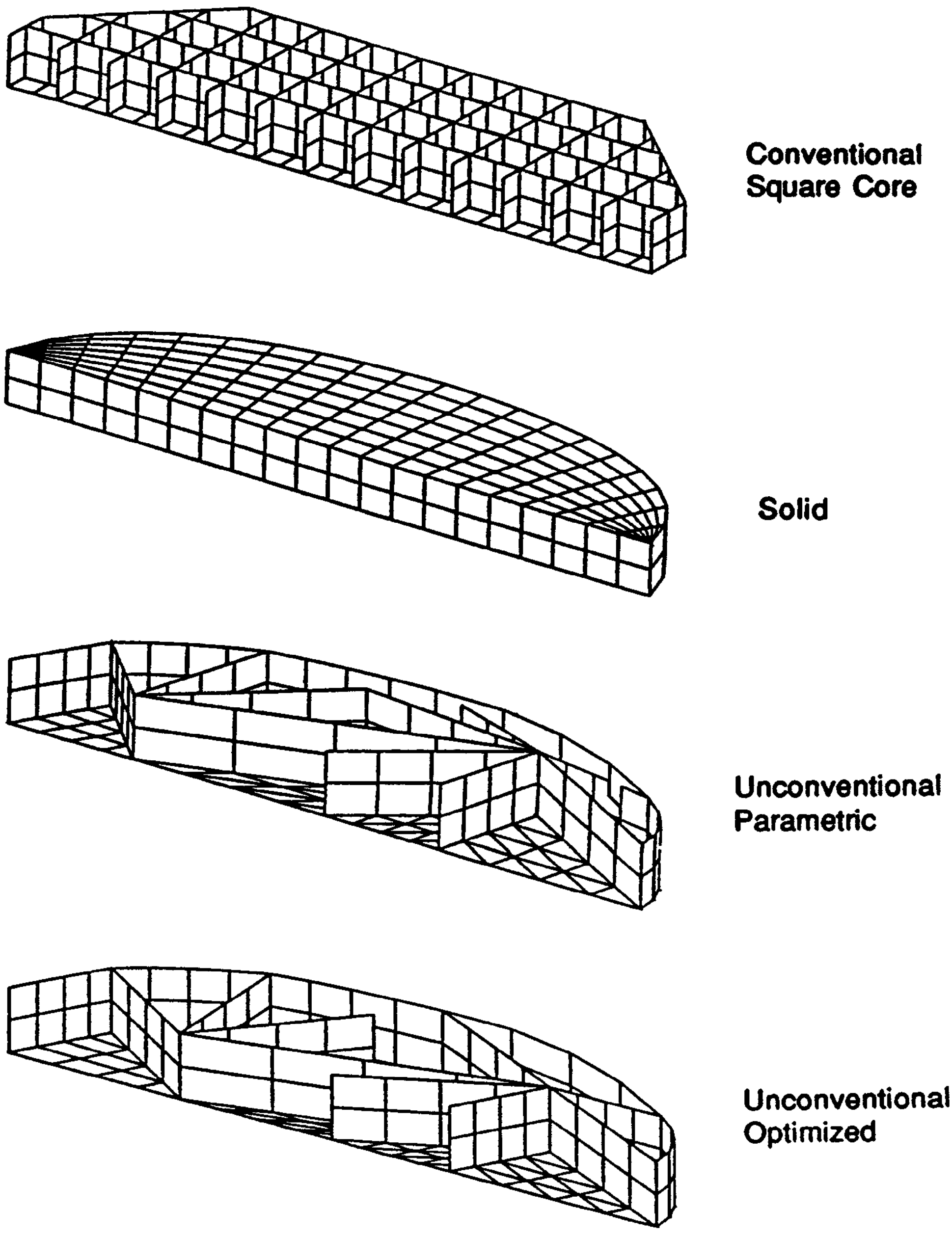

FIGURE 8.57 Elliptic turning mirror design.

The significant result is that the optimized design was the only design to meet the design requirement, but it did so with the lightest weight. From a design cost viewpoint, the parametric design required about three times as much labor and cpu time as the optimized design. The conclusion to be drawn is that the optimization techniques can produce better designs with less effort.

Another conclusion that can be drawn from the above study is that the new design freedom available from new fabrication (waterjet cutting) and processing (ion figuring) techniques has provided more design variables than an experienced design engineer can handle. Only the automated optimization techniques can utilize the many new variables successfully.

Optimization Summary

Since these lightweight mirrors must survive a variety of handling, transportation, launch, and inuse load conditions, all effects must be considered in the design process. A general design capability embedded in a finite element program must include the following tools as a minimum:

1. Sizing and shape variables
2. Static analysis with multiple load and boundary conditions and constraints on the displacements and stress
3. Natural frequency analysis with the constraints on frequency

Additional tools which are highly desirable include:

4. Frequency response with constraints on the displacement and stress
5. Transient response with constraints on the displacement and stress
6. Buckling analysis with constraints on the critical load
7. User-defined equations for the response functions
8. User defines subroutines/programs for the response functions

The above analyses must be available as simultaneous solutions, so that the design is not optimized for the static loads alone, and then separately for the natural frequency constraints. The design algorithm must work on all design constraints simultaneously.

For lightweight mirrors, the basis vector approach to the design variables is efficient and sufficiently general for most mirror designs. The use of automesh is not a viable tool unless there is also an error estimator to revise the mesh for sufficient accuracy. This automesh capability allows a wider design variation within a given run, but is more time consuming than the basis vector approach.

8.13 Summary

An optical structure's performance is more often limited by structural distortions than by stress. Thus, the typical assumptions and modeling techniques used for stress-limited structures may not be appropriate for determining the critical behavior of an optical structure. Even small bending moments caused by neutral axis offsets can seriously degrade optical performance. Several modeling techniques applicable to precision optical structures were discussed in this chapter including symmetry, adhesives, and surface evaluation.

References

1. Barnes, W. P. 1969. Optimal design of cored mirror structures, *Appl. Opt.*, 8, 1191.
2. Buettner, A. and Quesnel, D. 1992. Evaluation of fracture specimen using multimesh extrapolation. In *Proc. 1992 MSC World Users' Conf.* MacNeal-Schwendler, Los Angeles.
3. Cook, R. D., Malkus, D. S., and Plesha, M. E. 1989. *Concepts and Applications of Finite Element Analysis*, 3rd ed., Wiley, New York.

4. Devries, K. L., Gramoll, K. C., and Anderson, G. P. 1986. Analysis of adhesive tensile test methods, *Polym. Eng. Sci.*, 26.
5. Genberg, V. L. 1983. Optical surface evaluation. In *Proc. Structural Mechanics of Optics,* Vol. 450–08. SPIE, Bellingham.
6. Genberg, V. L. 1987. Optical pathlength calculations via finite elements. In *Proc. Structural Mechanics of Optics II,* Vol. 748–14. SPIE, Bellingham.
7. Genberg, V. L. 1993. Ray tracing from finite element results. In *Proc. Optomechanical Design*, Vol. 1998–08, SPIE, Bellingham.
8. Genberg, V. L. and Cormany, N. Y. 1993. Optimum design of lightweight mirrors. In *Proc. Optomechanical Design*, Vol. 1998–07, SPIE, Bellingham.
9. Juvinall, R. C. and Marshek, K. M. 1991. *Fundamentals of Machine Component Design,* 2nd ed. Wiley, New York.
10. Knight, C. E. 1993. *The Finite Element Method in Mechanical Design,* PWS-Kent, Boston.
11. Logan, D. L. 1991. *A First Course in the Finite Element Method*, 2nd ed. PWS-Kent, Boston.
12. MacNeal, R. H. and Harder, R. L. 1985. A proposed standard set of problems to test finite element accuracy, *Finite Element Anal. Design.*
13. Moore, G. J. 1992. *MSCX/NASTRAN Design Sensitivity and Optimization User's Guide.* MacNeal-Schwendler, Los Angeles.
14. Nowak, W. 1988. The analysis of structural dynamic effects on image motion in laser printers using MSC/NASTRAN. In *Proc. 1988 MSC World Users' Conf.* MacNeal-Schwendler, Los Angeles.
15. Schmit, L. A. 1960. Structural design by systematic synthesis, p. 105. In *Proc . of 2nd Conf. on Electronic Computation.* ASCE, New York.
16. Segerlind, L. J. 1984. *Applied Finite Element Analysis*, 2nd ed. Wiley, New York.
17. Thomas, H. L. and Genberg, V. 1994. *Integrated Structural/Optical/Optimization of Mirrors*, AIAA paper No. 94–4356CP.
18. Timoshenko, S. and Woinowsky-Krieger, S. 1959. *Theory of Plates and Shells*, p. 74. McGraw-Hill, New York.
19. Vanderplaats, G. N. 1984. *Numerical Optimization Techniques for Engineering Design*, McGraw-Hill, New York.
20. Vanderplaats, G. N. 1991. *DOT Users Manual.* VMA Engineering, Goleta.
21. Vanderplaats, G. N. 1993. *GENESIS Users Manual.* VMA Engineering, Goleta.
22. Wilson, T. and Genberg, V. L. 1993. Enabling advanced mirror blank design through modern optical fabrication technology. In *Proc. Fabrication and Testing of Optics and Large Optics*, Vol. 1994–27. SPIE, Bellingham.
23. Wolverton, T. and Brooks, J. 1987. Structural and optical analysis of a Landsat telescope mirror. In *Proc. 1987 MSC World Users' Conf.* MacNeal-Schwendler, Los Angeles.
24. Yang, T. Y. 1986. *Finite Element Structural Analysis*, Prentice-Hall, Englewood Cliffs, NJ.